Energy injection for mechanical systems through the method of Virtual Nonholonomic Constraints

by

Adan Moran-MacDonald

A thesis submitted in conformity with the requirements
for the degree of Master of Applied Science
Graduate Department of Electrical and Computer Engineering
University of Toronto

Abstract

Energy injection for mechanical systems through the method of Virtual Nonholonomic Constraints

Adan Moran-MacDonald
Master of Applied Science
Graduate Department of Electrical and Computer Engineering
University of Toronto
2020

This thesis develops a theoretical foundation for the framework of virtual nonholonomic constraints, which are relations between the generalized coordinates and generalized momenta of a mechanical system that can be enforced via feedback control. The theory is applied towards energy injection for two standard underactuated systems: the variable-length pendulum and the acrobot. Virtual nonholonomic constraints are designed for each system by examining human motion, and energy injection properties of these constraints are proven rigorously. The acrobot constraint is tested on a real-world acrobot, demonstrating highly effective energy-injection properties and robustness to a variety of external disturbances.

For Fry.

Contents

List of Tables

List of Figures

List of Symbols

Symbol	Definition
$\mathbb{R}^n$	Real numbers in n dimensions.
$[\mathbb{R}]_T$	Real numbers modulo $T > 0$, with $[\mathbb{R}]_\infty := \mathbb{R}$.
$\mathbb{S}^1$	The unit circle, diffeomorphic to $[\mathbb{R}]_{2\pi}$.
$\mathcal{Q}$	The configuration manifold of a system.
$C^r(X;Y)$	The space of r-times continuously differentiable functions from X to Y.
$\mathbb{R}^{n\times m}$	The space of real-valued matrices with n rows and m columns.
I_n	The $n \times n$ identity matrix.
$\mathbf{0}_{n\times m}$	The $n \times m$ matrix of all zeros.
M_i	If M is a vector, the ith element of M. If M is a matrix, the ith column of M.
$M_{i,j}$	The value of row i, column j for the matrix M.
$\dot{x}$	Derivative of x with respect to time t.
$\nabla_v F$	If F is $\mathbb{R}$-valued, the gradient of F with respect to v. If F is $\mathbb{R}^{n\times n}$-valued and $v \in \mathbb{R}^m$, the block gradient $\left[\nabla_{v_1} F^\mathsf{T} \dots \nabla_{v_m} F^\mathsf{T}\right]^\mathsf{T} \in \mathbb{R}^{nm\times n}$.
dF_v	Total differential (Jacobian) of F, equivalent to $(\nabla_v F)^\mathsf{T}$.
$\partial_v F$	Partial differential of F with respect to v, with i^{th} element $\frac{\partial F}{\partial v_i}$.
$\delta_{i,j}$	The Kronecker delta: 1 if $i = j$ and 0 otherwise.
$\otimes$	The matrix kronecker product.
$\|\cdot\|$	The euclidean norm on $\mathbb{R}^n$.
$\simeq$	Equivalent under diffeomorphism.

Chapter 1

Introduction

The Estonian sport of *Kiiking* (Figure 1.1) is the adult equivalent of a child playing on a standing swing, though here an athlete attempts to make a giant solid steel swing gain momentum. Naturally, the kiiker begins by pushing off the ground and proceeds to alternate between standing and squatting. This allows them to swing higher and faster over time, until they have reached their express goal of spinning at high speed around the bar.

FIGURE 1.1: Kiiking, which translates to "swing", involves a person standing and squatting on a giant swing until they are rotating around the bar. Image taken from [2].

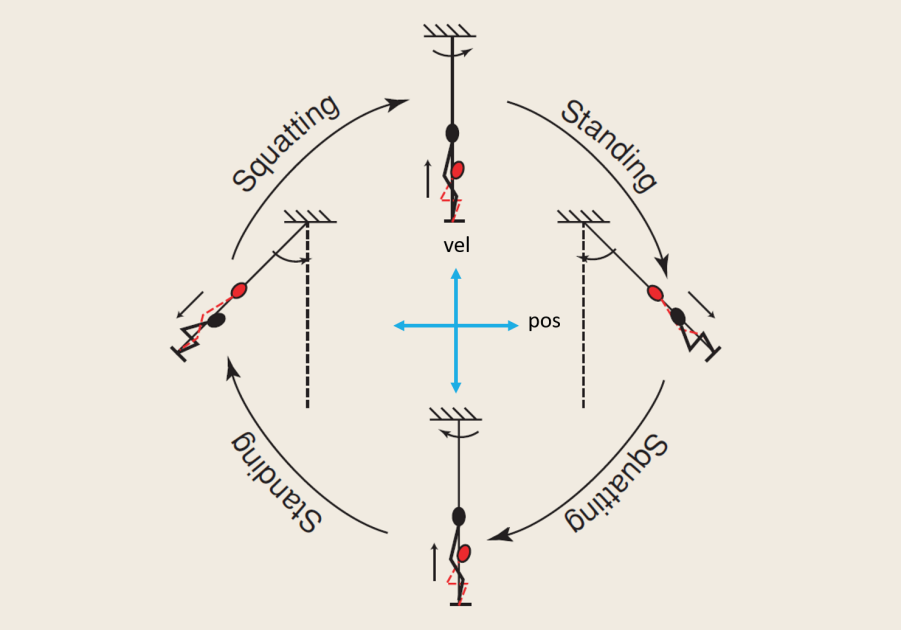

Figure 1.2: A person on a standing swing will stand at the bottom of the swing arc, and squat at the top. Figure modified from [3].

Now imagine that the kiiker is a robot, and their creator is teaching them to swing like a human. If the roboticist had studied classical control theory, they would plot a kiiker's squat depth as a trajectory over time and tell the robot to synchronize with this trajectory. In an ideal world, this technique would work perfectly; unfortunately, it is also entirely unnatural. After all, humans on swings do not have an internal stopwatch telling them when to squat. Rather, they adjust how much they bend their knees based on the current angle of the swing along with their direction of motion. This position-velocity adjustment allows humans to correct for external disturbances (like strong winds or enthusiastic swing pushers). Figure 1.2 shows this adjustment process: a person will squat when they reach the peak of their swing, and stand when they reach the fastest point at the bottom [3]. Even if the robot could perfectly track a time-based trajectory, an external disturbance may affect where squatting and standing occurs to the point that the swing actually slows down.

To fix this issue, a clever roboticist might use *virtual holonomic constraints*, which are controllers that track a function of position rather than time [4]. Sadly, this still fails since one needs velocity to determine when they have reached the peak of their swing. In other words, the robot needs to move according to a function of both position and velocity if it has any hope of behaving like a real person. These position-velocity controllers are known as *virtual nonholonomic constraints*, and they are the focus of this thesis.

Our goal throughout this thesis is to prove that virtual nonholonomic constraints can increase a robot's momentum through a process known as *energy injection*. We will use two benchmark robotic systems to build intuition and test our theory. The first system is the variable-length pendulum, which models a person on a swing. The second is the acrobot, an actuated double pendulum which models a gymnast hanging on a horizontal bar. For each of these examples, we will create virtual nonholonomic constraints which model human motion and will rigorously prove that these constraints inject energy.

1.1 Literature Review

Let us review some of the existing research on energy injection and virtual nonholonomic constraints.

Energy injection for mechanical systems is often performed by passivity-based control and energy shaping — one views the robot and its inputs as energy transformations which are moulded to enforce desired behaviour. Much of the theoretical work in this field has been performed by Ortega, van der Schaft, and others (see for example [5–7]). Energy shaping has been applied to both the variable-length pendulum [8] and the acrobot [9, 10]. This technique is useful and widely applicable, but it does not produce the structured human-like motion we wish to generate using virtual nonholonomic constraints.

The modern concept of virtual nonholonomic constraints was described by Griffin and Grizzle [11] in 2015, though there are references to more primitive versions going back as early as the the year 2000 [12]. Virtual nonholonomic constraints have been of most notable use in bipedal locomotion [13, 14], where they have shown marked improvements in the robustness of walking gaits when compared to previous control techniques. They have also been used for error-reduction in time-delayed teleoperation [15] and in the field of human-robot interaction [16, 17]. Horn et al. [18] have derived the zero dynamics for hybrid mechanical systems under virtual nonholonomic constraints. In particular, they study a class of constraints formed by taking an affine sum of holonomic functions with nonholonomic Bézier polynomials. They widen this class of constraints in [19] to improve bipedal locomotion on variable-slope terrain, and generate constraints through a specialized optimization routine.

The most recent literature surrounding virtual nonholonomic constraints has focused on enforcing stable periodic orbits for hybrid mechanical systems with impacts. To the best of our knowledge, no one has studied how virtual nonholonomic constraints can be

used for energy injection, where periodic motion is not desirable. This thesis attempts to fill this gap in the research. For more detail on the differences between this thesis and the existing research on virtual nonholonomic constraints, see Chapter 2.5.

Many of the contributions in this thesis are extensions of concepts from the field of virtual holonomic constraints. Of note is the framework devised by Mohammadi, Maggiore, and Consolini, among others [1, 4, 20, 21].

1.2 Statement of Contributions

Here are the contributions of this thesis.

Chapter 2 The development of virtual nonholonomic constraints. This includes the definition of simply actuated mechanical systems, virtual nonholonomic constraints, regular constraints, and energy injection. Theorem 2.10 yields a computational characterization of regularity, while Theorem 2.11 explicitly finds the constrained dynamics for a certain class of systems.

Chapter 3 An application of virtual nonholonomic constraints to the variable-length pendulum, based on a pumping technique used by children on standing swings. The chapter culminates in Theorem 3.2, which guarantees that a certain class of VNHCs will inject energy into this system.

Chapter 4 An application of virtual nonholonomic constraints to the acrobot, based on the motion performed by human gymnasts. The chapter ends with Theorem 4.2, which proves that the constraint we design does in fact inject energy into the acrobot.

1.3 Organization of the Thesis

The thesis is laid out as follows: in Chapter 2 we cover the requisite background on analytical mechanics, after which we develop the main theory of virtual nonholonomic constraints; in Chapter 3 we reformulate a time-optimal energy-injection strategy for the variable-length pendulum as a virtual nonholonomic constraint, and prove that the pendulum will gain enough energy to rotate around the bar with arbitrary speed; and in Chapter 4 we find a virtual nonholonomic constraint which enables the acrobot to kick its legs like a gymnast until it performs backflips on a horizontal bar. Finally, we

show experimental results on a physical acrobot which confirm that the theory works in the real world.

Chapter 2

Development of Virtual Nonholonomic Constraints

2.1 Preliminaries on Analytical Mechanics

A mechanical system can be represented by N point masses where each point represents the center of mass of a physical body, along with r *equations of constraint* (EOC) which model the physical restrictions between these masses. The position of each point mass is described using three cartesian coordinates (one for each spatial axis), so the system as a whole can be described by a vector in $\mathbb{R}^{3N}$ with r EOC. The dynamics of the system are computed by deriving the $3N$ *equations of motion* (EOM) produced by Newton's second law $F = ma$. While this technique works for simple systems, it is tedious and becomes impossible to apply to complex mechanical systems where the forces are not explicitly known.

Rather than modeling a mechanical system by cartesian positions and constraints, it is often feasible to represent the position of the system using n independent scalar-valued variables $q_1, \dots, q_n$ called *generalized coordinates*, where $n = 3N - r$ is the number of *degrees of freedom* (DOF) of the system [22]. For instance, Figure 2.1 shows a barbell on a $2D$-plane which can rotate freely on that plane. The barbell has $n = 3$ DOF, so it can be described by three independent generalized coordinates with no equations of constraint.

For the robotic systems of interest in this thesis, we assume that each generalized coordinate q_i represents either the distance or the angle between two parts of the system. Mathematically, each q_i takes values in $[\mathbb{R}]_{T_i}$, where $T_i = \infty$ if q_i represents a length or $T_i = 2\pi$ if q_i represents an angle. It is convention to collect the coordinates into a

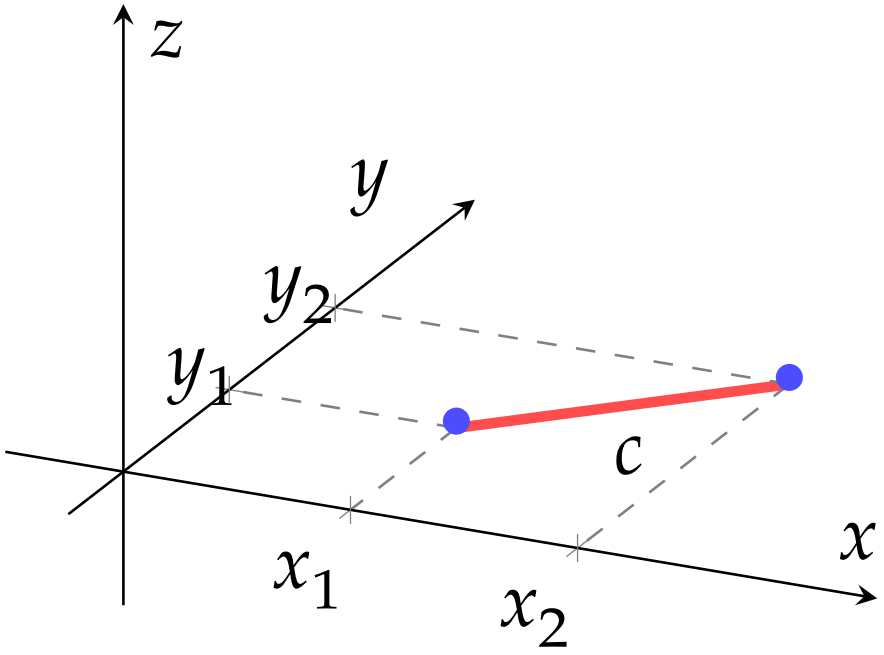

(A) The Newtonian representation of the barbell requires all six cartesian positions and the corresponding EOC.

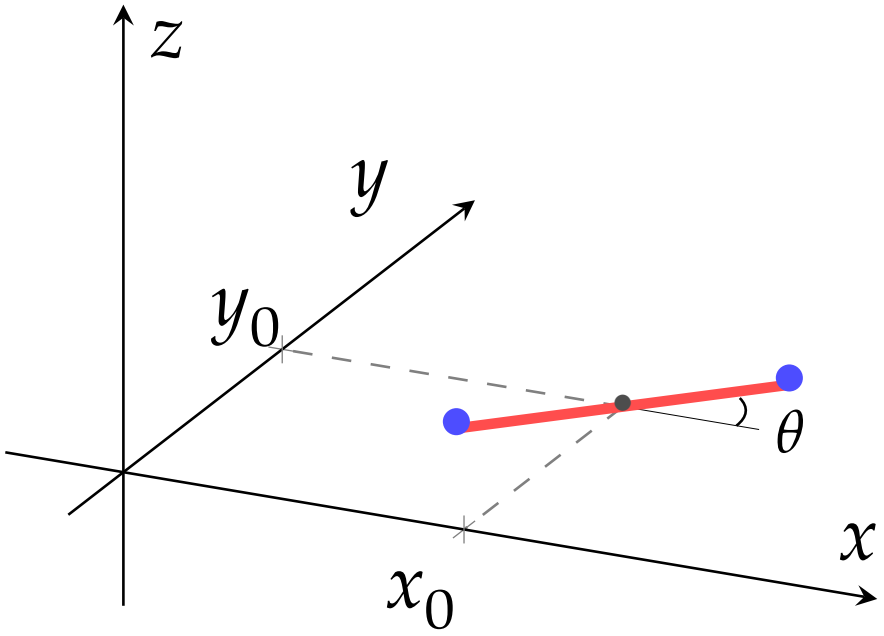

(B) One possible set of three generalized coordinates is (x_0, y_0, θ), which represent the position of the center of the bar and the angle of the barbell in the xy-plane.

Figure 2.1: A mechanical system with $N = 2$ point masses at $a = (x_1, y_1, z_1)$ and $b = (x_2, y_2, z_2)$, separated by a bar of length c. There are $r = 3$ EOC given by $\|a - b\| = c$, $z_1 = 0$, and $z_2 = 0$. This system has $n = 3$ degrees of freedom.

configuration $q = (q_1, \dots, q_n) \in \mathcal{Q}$ where the *configuration manifold* $\mathcal{Q}$ of the system is a so-called *generalized cylinder*

$$\mathcal{Q} = [\mathbb{R}]_{T_1} \times \cdot \times [\mathbb{R}]_{T_n}.$$

The derivative $\dot{q} = (\dot{q}_1, \dots, \dot{q}_n)$ of a configuration is called a *generalized velocity* of the system. For arbitrary systems, the space of allowable velocities depends on the current configuration of the system. However, since $\mathcal{Q}$ is a generalized cylinder, we find that $\dot{q} \in \mathbb{R}^n$. The combined vector $(q, \dot{q}) \in \mathcal{Q} \times \mathbb{R}^n$ is called a *state* of the system.

The field of analytical mechanics provides a computational method for finding the EOM of a system in generalized coordinates. The two most common analytical methods for modelling robotic systems are *Lagrangian* and *Hamiltonian* mechanics.

2.1.1 Lagrangian Mechanics

Lagrangian mechanics uses the kinetic energy $T(q, \dot{q})$ and potential energy $P(q)$ of the system to define the Lagrangian $\mathscr{L} : \mathcal{Q} \times \mathbb{R}^n \to \mathbb{R}$ defined by (2.1) [22],

$$\mathscr{L}(q, \dot{q}) = T(q, \dot{q}) - P(q). \tag{2.1}$$

When the mechanical system is actuated, the EOM are described by n second-order ordinary differential equations (ODEs) obtained from the *Euler-Lagrange equations* (2.2) with *generalized input forces* $\tau \in \mathbb{R}^k$,

$$\frac{d}{dt}\left\{\frac{\partial \mathscr{L}}{\partial \dot{q}_i}\right\} - \frac{\partial \mathscr{L}}{\partial q_i} = B_i^{\mathsf{T}}(q)\tau. \tag{2.2}$$

The vector $B_i^{\mathsf{T}} : \mathcal{Q} \to \mathbb{R}^{1\times k}$ describes how the input forces shape the dynamics of q_i. The matrix $B : \mathcal{Q} \to \mathbb{R}^{n\times k}$ with

$$B(q) = \begin{bmatrix} - & B_1^{\mathsf{T}}(q) & - \\ & \vdots & \\ - & B_n^{\mathsf{T}}(q) & - \end{bmatrix},$$

is called the *input matrix* for the system. If $k < n$, we say the system is *underactuated* with degree of underactuation $(n - k)$.

Many actuated mechanical systems have quadratic kinetic energies, so that the Lagrangian can be written explicitly as

$$\mathscr{L}(q, \dot{q}) = \frac{1}{2}\dot{q}^{\mathsf{T}} D(q)\dot{q} - P(q), \tag{2.3}$$

where the *inertia matrix* $D : \mathcal{Q} \to \mathbb{R}^{n\times n}$ is a symmetric, positive definite matrix for all $q \in \mathcal{Q}$ and the potential function $P : \mathcal{Q} \to \mathbb{R}$ is smooth.

2.1.2 Hamiltonian Mechanics

Hamiltonian mechanics converts the n second-order ODEs generated by Lagrangian mechanics into an equivalent set of $2n$ first-order ODEs.

To do this, we first define the *conjugate of momentum p_i to q_i* by

$$p_i(q,\dot{q}) := \frac{\partial \mathscr{L}}{\partial \dot{q}_i}(q,\dot{q}). \tag{2.4}$$

To ease notation, we write $p = (p_1, \dots, p_n) \in \mathbb{R}^n$ and call p the *conjugate of momenta to q*. Note that each p_i is a linear function of $\dot{q}$, and one can typically solve for $\dot{q}(q,p)$ by inverting all the expressions from (2.4). The combined vector $(q,p) \in \mathcal{Q} \times \mathbb{R}^n$ is called a *phase* of the system.

The *Hamiltonian* of the system in (q,p) coordinates is the "Legendre transform" (2.5) of the Lagrangian [23],

$$\mathscr{H}(q,p) := p^{\mathsf{T}}\dot{q}(q,p) - \mathscr{L}(q,\dot{q}(q,p)). \tag{2.5}$$

The EOM in the Hamiltonian framework are the $2n$ first-order equations called *Hamilton's equations*. They are given by

$$\begin{cases} \dot{q} = \nabla_p \mathscr{H}, \\ \dot{p} = -\nabla_q \mathscr{H} + B(q)\tau. \end{cases} \tag{2.6}$$

Here, $B(q) \in \mathbb{R}^{n\times k}$ is the same input matrix used by the Lagrangian framework, with $\tau \in \mathbb{R}^k$ the same vector of generalized input forces.

If the kinetic energy of the system is quadratic as in (2.3), the conjugate of momenta becomes $p = D(q)\dot{q}$. Since $D(q)$ is symmetric and positive definite, it is invertible at each $q \in \mathcal{Q}$. The Legendre transform (2.5) becomes

$$\begin{aligned} \mathscr{H}(q,p) &= p^{\mathsf{T}}D^{-1}(q)p - \left(\frac{1}{2}p^{\mathsf{T}}D^{-1}(q)p - P(q)\right) \\ &= \frac{1}{2}p^{\mathsf{T}}D^{-1}(q)p + P(q). \end{aligned}$$

Finding the derivative of each momentum coordinate yields

$$\dot{p}_i = -\frac{1}{2}p^\mathsf{T}\nabla_{q_i}D^{-1}(q)p - \frac{\partial P}{\partial q_i}(q) + B_i^\mathsf{T}(q)\tau.$$

Recall the Kronecker product of matrices [24], defined as follows.

Definition 2.1. Let $A \in \mathbb{R}^{n\times m}$ and $B \in \mathbb{R}^{r\times s}$. The Kronecker product $A \otimes B \in \mathbb{R}^{nr\times ms}$ is the matrix

$$A \otimes B = \begin{bmatrix} A_{1,1}B & \cdots & A_{1,m}B \\ \vdots & \ddots & \vdots \\ A_{n,1}B & \cdots & A_{n,m}B \end{bmatrix}.$$

Using the kronecker product, one can collect the derivative of momentum into the vector form

$$\dot{p} = -\frac{1}{2}(I_n \otimes p^\mathsf{T})\nabla_q D^{-1}(q)p - \nabla_q P(q) + B(q)\tau.$$

In sum, when the kinetic energy is quadratic the Hamiltonian system reduces to

$$\mathscr{H}(q,p) = \frac{1}{2}p^\mathsf{T}D^{-1}(q)p + P(q), \tag{2.7}$$

$$\begin{cases} \dot{q} = D^{-1}(q)p \\ \dot{p} = -\frac{1}{2}(I_n \otimes p^\mathsf{T})\nabla_q D^{-1}(q)p - \nabla_q P(q) + B(q)\tau. \end{cases} \tag{2.8}$$

Any set of coordinates (q,p) which satisfy Hamilton's equations under the Hamiltonian $\mathscr{H}$ are said to be *canonical coordinates* for the system. A change of coordinates $(q,p) \to (Q,P)$ is a *canonical transformation* if (Q,P) preserve the Hamiltonian structure; that is, if they are canonical coordinates under the Hamiltonian $\mathscr{H}\left(q(Q,P), p(Q,P)\right)$.

Landau and Lifschitz [23] provide a useful result for showing whether a given change of coordinates $(q,p) \to (Q,P)$ is a canonical transformation.

Definition 2.2. The *Poisson bracket* between the functions $f(q,p)$ and $g(q,p)$ is

$$[f,g] := \sum_{i=1}^{n} \frac{\partial f}{\partial p_i}\frac{\partial g}{\partial q_i} - \frac{\partial f}{\partial q_i}\frac{\partial g}{\partial p_i}. \tag{2.9}$$

Theorem 2.3. *A change of coordinates $(q,p) \to (Q,P)$ is a canonical transformation if and*

only if

$$[Q_i, Q_j] = 0,$$
$$[P_i, P_j] = 0,$$
$$[P_i, Q_j] = \delta_{i,j},$$

for all $i, j \in \{1, \dots, n\}$.

Proof. See (45.10) in [23]. □

Later in this chapter we will define a particular change of coordinates. The following Lemma allows us to prove it is a canonical transformation.

Lemma 2.4. *Let* $\mathscr{H}$ *be a Hamiltonian system in canonical coordinates* (q, p)*. Let* $A \in \mathbb{R}^{n\times n}$ *be an orthogonal matrix. The change of coordinates* $(q, p) \to (Q = Aq, P = Ap)$ *is a canonical transformation.*

Proof. For any constant matrix A, the transformation $(Q = Aq, P = Ap)$ satisfies $\frac{\partial Q_i}{\partial p_m} = \frac{\partial P_i}{\partial q_m} = 0$ for all $i, m \in \mathbf{n}$. Hence,

$$[Q_i, Q_j] = \sum_{m=1}^{n} \frac{\partial Q_i}{\partial p_m}\frac{\partial Q_j}{\partial q_m} - \frac{\partial Q_i}{\partial q_m}\frac{\partial Q_j}{\partial p_m} = 0,$$
$$[P_i, P_j] = \sum_{m=1}^{n} \frac{\partial P_i}{\partial p_m}\frac{\partial P_j}{\partial q_m} - \frac{\partial P_i}{\partial q_m}\frac{\partial P_j}{\partial p_m} = 0.$$

Since A is orthogonal, $(A_i)^{\mathsf{T}}(A^{\mathsf{T}})_j = (A_i)^{\mathsf{T}}(A^{-1})_j = \delta_{i,j}$. Using this fact we see that the Poisson brackets between P_i and Q_j are given by

$$\begin{aligned}
[P_i, Q_j] &= \sum_{m=1}^{n} \frac{\partial P_i}{\partial p_m}\frac{\partial Q_j}{\partial q_m} - \frac{\partial P_i}{\partial q_m}\frac{\partial Q_j}{\partial p_m} \\
&= \sum_{m=1}^{n} A_{i,m}A_{j,m} - 0 \\
&= \sum_{m=1}^{n} A_{i,m}(A^{\mathsf{T}})_{m,j} \\
&= (A_i)^{\mathsf{T}}(A^{\mathsf{T}})_j \\
&= \delta_{i,j}.
\end{aligned}$$

Therefore, by Theorem 2.3, the coordinate change $(Q = Aq, P = Ap)$ is a canonical transformation. □

2.2 Simply Actuated Hamiltonian Systems

Suppose we are given a Hamiltonian mechanical system (2.7). Because τ is transformed by the input matrix $B(q)$ before entering the EOM, it is not in general clear how any particular input force τ_i will affect the dynamics of the system. In this section, we define a new class of Hamiltonian systems where the effect of the input forces is made obvious. This class of systems will form the backbone for the rest of the theory developed in this thesis.

Definition 2.5. Let $\mathscr{H}$ be an n-DOF Hamiltonian system with $k \leq n$ actuators. A set of canonical coordinates (q, p) for this system are said to be *simply actuated coordinates* if the input matrix $B(q) \in \mathbb{R}^{n\times k}$ is of the form

$$B(q) = \begin{bmatrix} \mathbf{0}_{(n-k)\times k} \\ I_k \end{bmatrix}.$$

The first $(n-k)$ coordinates, labelled q_u, are called the *unactuated coordinates*. The remaining k coordinates, labelled q_a, are called the *actuated coordinates*. When grouping them together, we will always put them in the order (q_u, q_a) to fit with the definition. The corresponding (p_u, p_a) are called the *unactuated* and *actuated momenta*, respectively.

Under the following assumptions on the input matrix, we will show that there is a canonical transformation of (2.7) into simply actuated coordinates.

Assumption 1. The input matrix $B(q) \equiv B \in \mathbb{R}^{n\times k}$ is constant, full rank, and $k < n$.

Assumption 2. There exists a matrix $B^\perp \in \mathbb{R}^{(n-k)\times n}$ which is right semi-orthogonal $\left(B^\perp (B^\perp)^\mathsf{T} = I_{(n-k)}\right)$ and which is a left-annihilator for B. That is, $B^\perp B = \mathbf{0}_{(n-k)\times k}$.

Assumption 2 requires the rows of $B^\perp$ to be unit vectors that are mutually orthogonal. In the case that $k = (n-1)$, the existence of any left annihilator $A^0 \in \mathbb{R}^{1\times n}$ implies the left annihilator $B^\perp := A^0/\|A^0\|$ will be a unit vector satisfying Assumption 2.

Lemma 2.6. *Suppose Assumption 1 holds. Then there exists a nonsingular matrix $\hat{T} \in \mathbb{R}^{k\times k}$ so that the regular feedback transformation*

$$\tau = \hat{T}\hat{\tau}$$

has a new input matrix $\hat{B}$ for $\hat{\tau}$ which is left semi-orthogonal. That is, $\hat{B}^\mathsf{T}\hat{B} = I_k$.

Proof. Since B is a constant matrix, it has a singular-value decomposition $B = U\Sigma V^\mathsf{T}$ where $U^{-1} = U^\mathsf{T} \in \mathbb{R}^{n\times n}$, $V^{-1} = V^\mathsf{T} \in \mathbb{R}^{k\times k}$, and $\Sigma \in \mathbb{R}^{n\times k}$ is defined by

$$\Sigma = \begin{bmatrix} \sigma_1 & 0 & \cdots & 0 \\ 0 & \sigma_2 & \cdots & 0 \\ \vdots & & \ddots & \vdots \\ 0 & 0 & \cdots & \sigma_k \\ - & & \mathbf{0}_{(n-k)\times k} & - \end{bmatrix},$$

where $\sigma_i \neq 0$ because B is full-rank [25]. Define $T \in \mathbb{R}^{k\times k}$ by

$$T = \begin{bmatrix} \frac{1}{\sigma_1} & 0 & \cdots & 0 \\ 0 & \frac{1}{\sigma_2} & \cdots & 0 \\ \vdots & & \ddots & \vdots \\ 0 & 0 & \cdots & \frac{1}{\sigma_k} \end{bmatrix}.$$

Letting $\hat{T} = VT$ and assigning the regular feedback transformation $\tau = \hat{T}\hat{\tau}$, we get a new input matrix for $\hat{\tau} \in \mathbb{R}^k$ given by

$$\hat{B} = B\hat{T} = BVT = U \begin{bmatrix} I_k \\ \mathbf{0}_{(n-k)\times k} \end{bmatrix},$$

which is still constant and full-rank. In particular, $\hat{B}^\mathsf{T}\hat{B} = T^\mathsf{T}\Sigma^\mathsf{T}\Sigma T = I_k$. □

In light of Lemma 2.6, there is no loss of generality by making the following assumption.

Assumption 3. Assume that the input matrix B is left semi-orthogonal, *i.e.*,, $B^\mathsf{T}B = I_k$.

Let now $\mathbf{B} \in \mathbb{R}^{n\times n}$ be the following matrix:

$$\mathbf{B} = \begin{bmatrix} B^\perp \\ B^\mathsf{T} \end{bmatrix}.$$

Since $B^\perp$ is a left annihilator of B and both $B^\perp$ and B^T are right semi-orthogonal, it is easy to show that $\mathbf{B}$ is orthogonal.

Proof.

$$\mathbf{B}\mathbf{B}^\mathsf{T} = \begin{bmatrix} B^\perp(B^\perp)^\mathsf{T} & B^\perp B \\ (B^\perp B)^\mathsf{T} & B^\mathsf{T}B \end{bmatrix} = I_n.$$

Hence, $\mathbf{B}$ is invertible with $\mathbf{B}^{-1} = \mathbf{B}^\mathsf{T}$. □

The following theorem shows that $\mathbf{B}$ provides a canonical transformation into simply actuated coordinates, so that only the actuated momenta are affected by the input forces.

Theorem 2.7. *Under Assumptions 1,2, and 3, the Hamiltonian system* (2.7) *has simply actuated canonical coordinates* $(\tilde{q} = \mathbf{B}q, \tilde{p} = \mathbf{B}p)$*. The resulting dynamics are given by*

$$\mathscr{H}(\tilde{q}, \tilde{p}) = \frac{1}{2}\tilde{p}^\mathsf{T} M^{-1}(\tilde{q})\tilde{p} + V(\tilde{q}), \tag{2.10}$$
$$\begin{cases} \dot{\tilde{q}} = M^{-1}(\tilde{q})\tilde{p}, \\ \dot{\tilde{p}} = -\frac{1}{2}(I_n \otimes \tilde{p}^\mathsf{T})\nabla_{\tilde{q}} M^{-1}(\tilde{q})\tilde{p} - \nabla_{\tilde{q}} V(\tilde{q}) + \begin{bmatrix} \mathbf{0}_{(n-k)\times k} \\ I_k \end{bmatrix} \tau, \end{cases}$$

where

$$M^{-1}(\tilde{q}) := \mathbf{B}D^{-1}(\mathbf{B}^\mathsf{T}\tilde{q})\mathbf{B}^\mathsf{T},$$
$$V(\tilde{q}) := P(\mathbf{B}^\mathsf{T}\tilde{q}).$$

Proof. The change of coordinates $(\tilde{q} = \mathbf{B}q, \tilde{p} = \mathbf{B}p)$ satisfies Lemma 2.4, making it a canonical transformation. Furthermore, since $\dot{\tilde{p}} = \mathbf{B}\dot{p}$, the new input matrix is given by

$$\mathbf{B}B = \begin{bmatrix} B^\perp B \\ B^\mathsf{T} B \end{bmatrix} = \begin{bmatrix} \mathbf{0}_{(n-k)\times k} \\ I_k \end{bmatrix},$$

which means $\left(\tilde{q} = (q_u, q_a), \tilde{p} = (p_u, p_a)\right)$ are simply actuated coordinates for $\mathscr{H}$ as desired. □

2.3 Virtual Nonholonomic Constraints

Let us imagine a child on a swing who wants to reach the largest height possible. To begin, the child pushes off the ground to imbue the swing with small oscillations. What allows them to increase the amplitude of these oscillations is the appropriate extension and retraction of their feet. If a roboticist were creating a machine to replicate this behaviour, they might design a robot whose legs extend and retract at specific time intervals. At first glance, this technique should work perfectly because the leg motion would synchronize with the swinging frequency, thereby injecting energy as quickly as is physically possible.

Unfortunately, a deeper analysis reveals the flaw with this design. Most children are not counting out the time in their head; rather, they observe their current position and velocity and adjust their legs as required. For example, many children have an adult pushing the swing, or perhaps they are swinging on a windy day. In either case, they adjust their leg motion accordingly when presented with these external disturbances, without keeping track of time. Hence, the standard control technique of tracking a function of time (known as *trajectory tracking*) does not truly replicate human behaviour. Even if the robot's legs perfectly track a specified trajectory, an external disturbance will desynchronize the leg motion with the swing - thereby stopping the amplitude-increasing effects.

Rather than tracking a trajectory over time, a more human-like behaviour is to force the robot's legs track a function of the swing's state. One recent control method known as *virtual holonomic constraints* (VHCs) uses the actuators to enforce a relation $h(q) = 0$ of the configuration [4]. This method has provided incredible results in the development of walking robots [26, 27], vehicle motion [28, 29], and has even been used to design a snake-like swimming robot [30].

The downside to VHCs is that they only depend on the configuration of a mechanical system, and not its generalized velocity. For the child on a swing, whether they extend or retract their legs depends on their direction of motion. This inherently requires knowledge of their current velocity, which precludes the usage of VHCs. A few authors have attempted to extend the theory of VHCs to enforce relations $h(q, \dot{q}) = 0$ of the full state to account for this drawback. Since these relations use actuators to restrict both the configuration and velocity of a system, they are called virtual *nonholonomic* constraints. This idea has been used for human-robot interaction [12, 16, 17], error-reduction on time-delayed systems [15], and has shown marked improvements to the field of bipedal locomotion [11, 14, 18]. Most interestingly, this nonholonomic approach is more robust than standard VHCs when applied to bipedal robotics [19]. In particular, virtual nonholonomic constraints may be capable of injecting and dissipating energy from a system in a robust manner, all while producing realistic biological motion. This is what we aim to prove in this thesis.

Unlike the theory of VHCs, there does not appear to be a standard definition of virtual nonholonomic constraints: all the applications listed above use their own definitions, which makes it difficult to compare and generalize their work.

This section will provide a standard characterization of virtual nonholonomic constraints using Hamiltonian mechanics. The goal is to provide a consistent, rigorous foundation for designing constraints on a general class of systems.

Definition 2.8. A *virtual nonholonomic constraint* (VNHC) *of order k* is a relation $h(q,p) = 0$ where $h : \mathcal{Q} \times \mathbb{R}^n \to \mathbb{R}^k$ is C^2, $\operatorname{rank}\left(\left[dh_q, dh_p\right]\right) = k$ for all $(q,p) \in h^{-1}(0)$, and there exists a feedback controller $\tau(q,p)$ rendering the *constraint manifold* Γ invariant, where

$$\Gamma = \left\{(q,p) \mid h(q,p) = 0, dh_q\dot{q} + dh_p\dot{p} = 0\right\}.$$

From the definition of VNHCs, one finds that the constraint manifold Γ is a $2(n-k)$-dimensional closed embedded submanifold of $\mathcal{Q} \times \mathbb{R}^n$. The next obvious question is the following: when does there exists a feedback controller stabilizing Γ?

One approach to answering this question is to define the error term $e = h(q,p)$. If there exists some controller $\tau(q,p)$ driving $e \to 0$ and $\dot{e} \to 0$, then the same τ will necessarily stabilize Γ (under additional mild conditions, see [4]) [1].

We say that e is of *relative degree* $\{r_1, \dots, r_k\}$ if

1. Some component of τ appears at the r_i^{th} derivative of e_i for $i \in \{1, \dots, k\}$.

2. In the vector of time-derivatives $(e_1^{(r_1)}, \dots, e_k^{(r_k)})$, the vector τ is premultiplied by a nonsingular matrix.

With no further structure on $h(q,p)$, the control input τ usually appears after one derivative of e; unfortunately, if any e_i has relative degree $r_i = 1$ we may not be able to stabilize Γ. We could guarantee $e_i(t) \to 0$, but we could not in general guarantee $\dot{e}_i(t) \to 0$.

Requiring e to have relative degree $\{2, \dots, 2\}$ is much more useful, since it allows us to easily solve for a controller stabilizing Γ. This kind of relative degree requirement is already common in the VHC literature. Taking advantage of that precedent, we define a special type of VNHC that satisfies this property.

Definition 2.9. A VNHC $h(q,p) = 0$ of order k is *regular* if the output $e = h(q,p)$ is of relative degree $\{2, 2. \dots, 2\}$ everywhere on the constraint manifold Γ.

The authors of [11, 18, 19] observed that a relation which uses only the unactuated conjugate of momentum cannot have τ appearing after only one derivative. Of course, they performed their research in Lagrangian form; we will be using the Hamiltonian formulation from Chapter 2.2. As a reminder, our system is described in (q,p) coordinates

[1] The type of constraints we consider in this thesis are graphs of functions, and so meet these mild assumptions.

with $q = (q_u, q_a)$ and $p = (p_u, p_a)$ and has the dynamics

$$\mathscr{H}(q,p) = p^\mathsf{T} M^{-1}(q)p + V(q), \tag{2.11}$$

$$\begin{cases} \dot{q} = M^{-1}p, \\ \dot{p} = -\frac{1}{2}(I_n \otimes p^\mathsf{T})\nabla_q M^{-1}(q)p - \nabla_q V(q) + \begin{bmatrix} \mathbf{0}_{(n-k)\times k} \\ I_k \end{bmatrix}\tau. \end{cases} \tag{2.12}$$

Notation. We will write $q_u \in \mathscr{Q}_u$, $q_a \in \mathscr{Q}_a$ where $\mathscr{Q}_u \times \mathscr{Q}_a = \mathscr{Q}$. We also write $p_u \in \mathscr{P}_u := \mathbb{R}^{n-k}$ and $p_a \in \mathscr{P}_a := \mathbb{R}^k$, so that $p \in \mathscr{P} := \mathscr{P}_u \times \mathscr{P}_a = \mathbb{R}^n$. In this manner, the phase space of our system can be written as $\mathscr{Q} \times \mathscr{P}$.

Theorem 2.10. *A relation $h(q,p) = 0$ for system (2.11) is a regular VNHC of order k if and only if $dh_{p_a} = 0$ and*

$$\operatorname{rank}\left(\left(dh_q M^{-1}(q) - dh_{p_u}(I_{n-k} \otimes p^\mathsf{T})\nabla_{q_u} M^{-1}(q) \right) \begin{bmatrix} \mathbf{0}_{(n-k)\times k} \\ I_k \end{bmatrix} \right) = k,$$

everywhere on the constraint manifold Γ.

Proof. Let $e = h(q,p) \in \mathbb{R}^k$. Then

$$\begin{aligned} \dot{e} &= dh_q \dot{q} + dh_p \dot{p} \\ &= dh_q M^{-1}(q)p + \\ &\begin{bmatrix} dh_{p_u} & dh_{p_a} \end{bmatrix} \left(-\frac{1}{2} \begin{bmatrix} (I_{n-k} \otimes p^\mathsf{T})\nabla_{q_u} M^{-1}(q)p \\ (I_k \otimes p^\mathsf{T})\nabla_{q_a} M^{-1}(q)p \end{bmatrix} - \begin{bmatrix} \nabla_{q_u} V(q) \\ \nabla_{q_a} V(q) \end{bmatrix} + \begin{bmatrix} \mathbf{0}_{(n-k)\times k} \\ I_k \end{bmatrix} \tau \right). \end{aligned}$$

If $dh_{p_a} \neq \mathbf{0}_{k\times k}$ for some (q,p) on Γ, then τ appears in $\dot{e}$ and the VNHC is not of relative degree $\{2, 2, \dots, 2\}$. Hence, we must have that $dh_{p_a} = \mathbf{0}_{k\times k}$. Proceeding with this assumption, we now find that $h : \mathscr{Q} \times \mathscr{P}_u \to \mathbb{R}^k$, which means that

$$\dot{e} = dh_q M^{-1}(q)p - dh_{p_u}\left(\frac{1}{2}(I_{n-k} \otimes p^\mathsf{T})\nabla_{q_u} M^{-1}(q)p + \nabla_{q_u} V(q) \right).$$

Taking one further derivative provides

$$\ddot{e} = \left(\frac{d}{dt}dh_q\right)M^{-1}(q)p + dh_q\left(\sum_{i=1}^{n}\frac{\partial M^{-1}}{\partial q_i}(q)\dot{q}_i\right)p + dh_q M^{-1}(q)\dot{p} - \left(\frac{d}{dt}dh_{p_u}\right)\left(\frac{1}{2}(I_{n-k}\otimes p^\mathsf{T})\nabla_{q_u}M^{-1}(q)p + \nabla_{q_u}V(q)\right) - dh_{p_u}\left(\frac{1}{2}\frac{d}{dt}\left((I_{n-k}\otimes p^\mathsf{T})\nabla_{q_u}M^{-1}(q)p\right) + \left(\frac{d}{dt}\nabla_{q_u}V(q)\right)\right).$$

Most of these terms do not involve $\dot{p}$ and hence do not contain τ, so we shorten this to

$$\ddot{e} = (\star) - dh_{p_u}\left(\frac{1}{2}\frac{d}{dt}\left((I_{n-k}\otimes p^\mathsf{T})\nabla_{q_u}M^{-1}(q)p\right)\right) + dh_q M^{-1}(q)\begin{bmatrix}\mathbf{0}_{(n-k)\times k}\\ I_k\end{bmatrix}\tau.$$

Observe that the i^{th} row of $\frac{1}{2}\frac{d}{dt}\left((I_{n-k}\otimes p^\mathsf{T})\nabla_{q_u}M^{-1}(q)p\right)$ is given by

$$\frac{1}{2}\frac{d}{dt}\left(p^\mathsf{T}\frac{\partial M^{-1}}{\partial q_{u_i}}(q)p\right) = p^\mathsf{T}\frac{\partial M^{-1}}{\partial q_{u_i}}(q)\dot{p} + \frac{1}{2}p^\mathsf{T}\left(\sum_{j=1}^{n}\frac{\partial^2 M^{-1}}{\partial q_{u_i}\partial q_j}\dot{q}_j\right)p.$$

Highlighting only the term containing τ, we get the vector form

$$\frac{1}{2}\frac{d}{dt}\left((I_{n-k}\otimes p^\mathsf{T})\nabla_{q_u}M^{-1}(q)p\right) = (\star) + (I_{n-k}\otimes p^\mathsf{T})\nabla_{q_u}M^{-1}(q)\begin{bmatrix}\mathbf{0}_{(n-k)\times k}\\ I_k\end{bmatrix}\tau.$$

Plugging this into $\ddot{e}$ reveals that

$$\ddot{e} = (\star) + \left(dh_q M^{-1}(q) - dh_{p_u}(I_{n-k}\otimes p^\mathsf{T})\nabla_{q_u}M^{-1}(q)\right)\begin{bmatrix}\mathbf{0}_{(n-k)\times k}\\ I_k\end{bmatrix}\tau,$$

where $(\star)$ is a continuous function of q and p. For shorthand, we'll write

$$\ddot{e} = E(q,p) + H(q,p)\tau,$$

where E and H are defined appropriately. From the definition of regularity, the VNHC h is regular when e is of relative degree $\{2,\dots,2\}$, which is true if and only if the matrix premultiplying τ is nonsingular, and hence that H is invertible. This proves the theorem. □

Using the expression $\ddot{e} = E(q,p) + H(q,p)\tau$ from the proof of Theorem 2.10, a regular

VNHC of order k can be stabilized by[2] the output-linearizing phase-feedback controller

$$\tau(q,p) = -H^{-1}(q,p)\left(E(q,p) + k_p e + k_d \dot{e}\right), \tag{2.13}$$

where $k_p, k_d \in \mathbb{R}_{>0}$ are control parameters which can be tuned on the resulting linear system $\ddot{e} = -k_p e - k_d \dot{e}$.

Note that one generally cannot measure conjugate of momenta directly, as sensors on mechanical systems will only measure the state $(q, \dot{q})$. To implement this controller in practice, one must compute $p = M(q)\dot{q}$ at every iteration. In other words, this controller requires knowledge of the full state of the system.

Now that we have found a controller to enforce a regular VNHC of order k, we would like to determine the dynamics on the constraint manifold Γ. Intuitively, these dynamics should be parameterized by (q_u, p_u) since q_a is a function of these as specified by $h(q, p_u) = 0$. Unfortunately, $\dot{q}_u$ depends on p_a, and for general systems one cannot solve explicitly for p_a in terms of (q_u, p_u). This is because the $\dot{p}$ dynamics contains the coupling term $(I_n \otimes p^\mathsf{T})\nabla_{q_u} M(q)p$.

We now introduce an assumption so we can solve explicitly for the constrained dynamics.

Assumption 4. The Hamiltonian system has an inertia matrix that does not depend on the unactuated coordinates:

$$\nabla_{q_u} M(q) = \mathbf{0}_{n(n-k)\times n}.$$

Theorem 2.11. *Let $\mathscr{H}$ be a mechanical system in simply actuated coordinates satisfying Assumption 4. Let $h(q, p_u) = 0$ be a regular VNHC of order k with constraint manifold Γ. Suppose that on Γ one can solve for q_a as a function $q_a = f(q_u, p_u)$. Then the constrained dynamics are given by*

$$\left.\begin{aligned} \dot{q}_u &= \begin{bmatrix} I_{(n-k)} & \mathbf{0}_{(n-k)\times k} \end{bmatrix} M^{-1}(q)p \\ \dot{p}_u &= -\nabla_{q_u} V(q) \end{aligned}\right|_{\substack{q_a = f(q_u,p_u) \\ p_a = g(q_u,p_u)}}, \tag{2.14}$$

where

$$g(q_u, p_u) := \left(dh_q M^{-1}(q)\begin{bmatrix} \mathbf{0}_{(n-k)\times k} \\ I_k \end{bmatrix}\right)^{-1}\left(dh_{p_u}\nabla_{q_u} V(q) - dh_q M^{-1}(q)\begin{bmatrix} I_{n-k} \\ \mathbf{0}_{k\times(n-k)} \end{bmatrix} p_u\right)\Bigg|_{q_a = f(q_u,p_u)}. \tag{2.15}$$

[2] Under additional mild conditions [4].

Proof. Setting $e = h(q, p_u)$ and using the fact that $\nabla_{q_u} M^{-1}(q) = 0$, we find that

$$\dot{e} = dh_q M^{-1}(q)p - dh_{p_u} \nabla_{q_u} V(q).$$

Observe that

$$\begin{aligned} dh_q M^{-1}(q)p &= dh_q M^{-1}(q) \begin{bmatrix} p_u \\ p_a \end{bmatrix} \\ &= dh_q M^{-1}(q) \begin{bmatrix} I_{n-k} & \mathbf{0}_{(n-k)\times k} \\ \mathbf{0}_{k\times(n-k)} & I_k \end{bmatrix} \begin{bmatrix} p_u \\ p_a \end{bmatrix} \\ &= dh_q M^{-1}(q) \begin{bmatrix} I_{n-k} \\ \mathbf{0}_{k\times(n-k)} \end{bmatrix} p_u + dh_q M^{-1}(q) \begin{bmatrix} \mathbf{0}_{(n-k)\times k} \\ I_k \end{bmatrix} p_a. \end{aligned}$$

On the constraint manifold, we have $e = \dot{e} = 0$, which means

$$dh_q M^{-1}(q) \begin{bmatrix} \mathbf{0}_{(n-k)\times k} \\ I_k \end{bmatrix} p_a = dh_{p_u} \nabla_{q_u} V(q) - dh_q M^{-1}(q) \begin{bmatrix} I_{n-k} \\ \mathbf{0}_{k\times(n-k)} \end{bmatrix} p_u.$$

Since h is regular and $\nabla_{q_u} M^{-1}(q) = 0$, we have that

$$\operatorname{rank}\left(dh_q M^{-1}(q) \begin{bmatrix} \mathbf{0}_{(n-k)\times k} \\ I_k \end{bmatrix} \right) = k.$$

Solving for p_a gives

$$p_a(q, p_u) = \left(dh_q M^{-1}(q) \begin{bmatrix} \mathbf{0}_{(n-k)\times k} \\ I_k \end{bmatrix} \right)^{-1} \left(dh_{p_u} \nabla_{q_u} V(q) - dh_q M^{-1}(q) \begin{bmatrix} I_{n-k} \\ \mathbf{0}_{k\times(n-k)} \end{bmatrix} p_u \right).$$

This yields a function $p_a(q, p_u)$. However, on Γ we have $q_a = f(q_u, p_u)$, which we use to solve for $p_a = g(q_u, p_u)$. Since q_a and p_a can be computed directly from (q_u, p_u), the dynamics on Γ are parameterized only by $(\dot{q}_u, \dot{p}_u)$. □

Theorem 2.11 shows that, for a particular class of systems and constraints, the dynamics on Γ are entirely described by the $2(n-k)$ unactuated coordinates. This is true regardless of the number of degrees of freedom of the system.

The following corollay applies Theorem 2.11 to systems with only one unactuated coordinate.

Corollary. *Let $\mathscr{H}$ be the system* (2.10) *with degree of underactuation one. Suppose $\mathscr{H}$ satisfies*

Assumption 4. Let $h(q, p_u) = 0$ be a regular VNHC of order $(n-1)$ of the form $h(q, p_u) = q_a - f(q_u, p_u)$, where f is a suitably defined C^2 function. Then $dh_q = \begin{bmatrix} -\partial_{q_u} f & I_{(n-1)} \end{bmatrix}$. Defining $e_1 := (1, 0, \dots, 0)^\mathsf{T} \in \mathbb{R}^n$, the actuated momentum is

$$p_a = -\left(dh_q M^{-1}(q) \begin{bmatrix} \mathbf{0}_{1\times(n-1)} \\ I_{(n-1)} \end{bmatrix} \right)^{-1} \left(\partial_{p_u} f \partial_{q_u} V + dh_q M^{-1}(q) e_1 p_u \right) \Big|_{q_a = f(q_u, p_u)} . \tag{2.16}$$

Since $q_u \in [\mathbb{R}]_{T_u}$ for some $T_u \in]0, \infty]$ and $p_u \in \mathbb{R}$, the orbit $(q_u(t), p_u(t))$ traces out a curve on the constraint manifold $\Gamma \simeq [\mathbb{R}]_{T_u} \times \mathbb{R}$ which we call the (q_u, p_u)-plane.

We conclude this chapter by formalizing the notion of energy injection for VNHCs. To glean some intuition for this idea, suppose our mechanical system satisfies the above corollary so that the constraint manifold Γ is the (q_u, p_u)-plane. If any initial condition of the constrained dynamics converges to the origin, the system must be losing energy because the unactuated momentum p_u is decreasing. Any notion of energy injection must therefore require that the origin of Γ repels all solutions. Furthermore, periodic solutions prevent the system from attaining higher speeds, so the constrained dynamics should not have closed orbits or limit cycles. Finally, we want the unactuated momentum to increase on average, regardless of its initial value. This intuition is generalized to ODEs on manifolds by the following definition.

Definition 2.12. Let $\mathcal{Q}$ be an n-dimensional generalized cylinder. Let $f : \mathcal{Q} \to \mathcal{Q} \times \mathbb{R}^n$ be a smoth vector field and let $D \subset M$ be open. The system described by $\dot{x} = f(x)$ *gains energy on D* if, for all compact sets $K \subset D$ and for almost every initial condition $x(0) \in K$, there exists $T > 0$ such that $x(t) \notin K$ $(\forall t > T)$. The system *loses energy on D* if it gains energy in negative-time.

Any system satisfying Definition 2.12 can have unstable equilibria on D, but not limit cycles nor closed orbits. The next definition ties this notion of energy gain to VNHCs.

Definition 2.13. A regular VNHC $h(q, p) = 0$ with constraint manifold Γ *injects (dissipates) energy on $D \subset \Gamma$* if the constrained dynamics gain (lose) energy everywhere on D, except possibly on a set of measure zero.

2.4 Summary of Results

In this chapter, we developed the framework of virtual nonholonomic constraints for underactuated Hamiltonian mechanical systems. We made the following assumptions:

1. The input matrix $B(q) \equiv B \in \mathbb{R}^{n\times k}$ is constant and full rank.

2. The input matrix has a left-annihilator $B^\perp \in \mathbb{R}^{(n-k)\times n}$.

3. The annihilator matrix $B^\perp$ is right semi-orthogonal.

These assumptions allowed us to define a canonical change of coordinates into the simply actuated coordinates $(q,p) \in \mathcal{Q} \times \mathcal{P}$, where $q = (q_u, q_a)$ and $p = (p_u, p_a)$.

We defined a virtual nonholonomic constraint as a function $h \in C^2(\mathcal{Q} \times \mathcal{P}; \mathbb{R}^k)$ which has no singular points on its constraint manifold

$$\Gamma = \left\{(q,p) \mid h(q,p) = 0, dh_q\dot{q} + dh_p\dot{p} = 0\right\}.$$

We then showed that a VNHC $h : \mathcal{Q} \times \mathcal{P}_u \to \mathbb{R}^k$ is regular if and only if the square matrix

$$\left(dh_q M^{-1}(q) - dh_{p_u}(I_{n-k} \otimes p^\mathsf{T})\nabla_{q_u} M^{-1}(q)\right)\begin{bmatrix}\mathbf{0}_{(n-k)\times k}\\ I_k\end{bmatrix}$$

is invertible on Γ.

To find the explicit equations for constrained dynamics of a regular VNHC, we made the following assumptions:

- The inertia matrix satisfies $\nabla_{q_u} M(q) = \mathbf{0}_{n(n-k)\times n}$.

- On Γ, one can solve for q_a as a function of (q_u, p_u).

If these assumptions hold, one can solve for $p_a = g(q_u, p_u)$ on Γ. The constrained dynamics are then given by $(\dot{q_u}, \dot{p_u})$ subject to $h(q, p_u) = 0$ and $p_a = g(q_u, p_u)$.

Finally, we saw the benefit of using VNHCs is that they reduce the dimensionality of the system from $2n$ equations of motion to $2(n-k)$ equations, which significantly reduces the complexity of analyzing large systems. In particular, if the system has degree of underactuation one, the dynamics reduce to a 2D system on the "(q,p)-plane" $[\mathbb{R}]_T \times \mathbb{R}$.

2.5 Comparison with Existing VNHC Literature

Griffin and Grizzle were the first to define relative degree $\{2, \dots, 2\}$ VNHCs (see [11] and [13]). They required that the first coordinate be unactuated, so Horn et al. [18] extended their work to more general mechanical systems by defining the unactuated coordinate

$q_u = B^\perp q$. These ideas are what inspired us to use simply actuated Hamiltonian systems, which are more suitable for the study of VNHCs than Lagrangian mechanics.

Our definition of a VNHC is more general than that of Griffin and Grizzle. They define a VNHC as a relation $h(q, \sigma_u)$, where σ_u is the Lagrangian mechanics proxy for p_u. Their definition carries an implicit assumption that VNHCs are of relative degree $\{2, \dots, 2\}$, which are what we call regular VNHCs. By contrast, our definition of a VNHC allows for relations $h(q, p)$ that use the full phase. We are the first to distinguish these from regular VNHCs, and to provide the characterization of regularity in Theorem 2.10.

Horn et al. [18] derive the constrained dynamics for VNHCs of the form $h(q, \sigma_u)$. Our derivation of the constrained dynamics in Theorem 2.11 uses the same assumptions they require, with the additional assumption that one can solve for $q_a = f(q_u, p_u)$ on the constraint manifold. While this means Horn et al.'s constrained dynamics hold for a larger class of VNHCs, their derivations are obscured by a complicated change of coordinates when finding the closed form of the dynamics. By making the aforementioned additional assumption, we are instead able to find the constrained dynamics in terms of the unactuated coordinates. This makes our constrained dynamics more physically intuitive, since they describe the behaviour of a specific part of the mechanical system. This additional structure will facilitate our analysis of the energy injection properties of VNHCs across the next two chapters.

Chapter 3

Application of VNHCS: The Variable Length Pendulum

3.1 Motivation

The variable length pendulum (VLP) is a classical underactuated dynamical system which is often used to model the motion of a person on a swing [3, 31]. The VLP also represents the motion of the load at the end of a crane, the (simplified) motion of a gymnast on a bar [32], and the tuned-mass-damper systems which stabilize skyscrapers [33].

The motion of the VLP has been well studied (see for instance [34]), and many control mechanisms exist to stabilize trajectories of the system. While many of these controllers are time-dependent, Xin and Liu [8] offer a time-independent technique to inject energy into the VLP. They design a controller through a technique called *energy shaping* and prove that it stabilizes any desired energy level set. However, their control input depends on a pre-specified target energy and requires knowledge of the current total energy of the VLP. This makes their energy injection mechanism "ad-hoc" in the sense that it is tailored very specifically to the VLP, and is not generalizable to a larger methodology.

It may be better to base the control design on natural biological behaviour. In this chapter we will make use of the general VNHC framework developed in Chapter 2 to add and remove energy from the VLP in a time-independent manner. We'll show that, unlike energy shaping, VNHCs can be used to stabilize energy levels while maintaining the structured motion of a human on a swing.

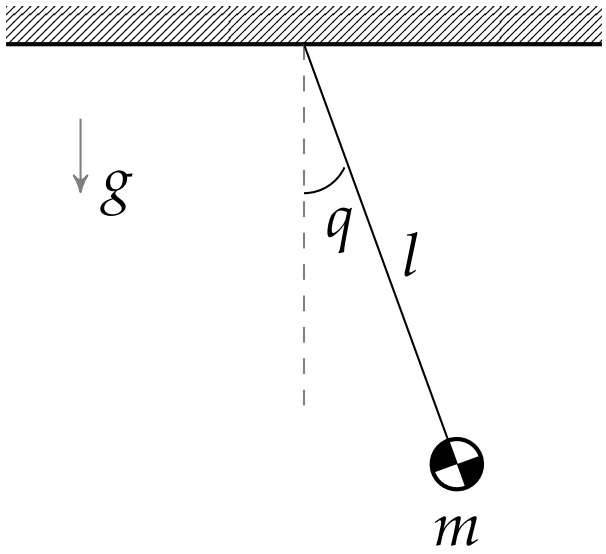

Figure 3.1: The variable length pendulum is a mass attached to the tip of a massless rod which can change length.

3.2 Dynamics of the Variable Length Pendulum

We will model the VLP as a point mass m connected to a fixed pivot by a massless rod of varying length l with angle $q \in \mathbb{S}^1$ from the vertical, as in Figure 3.1. We will ignore any damping and frictional forces in this model. In a realistic VLP, the rod length l varies between some minimum length $\underline{l} \geq 0$ and some maximum length $\bar{l} > \underline{l}$. The configuration of the VLP is the vector $\mathbf{q} := (q, l) \in \mathbb{S}^1 \times [\underline{l}, \bar{l}]$.

Using this configuration, we will compute the Hamiltonian dynamics of the system. The Cartesian position of the mass at the tip of the pendulum is given by $x = (l\sin(q), -l\cos(q))$, while its velocity is $\dot{x} = (\dot{l}\sin(q) + l\cos(q)\dot{q}, -\dot{l}\cos(q) + l\sin(q)\dot{q})$. Computing the kinetic energy T yields

$$T(\mathbf{q}, \dot{\mathbf{q}}) = \frac{1}{2}m\|\dot{x}\|^2 = \frac{1}{2}m\left(\dot{l}^2 + l^2\dot{q}^2\right).$$

The potential energy P with respect to the pivot (under a gravitational acceleration g) is

$$P(\mathbf{q}) = -mgl\cos(q).$$

Collecting the kinetic energy into a quadratic form, we get the Lagrangian

$$\mathscr{L}(\mathbf{q}, \dot{\mathbf{q}}) = \frac{1}{2}\dot{\mathbf{q}}^\mathsf{T} D(\mathbf{q})\dot{\mathbf{q}} - P(\mathbf{q}) = \frac{1}{2}\begin{bmatrix}\dot{q} & \dot{l}\end{bmatrix}\begin{bmatrix}ml^2 & 0 \\ 0 & m\end{bmatrix}\begin{bmatrix}\dot{q} \\ \dot{l}\end{bmatrix} + mgl\cos(q).$$

Computing the conjugate of momenta to $\mathbf{q}$, we get

$$\mathbf{p} := \begin{bmatrix} p \\ p_l \end{bmatrix} = \begin{bmatrix} ml^2\dot{q} \\ m\dot{l} \end{bmatrix}.$$

Performing the Legendre transform on $\mathscr{L}$ and setting $M(\mathbf{q}) := D(\mathbf{q})$, $V(\mathbf{q}) := P(\mathbf{q})$, we get the Hamiltonian (2.11) whose dynamics (2.12) resolve to

$$\mathscr{H} = \frac{1}{2}\begin{bmatrix} p & p_l \end{bmatrix}\begin{bmatrix} \frac{1}{ml^2} & 0 \\ 0 & \frac{1}{m} \end{bmatrix}\begin{bmatrix} p \\ p_l \end{bmatrix} - mgl\cos(q), \tag{3.1}$$

$$\begin{cases} \dot{q} = \frac{p}{ml^2}, \\ \dot{l} = \frac{p_l}{m}, \\ \dot{p} = -mgl\sin(q), \\ \dot{p}_l = \frac{p^2}{ml^3} + mg\cos(q) + \tau. \end{cases}$$

The control input is a force $\tau \in \mathbb{R}$ affecting the dynamics of p_l, acting collinearly with the rod. We assume the force does not affect the dynamics of p in any way - that is, the control input cannot enact any lateral force on the pendulum. This makes the VLP into an underactuated mechanical system with degree of underactuation one. It is also a useful assumption because it means $(\mathbf{q}, \mathbf{p})$ are simply actuated coordinates, which allows us to apply the theory of VNHCs we developed in Chapter 2.

Let us define the VNHC $l = L(q, p)$, by which we mean we are actually defining the VNHC $h(\mathbf{q}, \mathbf{p}) = l - L(q, p) = 0$ of order 1. The VLP satisfies $\nabla_q M^{-1}(\mathbf{q}) = \mathbf{0}_{2\times 2}$. By Theorem 2.10, $h(\mathbf{q}, \mathbf{p})$ is a regular VNHC whenever $L(q, p)$ is C^2 because

$$dh_{\mathbf{q}} M^{-1}(\mathbf{q}) B = \begin{bmatrix} -\frac{\partial L}{\partial q} & 1 \end{bmatrix}\begin{bmatrix} \frac{1}{ml^2} & 0 \\ 0 & \frac{1}{m} \end{bmatrix}\begin{bmatrix} 0 \\ 1 \end{bmatrix} = \frac{1}{m},$$

is always full rank. The constraint manifold Γ is diffeomorphic to $\mathbb{S}^1 \times \mathbb{R}$, which is parameterized by the unactuated phase (q, p). By Theorem 2.11, the constrained dynamics are described entirely by $(\dot{q}, \dot{p})$ with l replaced by $L(q, p)$:

$$\begin{cases} \dot{q} = \frac{p}{mL^2}, \\ \dot{p} = -mgL\sin(q). \end{cases} \tag{3.2}$$

Note that we suppress the function notation of $L(q, p)$ for clarity.

The total mechanical energy of the system restricted to the constraint manifold is

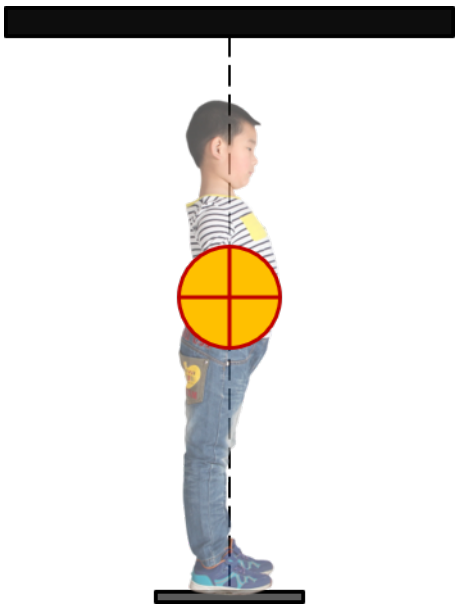

(A) A person standing on a swing has their center of mass close to the pivot.

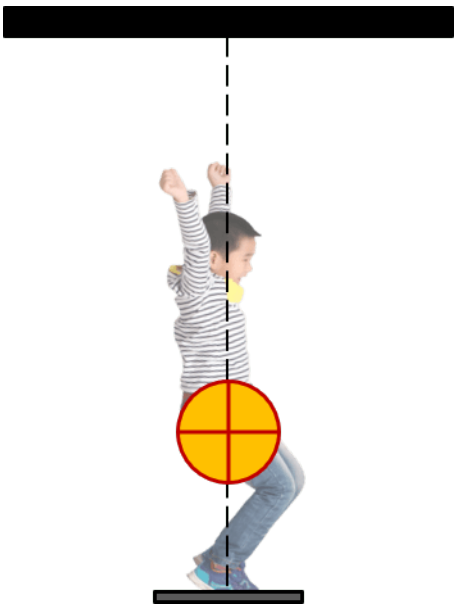

(B) When a person squats on a swing, their center of mass extends away from the pivot.

Figure 3.2: The VLP representation of a person on a standing swing.

given by (3.3), where $L(q,p)$ and $\dot{L}(q,p)$ are known.

$$E(q,p) = \frac{1}{2}\frac{p^2}{mL^2} + \frac{1}{2}\dot{L}^2 - mgL\cos(q). \tag{3.3}$$

In the rest of this chapter, we will derive a C^2 function $L(q,p)$ based on natural human motion. This function will produce constrained dynamics that inject energy into the VLP.

3.3 The VLP Constraint

To motivate why a VNHC could inject energy into the VLP in a human-like manner, we will examine a person standing on a swing. As can be seen in Figure 3.2, a person's center of mass moves closer to the swing's pivot when they stand, and moves away from the pivot when they squat. This is equivalent to the VLP model from Figure 3.1, where standing and squatting correspond to shortening and lengthening the pendulum respectively.

The action of regulating pendulum length to inject energy into the VLP is known as "pumping". Piccoli and Kulkarni [3] asked whether the pumping strategy performed by children is time-optimal, assuming they can squat or stand instantaneously. Indeed,

they discovered that children increase the height of their swing as fast as is physically possible.

A child's optimal pumping strategy is the following: they stand at the lowest point of the swing, and squat at the highest point. Looking at the VLP representation, the pendulum shortens at the bottom of the swing, and lengthens at the top. For an intuitive explanation, conservation of angular momentum indicates that shortening the pendulum at the bottom forces the mass to gain speed to compensate for the reduced length [31]. Energy is not conserved in this process, so the pendulum gains kinetic energy and reaches a higher point at the peak of its swing. Lengthening the pendulum when it reaches this peak means gravity imparts a larger angular momentum to the mass by the time it reaches the bottom of its swing, which in turn is converted to a higher velocity when the pendulum is shortened. By alternating these processes, the pendulum experiences an average net gain in rotational energy.

Notice that the child's pumping strategy requires knowledge of when the system is at the "bottom" or "top" of the swing. Since being at the bottom is equivalent to having angle $q = 0$ and being at the top is equivalent to having momentum $p = 0$, a controller based on this strategy will necessarily involve the full unactuated phase (q, p). This is why we must use VNHCs instead of other methods (such as VHCs) to perform this maneuver.

The time-optimal controller from [3] is, in our notation,

$$L^\star(q, p) := -\operatorname{sgn}(qp),$$

which is a piecewise-continuous controller that varies between ± 1. We could set our constraint to be $l = L^\star(q, p)$, but this is not a VNHC because it is not C^2. Additionally, it would force us to assume that $l \in \{-1, 0, 1\}$ and that one can switch l instantaneously. Since we need to enforce the constraint using the physical input τ (which would ideally emulate realistic human motion), we cannot use $L^\star$ as our VNHC. We will instead find an alternate representation of $L^\star$ which can be converted into a VNHC, and which allows $l \in [\underline{l}, \bar{l}]$.

Figure 3.3a displays $L^\star(q, p)$ on the (q, p)-plane. Note that the length remains constant inside each quadrant and changes only when it crosses one of the axes. Using this fact, we can redefine the time-optimal pumping strategy as a function of $\theta := \arctan_2(p, q)$. Abusing notation, we denote this by $L^\star(\theta)$, which is defined in (3.4). Figure 3.3b shows

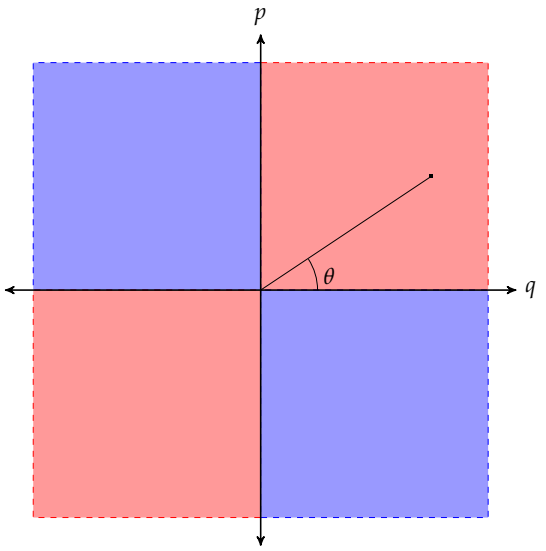

(A) The time-optimal controller $L^\star(q,p)$ mapped onto the (q,p)-plane. Here, red corresponds to $L^\star(q,p) = -1$ and blue to $L^\star(q,p) = 1$.

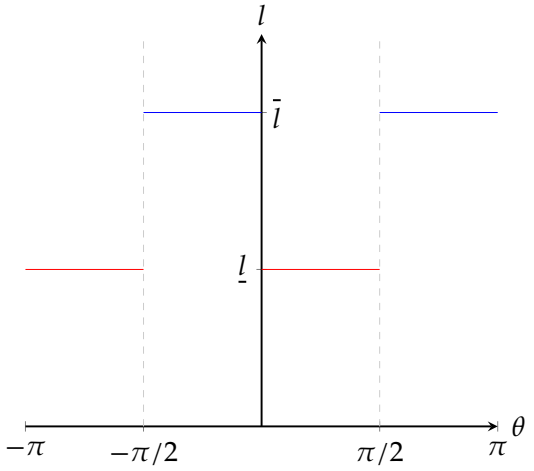

(B) The time-optimal controller converted to the alternate representation $L^\star(\theta)$.

Figure 3.3: The time-optimal controller for a standing swing as derived by [3]. Red corresponds to standing, blue to squatting, and $\theta := \arctan_2(p,q)$ is the angle of the VLP phase in the (q,p)-plane.

the graph of $L^\star(\theta)$, where now the length varies between $[\underline{l}, \bar{l}]$ rather than $\{-1, 0, 1\}$.

$$L^\star(\theta) := \begin{cases} \bar{l} & \theta \in [-\frac{\pi}{2}, 0[\cup [\frac{\pi}{2}, \pi[\\ \underline{l} & \theta \in [-\pi, -\frac{\pi}{2}[\cup [0, \frac{\pi}{2}[. \end{cases} \tag{3.4}$$

We now define a continuous function which approximates $L^\star(\theta)$. Let $\Delta l := (\bar{l} - \underline{l})/2$ and $l_{\text{avg}} := (\bar{l} + \underline{l})/2$. Let $T \in]0, \frac{\pi}{2}]$ be a parameter of our choosing. By intelligently attaching sinusoids of frequency $\omega = \frac{\pi}{T}$ to $L^\star(\theta)$ (see Figure 3.4), we get a family of C^1 constraints $L_T(\theta)$ parameterized by T:

$$L_T(\theta) := \begin{cases} \bar{l} & \theta \in \left[-\frac{\pi}{2} + \frac{T}{2}, -\frac{T}{2}\right] \cup \left[\frac{\pi}{2} + \frac{T}{2}, \pi - \frac{T}{2}\right] \\ \underline{l} & \theta \in \left[-\pi + \frac{T}{2}, -\frac{\pi}{2} - \frac{T}{2}\right] \cup \left[\frac{T}{2}, \frac{\pi}{2} - \frac{T}{2}\right] \\ -\Delta l \sin(\omega(\theta + \pi)) + l_{\text{avg}} & \theta \in \left[-\pi, -\pi + \frac{T}{2}\right] \\ -\Delta l \sin(\omega\theta) + l_{\text{avg}} & \theta \in [-\frac{T}{2}, \frac{T}{2}] \\ \Delta l \sin(\omega(\theta - a)) + l_{\text{avg}} & \theta \in \left[a - \frac{T}{2}, a + \frac{T}{2}\right] \text{ for } a \in \left\{-\frac{\pi}{2}, \frac{\pi}{2}\right\} \\ -\Delta l \sin(\omega(\theta - \pi)) & \theta \in \left[\pi - \frac{T}{2}, \pi\right]. \end{cases} \tag{3.5}$$

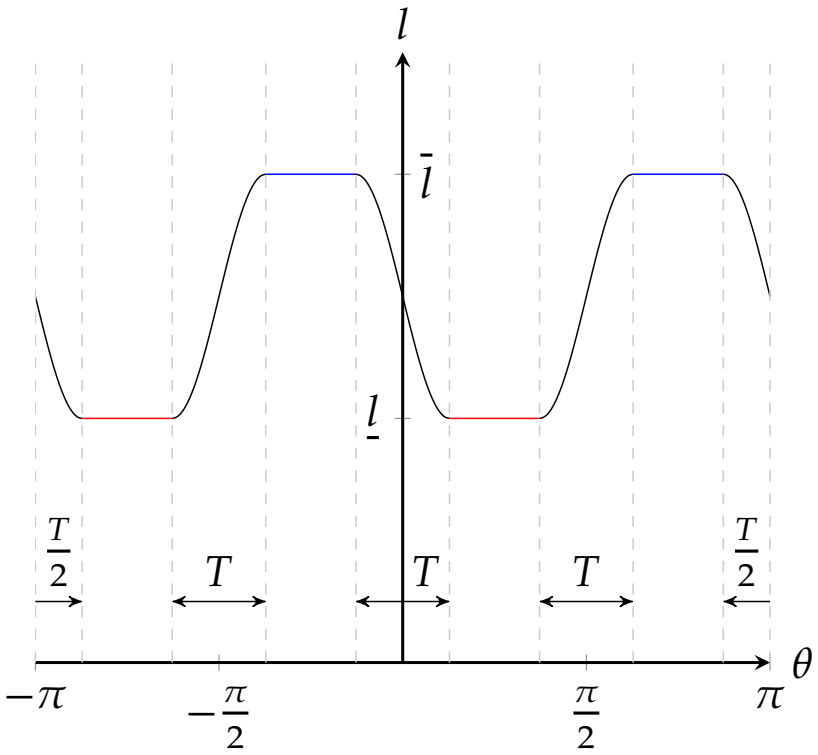

Figure 3.4: The continuous VLP constraint $l = L_T(\theta)$.

This family of constraints approximates $L^\star(\theta)$ because

$$\lim_{T\to 0} L_T(\theta) = L^\star(\theta).$$

Unfortunately, while $L_T(\theta)$ is continuously-differentiable, it is not twice-differentiable for most values of T. If we wish to use it as a VNHC, we must ensure that either the generalized forces τ acting on p_l can be discontinuous (which is certainly achievable by humans), or we must find a value of T where this constraint is at least C^2. Thankfully, setting $T = \frac{\pi}{2}$ yields the smooth function $L_{\frac{\pi}{2}}(\theta)$, which can be simplified from (3.5) into

$$L_{\frac{\pi}{2}}(\theta) = -\Delta l \sin(2\theta) + l_{\text{avg}}. \tag{3.6}$$

This smooth constraint is plotted for demonstration in Figure 3.5.

Because $L_{\frac{\pi}{2}}(\theta)$ is smooth and it approximates $L^\star(\theta)$, we set our VNHC to be

$$h(\mathbf{q},\mathbf{p}) = l - L_{\frac{\pi}{2}}\left(\theta(q,p)\right).$$

We can now prove our VNHC injects energy into the VLP. As part of the proof, we will require the following lemma.

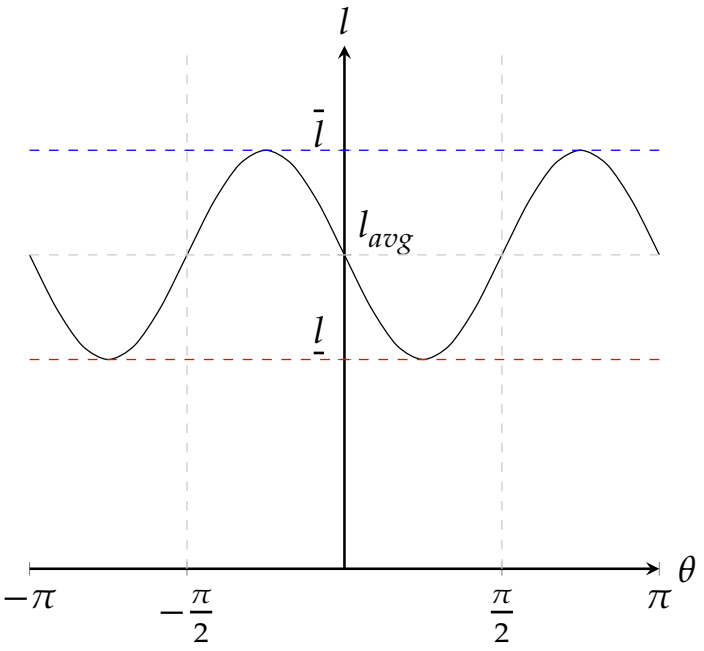

Figure 3.5: The smoothed VLP constraint $l = L_{\frac{\pi}{2}}(\theta)$.

Lemma 3.1. *For any $x, y \in \mathbb{R}$,*

$$\operatorname{sgn}\left(x^3 - y^3\right) = \operatorname{sgn}\left(x - y\right).$$

Proof. Observe that $x^3 - y^3 = (x - y)(x^2 + xy + y^2)$. The inequality $x^2 + xy + y^2 \geq 0$ holds because

$$x^2 + xy + y^2 = \left(x + \frac{y}{2}\right)^2 + \frac{3y^2}{4} \geq 0,$$

which proves the lemma. □

We will show that the constrained dynamics trace out a curve on the (q, p)-plane which is diverging from the origin. This implies that the momentum p is increasing in magnitude whenever the curve hits the p-axis, which in turn means the VLP is gaining energy on average.

Theorem 3.2. *Define $\theta := \arctan_2(p, q)$. Let $L : \mathbb{S}^1 \to [\underline{l}, \bar{l}]$ be a C^2 function of θ. A regular VNHC of the form $h(\mathbf{q}, \mathbf{p}) = l - L(\theta)$ for the VLP injects energy on the constraint manifold $\Gamma \simeq \mathbb{S}^1 \times \mathbb{R}$ if there exists $l_{avg} \in [\underline{l}, \bar{l}]$ such that*

$$\left(l_{avg} - L(\theta)\right) sin(2\theta) \geq 0 \ \forall \theta \in \mathbb{S}^1, \tag{3.7}$$

with the property that the inequality is strict except at $\theta \in \left\{0, \frac{\pi}{2}, \pi, \frac{3\pi}{2}\right\}$. *If instead*

$$\left(l_{avg} - L(\theta)\right) sin(2\theta) \leq 0 \ \forall \theta \in \mathbb{S}^1,$$

the VNHC dissipates energy on Γ.

Proof. Since a system that gains energy per Definition 2.12 cannot have stable equilibria, we will first show that, under the given assumptions, the origin of the constrained dynamics (3.2) is a repeller. For that we consider the negative time system obtained from (3.2) by reversing the sign of the vector field:

$$\begin{cases} \dot{q} = -\frac{p}{mL^2}, \\ \dot{p} = mgL\sin(q). \end{cases} \tag{3.8}$$

The state space of (3.8) is $\mathbb{S}^1 \times \mathbb{R}$, and the system has two equilibria, $(q,p) = (0,0)$ and $(q,p) = (\pi, 0)$. We need to show that the equilibrium $(q,p) = (0,0)$ is asymptotically stable for (3.8).

Consider the Lyapunov function candidate

$$E_{\text{avg}}(q,p) := \frac{1}{2}\frac{p^2}{ml_{\text{avg}}^2} + mgl_{\text{avg}}(1 - \cos(q)),$$

which corresponds to the energy of VLP when the pendulum length is fixed at l_{avg}. The function E_{avg} is positive definite at $(0,0)$, and has compact sublevel sets on $\mathbb{S}^1 \times \mathbb{R}$. The derivative of E_{avg} along (3.8) is

$$\dot{E}_{\text{avg}} = \frac{g\sin(q)p\left(L(\theta)^3 - l_{\text{avg}}^3\right)}{l_{\text{avg}}^2 L(\theta)^2}. \tag{3.9}$$

It is easy to show that

$$\operatorname{sgn}\left(\sin(q)p\right) = \operatorname{sgn}\left(\sin(2\theta)\right).$$

Furthermore, by Lemma 3.1 we have

$$\operatorname{sgn}\left(L(\theta)^3 - l_{\text{avg}}^3\right) = \operatorname{sgn}\left(L(\theta) - l_{\text{avg}}\right),$$

and therefore,

$$\begin{aligned}\operatorname{sgn}\left(\dot{E}_{\text{avg}}\right) &= \operatorname{sgn}\left(\sin(q)p\left(L(\theta)^3 - l_{\text{avg}}^3\right)\right)\\ &= \operatorname{sgn}\left(\sin(2\theta)\left(L(\theta) - l_{\text{avg}}\right)\right)\\ &= -\operatorname{sgn}\left(\left(l_{\text{avg}} - L(\theta)\right)\sin(2\theta)\right)\\ &\leq 0 \text{ (by assumption).}\end{aligned} \tag{3.10}$$

We have thus shown that $\dot{E}_{\text{avg}} \leq 0$, and therefore the equilibrium $(q,p) = (0,0)$ is stable for (3.8). We now apply the Krasovskii-LaSalle invariance principle, and consider the largest subset of $Z = \left\{(q,p) \in \mathbb{S}^1 \times \mathbb{R} \mid \dot{E}_{\text{avg}}(q,p) = 0\right\}$. We see from (3.9) that $\dot{E}_{\text{avg}}(q,p)$ is zero when $p = 0$, $\sin(q) = 0$, or $L(\theta) = l_{\text{avg}}$. This latter condition by assumption is met when $\theta \in \{0, \pi/2, \pi, 3\pi/2\}$, or equivalently when either $q = 0$ or $p = 0$. All in all, we have that

$$Z = \left\{(q,p) \in \mathbb{S}^1 \times \mathbb{R} \mid q = 0\right\} \cup \left\{(q,p) \in \mathbb{S}^1 \times \mathbb{R} \mid p = 0\right\}.$$

It is easily seen that the largest invariant subset of Z is the union of the two equilibria

$$\Omega = \{(0,0)\} \cup \{(\pi,0)\}.$$

Since all sublevel sets of E_{avg} are compact, the Krasovskii-LaSalle invariance principle implies that the set Ω is globally attractive [35]. Since the two equilibria are isolated, and since $(q,p) = (0,0)$ is stable, we deduce that the equilibrium $(q,p) = (0,0)$ is asymptotically stable for the negative time system (3.8), and thus it is a repeller for the constrained dynamics in (3.2).

We now prove that almost all solutions of the reduced dynamics (3.2) escape compact sets in finite time, *i.e.*,, that for each compact subset K of $\mathbb{S}^1 \times \mathbb{R}$, and for almost every condition $(q_0, p_0) \in K$, there exists $T > 0$ such that $(q(t), p(t)) \notin K$ for all $t > T$, where $(q(t), p(t))$ denotes the solution of (3.2) with $(q(0), p(0)) = (q_0, p_0)$. In what follows, we denote by $x = (q,p)$ the state of the reduced dynamics (3.2). Also, we denote by Π^+ the stable manifold of the equilibrium $(\pi, 0)$ for system (3.2), defined as

$$\Pi^+ := \left\{x(0) \in \mathbb{S}^1 \times \mathbb{R} \mid \lim_{t\to\infty} x(t) = (\pi,0)\right\}.$$

The linearization of system (3.2) at the equilibrium $(\pi, 0)$ has a system matrix given by

$$\begin{bmatrix} 0 & -\frac{1}{mL(0)^2} \\ -mgL(0) & 0 \end{bmatrix}, \tag{3.11}$$

whose spectrum is $\{\pm\sqrt{g/L(0)}\}$. Since one eigenvalue of (3.11) is positive and one is negative, the stable manifold theorem implies that the stable manifold Π^+ is a one-dimensional immersed submanifold of $\mathbb{S}^1 \times \mathbb{R}$, and thus is a set of measure zero [36].

Let $K \subset \mathbb{S}^1 \times \mathbb{R}$ be an arbitrary compact set and let $x(0) \in K \setminus \left(\Pi^+ \cup \{(0,0)\}\right)$. Since $x(0) \notin \Pi^+$, we have that

$$x(t) \nrightarrow_{t\to\infty} (\pi, 0). \tag{3.12}$$

Suppose, by way of contradiction, that for each $T > 0$ there exists $t' > T$ such that $x(t') \in K$. Letting

$$k := \max_{x\in K} E_{\text{avg}}(x),$$

and $E_k = \{x \mid E_{\text{avg}}(x) \leq k\}$, we have that $K \subset E_k$, and thus $x(t') \in E_k$. We have shown earlier that the function E_{avg} is nonincreasing along solutions of (3.8), which implies that $E_{\text{avg}}(x(t))$ is nondecreasing for solutions of the reduced dynamics (3.2), and therefore the half orbit $x([0, t'])$ is contained fully within E_k. In particular, $x(T) \in E_k$. Since this is true for each $T > 0$, we deduce that $x(t) \in E_k$ for all $t \in [0, \infty[$. Since E_k is compact, $x(t)$ has a positive limit set in E_k which, by the Poincaré-Bendixson theorem, is either an equilibrium or a closed orbit [37]. We will show this positive limit set must be an equilibrium and thereby reach a contradiction.

In order to rule out closed orbits, suppose that the reduced dynamics (3.2) have a periodic solution $z(t)$. Since $E_{\text{avg}}(z(t))$ is nondecreasing and $z(t)$ is periodic, it must be that $E_{\text{avg}}(z(t))$ is constant, or $\dot{E}_{\text{avg}}(z(t)) \equiv 0$. We have shown earlier that[1]

$$\left\{x \mid \dot{E}_{\text{avg}}(x) = 0\right\} = \{(q,p) \mid q = 0\} \cup \{(q,p) \mid p = 0\},$$

and the only invariant subset of this set is the union of two disjoint equilibria. Since the orbit $z(\mathbb{R})$ is an invariant set which is connected, $z(\mathbb{R})$ must be an equilibrium and cannot be a nontrivial closed orbit.

Returning to the Poincaré-Bendixson theorem, the positive limit set of $x(t)$ must be an equilibrium and, by (3.12), this equilibrium must be $(0,0)$. Since we have chosen $x(0) \neq (0,0)$, and since $(q,p) = (0,0)$ is a repeller, $x(t)$ cannot converge to $(0,0)$, which gives a contradiction.

We conclude that the VNHC injects energy into the VLP on $\mathbb{S}^1 \times \mathbb{R}$. By flipping the inequality of (3.7) we find the VLP is gaining energy in negative-time, so the VNHC is dissipating energy. □

[1] We have shown it for the negative time system (3.8), but changing the sign of the vector field does not change the set where $\dot{E}_{\text{avg}} = 0$ nor the invariant sets.

Corollary. *Recall that*

$$L_{\frac{\pi}{2}}(\theta) := -\Delta l \sin(2\theta) + l_{avg},$$

and define

$$L^{-}_{\frac{\pi}{2}}(\theta) := \Delta l \sin(2\theta) + l_{avg}.$$

The VNHC $l = L_{\frac{\pi}{2}}(\theta)$ injects energy into the VLP, while $l = L^{-}_{\frac{\pi}{2}}(\theta)$ dissipates energy.

Proof. Both VNHCs satisfy Theorem 3.2 because

$$\left(l_{\text{avg}} - L_{\frac{\pi}{2}}(\theta)\right)\sin(2\theta) = \Delta l \sin^2(2\theta) \geq 0,$$

and

$$\left(l_{\text{avg}} - L^{-}_{\frac{\pi}{2}}(\theta)\right)\sin(2\theta) = -\Delta l \sin^2(2\theta) \leq 0,$$

where the inequalities are strict everywhere except the coordinate axes. □

Remark. Theorem 3.2 not only guarantees that our VNHC only injects energy, but that the lower equilibrium is a repeller. If the VLP is initialized at the origin, any slight push along q will allow it to start gaining energy.

The class of VNHCs which satisfies Theorem 3.2 is illustrated graphically in Figure 3.6. To stabilize specific energy level sets, one simple approach is to switch between injection and dissipation VNHCs when the momentum p reaches a pre-determined value at the bottom of the swing. For the VNHCs we designed in this chapter, this means toggling between $L_{\frac{\pi}{2}}(\theta)$ and $L^{-}_{\frac{\pi}{2}}(\theta)$, with some hysteresis to avoid infinite switching.

Theorem 3.2 provides an alternate explanation for why the optimal pumping strategy $L^{\star}(\theta)$ works so well at injecting energy: it maximizes the derivative of E_{avg} under the restriction $l \in [\underline{l}, \bar{l}]$, so that the orbit in the (q,p)-plane diverges from the origin as fast as possible.

Let us define $(L^{\star})^{-}(\theta)$ by swapping the order of $\underline{l}$ and $\bar{l}$ in $L^{\star}(\theta)$:

$$(L^{\star})^{-}(\theta) := \begin{cases} \underline{l} & \theta \in [-\frac{\pi}{2}, 0[\cup [\frac{\pi}{2}, \pi[\\ \bar{l} & \theta \in [-\pi, -\frac{\pi}{2}[\cup [0, \frac{\pi}{2}[. \end{cases}$$

Since this function *minimizes* the derivative of E_{avg} under the restriction $l \in [\underline{l}, \bar{l}]$, one might predict that $(L^{\star})^{-}(\theta)$ is the optimal energy dissipation strategy for the VLP. This is, in fact, true. Piccoli and Kulkarni [3] showed that squatting at the lowest point of a swing and standing at the highest (instead of standing and squatting, respectively) produces the time-optimal trajectory for *stopping* a standing swing.

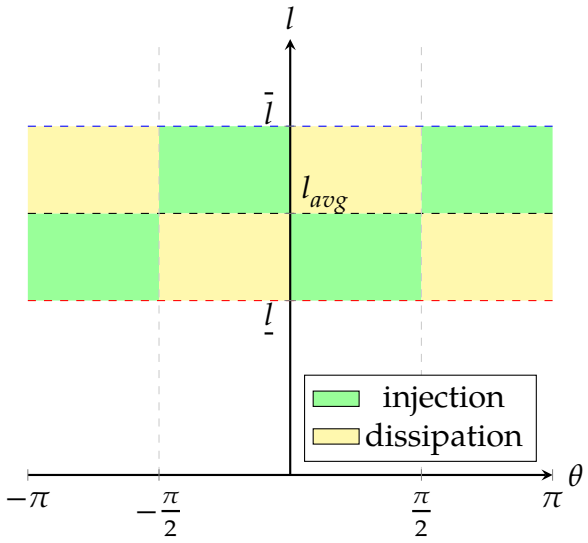

Figure 3.6: Any VNHC of the form $l = L(\theta)$ where $L(\theta)$ is entirely contained within the green (yellow) regions will inject (dissipate) energy.

All together, the theory developed in this chapter shows that VNHCs can replicate the time-optimal pumping/dissipation strategies performed by humans on swings. Furthermore, we see that VNHCs are a powerful tool for creating simple energy stabilization techniques based on natural human motion.

3.4 Simulation Results

In this section, we compare the energy injection properties of our smooth VNHC $L_{\frac{\pi}{2}}(\theta)$, the time-optimal VNHC $L^\star(\theta)$ from Equation (3.4), and the differentiable VNHC $L_T(\theta)$ from Equation (3.5) with $T = 0.01$. To do this comparison, we simulate an adult Estonian performing a Kiiking routine.

The average weight of a 25 year old Estonian man is 80.17kg [38], so we set the VLP mass m to this value. To find our upper and lower bounds on length, we first need to choose the size of a swing. The common model of a Kiiking swing is between $3-4$m tall [39], so we take the length to be 3m. The average 25 year old Estonian is 1.8m tall [38], and we assume their squat height is half that at 0.9m tall. We further assume that their center of mass (COM) is always located at half their current height, which means their standing COM is 0.9m from the ground while their squatting COM is 0.45m from the ground. This means the distance from their standing COM to the pivot is 2.1m, while the distance from their squatting COM to the pivot is 2.55m. Hence, we set $\underline{l} = 2.1$ and $\bar{l} = 2.55$. We initialize a VLP with these parameters at $(q, p) = \left(\frac{\pi}{32}, 0\right)$ and plot the

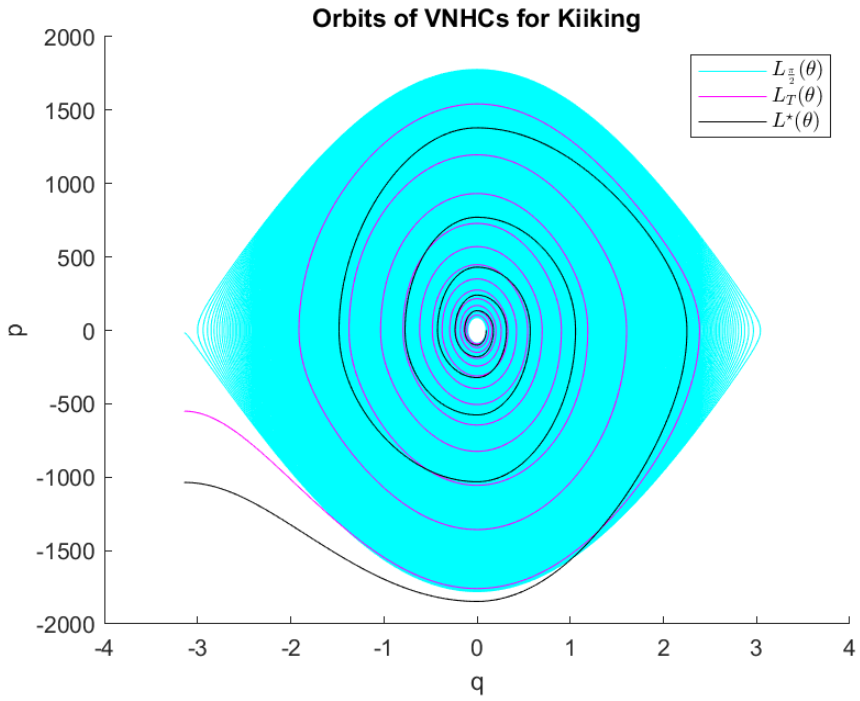

Figure 3.7: The orbits of the time-optimal controller $L^\star(\theta)$ (black), the differentiable controller $L_T(\theta)$ (magenta), and the smooth VNHC $L_{\frac{\pi}{2}}(\theta)$ (cyan) employed by a 25 year old Estonian male on a 3m tall Kiiking swing. All the controllers are initialized at $q(0) = \frac{\pi}{32}$, and they each steadily gain energy until they reach a rotation.

resulting orbits in Figure 3.7.

The time-optimal controller reaches a rotation within 18 seconds, the differentiable controller rotates in 41 seconds, and the smooth VNHC takes 4691 seconds (78 minutes). Despite the fact that the smooth VNHC is several orders of magnitude slower than the other controllers, it still succeeds at injecting energy into the system. This is especially clear when looking at Figure 3.8, which shows the smooth VNHC steadily gaining energy over time.

Overall, this simulation confirms that VNHCs are capable of injecting energy into the VLP. Moreover, if one can use the differentiable controller $L_T(\theta)$ (which humans certainly can), one is able to approximate the time-optimal controller arbitrarily well. We conclude that VNHCs are powerful tools for injecting energy into the VLP while maintaining the natural structure of human motion.

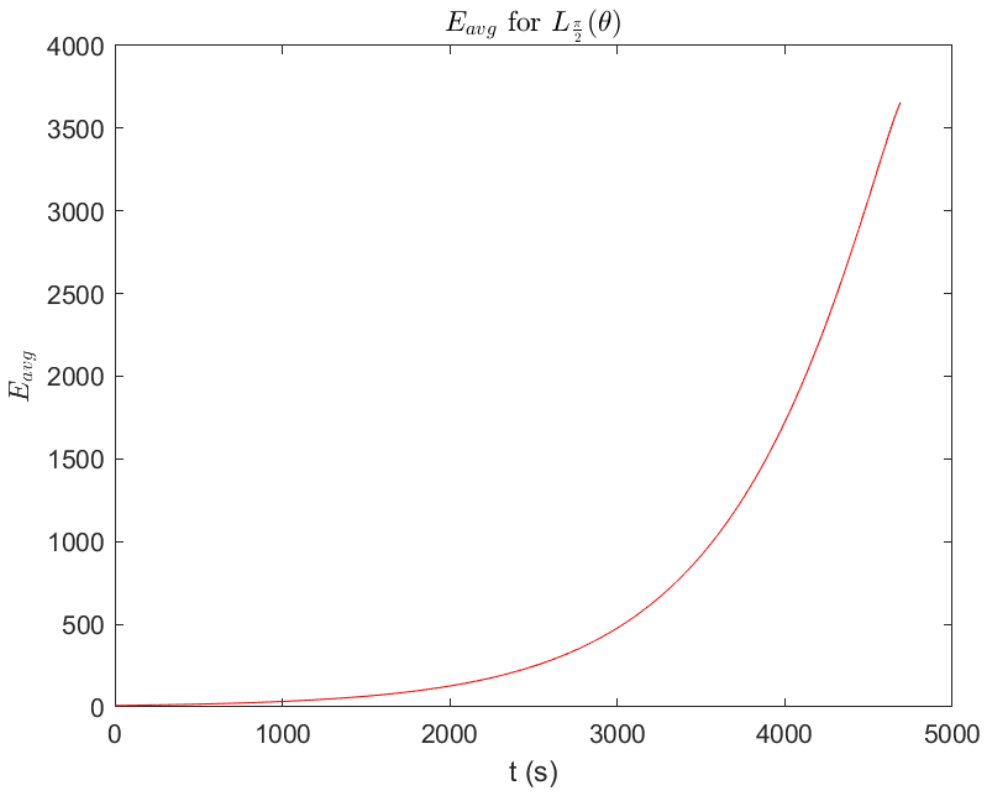

Figure 3.8: The energy $E_{\text{avg}}(q,p)$ of a 25 year old Estonian male on a 3m tall Kiiking swing who employs the smooth VNHC $L_{\frac{\pi}{2}}(\theta)$.

Chapter 4

Application of VNHCs: The Acrobot

4.1 Motivation

The acrobot is a two-link pendulum, actuated at the center joint (as in Figure 4.1). Since its first description in 1990 [40], the acrobot has become a benchmark problem in control theory; it is an underactuated mechanical system which produces complex nonlinear motion from an easy-to-describe model. The acrobot models a gymnast on a bar, since it represents a torso (top link) and legs (bottom link) with motion generated by the swinging of the legs at the hips. It is also one of the simplest models for a biped walking robot [41].

Controlling the acrobot is a nontrivial task because it is not feedback linearizable [40]. Several researchers have studied the swing-up problem of driving the acrobot to its equilibrium point above the bar using partial feedback linearization [42], energy-based control [9, 43], and through studying human motion [10, 44].

In gymnastics terminology, a "giant" is the motion a gymnast performs to achieve full rotations around the bar [45]. We are interested in using VNHCs to generate giant motion, with the aim of stabilizing desired energy levels. The control of giant motion for the acrobot has been studied in [10, 46], and some authors have used virtual holonomic constraints to achieve this behaviour [1, 47, 48]. However, these controllers are neither intuitive nor easy to design: [48] defines a constraint by inverting a trajectory in time onto the state space; [47] requires a cascade controller to stabilize both a constraint and a desired limit cycle in the state space; and [1] enforces the giant by adding an extra state to estimate velocity, which increases the dimensionality of the problem in a crude approach to using VNHCs.

In this chapter we will design a physically-intuitive VNHC which generates giant motion and prove the acrobot gains energy. In the process of completing this proof,

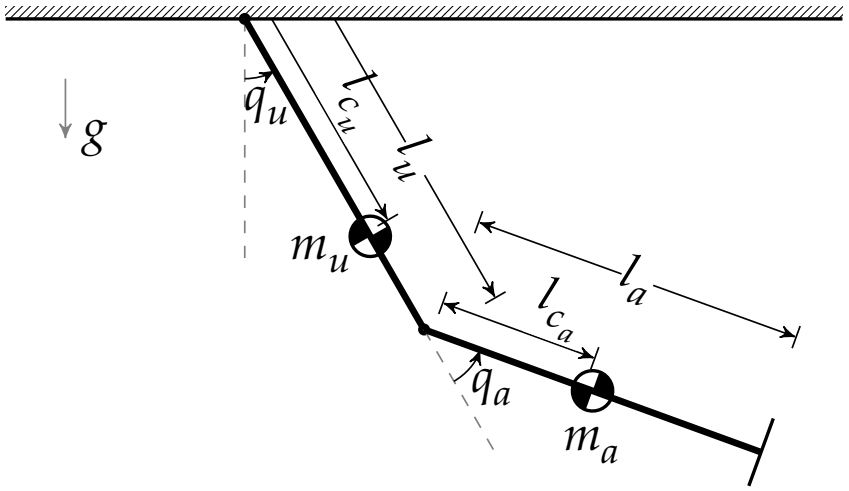

Figure 4.1: The general acrobot model, represented by two weighted rods differing in both length and mass.

we will arrive at a promising method which might one day be useful for generating energy-injecting VNHCs on arbitrary mechanical systems.

4.2 Dynamics of the Acrobot

Suppose we are given an acrobot as in Figure 4.1 modelling a gymnast hanging on a horizontal bar, where the "torso" has moment of inertia J_u and the "leg" has moment of inertia J_a (each with respect to their own center of mass). Let $q_u \in \mathbb{S}^1$ be the shoulder angle and $q_a \in \mathbb{S}^1$ be the hip angle, where only q_a is actuated. Collecting them together provides the configuration $q = (q_u, q_a) \in \mathbb{S}^1 \times \mathbb{S}^1$. The acrobot has inertia matrix D, potential function P (with respect to the horizontal bar), and input matrix B given as follows [1]:

$$D(q) = \begin{bmatrix} m_a l_u^2 + 2m_a \cos(q_a) l_u l_{c_a} + m_a l_{c_a}^2 + m_u l_{c_u}^2 + J_u + J_a & m_a l_{c_a}^2 + m_a l_u l_{c_a} \cos(q_a) + J_a \\ m_a l_{c_a}^2 + m_a l_u l_{c_a} \cos(q_a) + J_a & m_a l_{c_a}^2 + J_a \end{bmatrix}, \tag{4.1}$$

$$P(q) = g\left(m_a l_{c_a}(1 - \cos(q_u + q_a)) + (m_a l_u + m_u l_{c_u})(1 - \cos(q_u))\right), \tag{4.2}$$

$$B(q) = \begin{bmatrix} 0 \\ 1 \end{bmatrix}. \tag{4.3}$$

While this is the most general representation of an acrobot, the dynamics are unwieldy. To make rigorous analysis of these dynamics more tractable, we begin by assuming the acrobot is comprised of two massless rods of equal length l, with equal

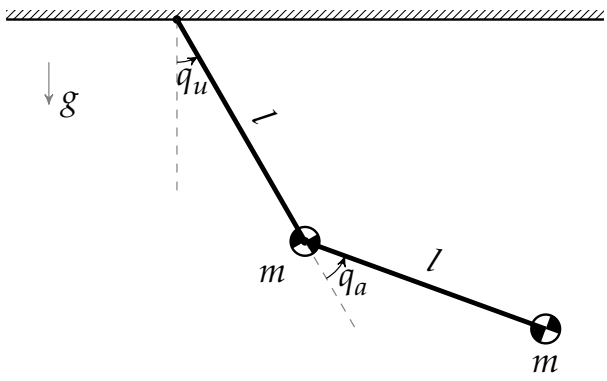

Figure 4.2: A simple acrobot has massless rods of equal length l and equal masses m at the tips.

point masses m at the tips. We call this a *simple* acrobot, which is displayed in Figure 4.2. We will also ignore any frictional forces at both the hip and shoulder joints. Finally, it is important to note that a real gymnast cannot swing their legs in full circles, though they are usually flexible enough to raise them parallel to the floor; for this reason, we assume that $q_a \in [-Q_a, Q_a]$ where $Q_a \in [\frac{\pi}{2}, \pi[$.

Since we are now working with a simple acrobot, we have $l_{c_u} = l_{c_a} = l_u = l_a = l$ and $m_u = m_a = m$. On top of this, the moments of inertia J_u and J_a of the rods vanish. Reducing (4.1)-4.2 yields the simplified inertia matrix D_s and potential function P_s, where

$$D_s(q) = \begin{bmatrix} ml^2\left(3 + 2\cos(q_a)\right) & ml^2\left(1 + \cos(q_a)\right) \\ ml^2\left(1 + \cos(q_a)\right) & ml^2 \end{bmatrix}, \tag{4.4}$$

$$P_s(q) = -mgl\left(2\cos(q_u) + \cos(q_u + q_a)\right). \tag{4.5}$$

Notation. For shorthand, we write $c_u := \cos(q_u)$, $c_a := \cos(q_a)$, and $c_{ua} := \cos(q_u + q_a)$. Likewise, $s_u := \sin(q_u)$, $s_a := \sin(q_a)$, and $s_{ua} := \sin(q_u + q_a)$.

Defining $M(q) := D_s(q)$ and $V(q) := P_s(q)$, we find the conjugate of momenta is $p = (p_u, p_a) = M(q)\dot{q}$. The dynamics in (q, p) coordinates are given by

$$\mathscr{H}(q,p) = \frac{1}{2}p^\mathsf{T}M^{-1}(q)p - mgl\left(2c_u + c_{ua}\right), \tag{4.6}$$

$$\begin{cases} \dot{q} = M^{-1}(q)p, \\ \dot{p}_u = -mgl\left(2s_u + s_{ua}\right), \\ \dot{p}_a = -\frac{1}{2}p^\mathsf{T}\nabla_{q_a}M^{-1}(q)p - mgls_{ua} + \tau, \end{cases}$$

where the inverse inertia matrix is

$$M^{-1}(q) = \frac{1}{ml^2\left(2 - c_a^2\right)} \begin{bmatrix} 1 & -\left(1 + c_a\right) \\ -\left(1 + c_a\right) & 3 + 2c_a \end{bmatrix}. \tag{4.7}$$

The control input is a force $\tau \in \mathbb{R}$ affecting only the dynamics of p_a, representing a torque acting on the hip joint. This means (q, p) are simply actuated coordinates inside the phase space $\mathcal{Q} \times \mathcal{P}$ where $\mathcal{Q} = \mathcal{Q}_u \times \mathcal{Q}_a := \mathbb{S}^1 \times \mathbb{S}^1$, and $\mathcal{P} = \mathcal{P}_u \times \mathcal{P}_a := \mathbb{R} \times \mathbb{R}$. This allows us to apply the theory of VNHCs from Chapter 2.

Let us define the VNHC $h(q, p) = q_a - f(q_u, p_u)$ of order 1, where $f \in C^2\left(\mathcal{Q}_u \times \mathcal{P}_u; \mathcal{Q}_a\right)$. Since $\nabla_{q_u} M^{-1}(q) = \mathbf{0}_{2\times 2}$, Theorem 2.10 tells us that this VNHC will be regular when the regularity matrix

$$dh_q M^{-1}(q) \begin{bmatrix} 0 \\ 1 \end{bmatrix},$$

is of full rank 1 on the constraint manifold Γ. Given that $dh_q = \begin{bmatrix} -\partial_{q_u} f & 1 \end{bmatrix}$, the regularity matrix evaluates to the scalar equation

$$\frac{(1 + c_a)\partial_{q_u} f(q_u, p_u) + (3 + 2c_a)}{ml^2(2 - c_a^2)}. \tag{4.8}$$

This is full rank if and only if the numerator does not change sign. The following proposition provides a sufficient condition for regularity.

Proposition 4.1. *A relation $h(q, p) = q_a - f(p_u) = 0$ with $f \in C^2\left(\mathcal{P}_u; \mathcal{Q}_a\right)$ is a regular VNHC of order 1 for the simple acrobot.*

Proof. Since $\partial_{q_u} f = 0$, the regularity equation (4.8) is strictly positive for all values of q_a, and hence is full rank everywhere on the constraint manifold. By Theorem 2.10, h is a regular VNHC of order 1. □

Proposition 4.1 will be useful later, as we will not need to check regularity if we design a function of the unactuated momentum.

The acrobot is noticeably more complex than the VLP, as the dynamics of (q_u, p_u) and (q_a, p_a) are coupled through $M^{-1}(q)$. Because of this, the constrained dynamics of an arbitrary VNHC may not be easy to write out. In the rest of this chapter, our goal is to design the function $f(q_u, p_u)$ based on the natural human motion of a gymnast, with one caveat: we must be able to prove the constrained dynamics will inject energy into the acrobot.

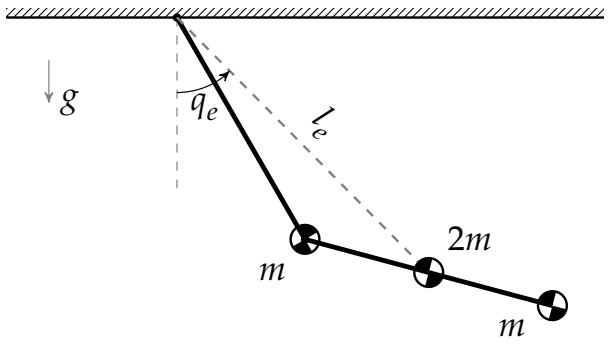

Figure 4.3: A simple acrobot modelled as a VLP with equivalent center of mass $2m$. The length of the VLP changes according to q_a.

4.3 Previous Constraint Approaches

Let us examine some of the existing approaches to generating giant motion for the acrobot, since these may be viable candidates on which to base a VNHC.

One initial approach to controlling the acrobot is to model it as a variable-length pendulum by collapsing the two rods and masses into one equivalent center of mass (ECM), as in Figure 4.3. This seems a reasonable model reduction, since the length from the pivot to the ECM changes depending on the angle q_a of the leg. Indeed, Henmi et al. [10] use this approach to design a trajectory for the ECM, then determine which leg angles $q_a(t)$ are required to generate that trajectory. Following in their footsteps, we might consider using the results from Chapter 3 to find the leg angles that allow the ECM to gain energy. Then we could apply Theorem 3.2 to prove the acrobot is gaining energy.

Unfortunately, the VLP is not a true representation of the acrobot. The effective length of the ECM is

$$l_e(q_a) := l\sqrt{\frac{5}{4} + c_a},$$

and its effective angle is

$$q_e := \arctan_2\left(s_u + \frac{1}{2}s_{ua}, -c_u - \frac{1}{2}c_{ua}\right).$$

There are two important notes to consider based on these equations. First, Figure 4.4 shows that for each pose of the VLP representation, there are two configurations of the acrobot which give the same effective length and angle. This means the acrobot and the VLP are not equivalent representations; designing a VNHC that injects energy using the ECM may not produce human-like leg motion on the acrobot.

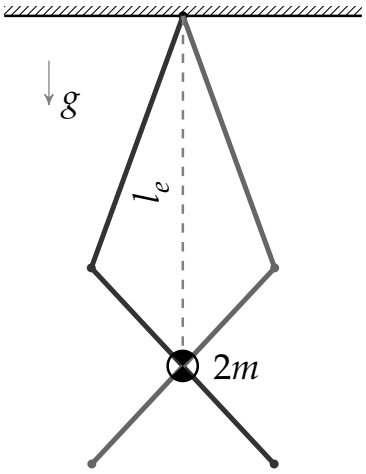

Figure 4.4: The equivalent center of mass of the acrobot generally has two configurations which correspond to the same effective length and angle. These configurations are symmetric about the line connecting the pivot to the ECM.

Second, if we were to compute the conjugate of momenta p_{l_e} to l_e and p_e to q_e, we would see the torque input τ appearing in both of their dynamic equations. In the VLP model from Chapter 3, the control input only affects the dynamics of the length variable. If we want to design a VNHC for this system, we cannot use any of the results from Chapter 3 because the VLP models do not match.

Since we cannot apply the results of Chapter 3 to simplify the proof of energy injection, and the resulting ECM motion may not even produce realistic leg motion, this model reduction is ineffective for our purposes.

Let us turn next to the thesis of Wang [1], who designs a VHC to enforce a so-called "tap" motion with the purpose of injecting energy into the acrobot. First, he defines a compensator variable s which tracks $\dot{q}_u$, so that he can use the theory of VHCs with the extended configuration (q_u, q_a, s). He then finds $h_1, h_2 \in \mathbb{R}_{>0}$ to define the normalized radius ρ and normalized angle ξ in the (q_u, s)-plane. These normalized variables are given by

$$\begin{aligned}\rho &:= \sqrt{h_1 q_u^2 + h_2 s^2},\\ \xi &:= \arctan_2(h_2 s, h_1 q_u).\end{aligned}$$

He then sets the VHC to be $h(q) = q_a - f_{\text{rad}}(\rho) f_{\text{ang}}(\xi)$ with the control parameters $\bar{q}_u$

and ρ_0, where

$$f_{\text{rad}}(\rho) := \tanh^2(\rho/\rho_0), \tag{4.9}$$

$$f_{\text{ang}}(\xi) := \begin{cases} 0 & -\pi < \xi \leq 0 \\ \bar{q}_u \exp\left(1 - \frac{1}{1-(\frac{4\xi}{\pi}-1)^2}\right) & 0 < \xi \leq \frac{\pi}{2} \\ 0 & \frac{\pi}{2} < \xi \leq \pi. \end{cases} \tag{4.10}$$

While this constraint shows promising experimental results and it accurately emulates true human motion, Wang does not provide analytical proof that the acrobot will gain energy. His lack of analysis is tied to the fact that the constrained dynamics are incredibly complicated. In fact, just showing the constraint is regular is a challenging task. While we could very easily convert his VHC into a VNHC by replacing s with p_u, we would run into the same problem. Since we want our constraint to *provably* inject energy, we must forgo this type of constraint in favour of something less complex.

4.4 The Acrobot Constraint

One may be tempted to design a constraint of the form $q_a = \bar{q}_a \sin(\theta)$, with $\theta := \arctan_2(p_u, q_u)$, since a similar approach was so effective for the VLP in Chapter 3. Unfortunately, this constraint is not regular, and it is difficult to find any VNHC of the form $q_a = f(\theta)$ where regularity can be proven easily. Instead, we will develop a constraint $h(q,p) = q_a - f(p_u)$ because these constraints are always regular (as per Proposition 4.1).

To design this constraint, let us begin (perhaps unexpectedly) by examining a person on a seated swing. The person extends their legs when the swing moves forwards, and retracts their legs when the swing moves backwards. As the swing gains speed, the person leans their body back while extending their legs. This allows them to bring their legs higher, shortening the distance from their center of mass to the pivot and adding more energy to the swing. When the swing moves backward, they sit up and fully retract their legs underneath them [31].

Now imagine the person's torso is affixed to the swing's rope so they are always upright. Imagine further that the swing has no seat at all, allowing the person to extend their legs beneath them. This position is identical to that of a gymnast on a bar, which is why we can use leg motion from the seated swing to design a controller for the acrobot.

The acrobot's legs are rigid rods which cannot retract, so we emulate the person

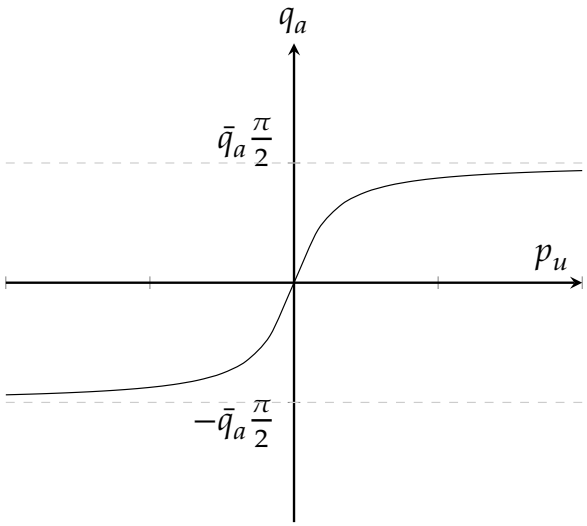

Figure 4.5: The acrobot constraint $q_a = \bar{q}_a \arctan(Ip_u)$.

on a swing by pivoting the legs toward the direction of motion. To account for how a person leans back at higher speeds, the legs should pivot to an angle proportional to the swing's speed. Since the direction of motion is entirely determined by p_u, one such VNHC which emulates this process is $q_a = \bar{q}_a \arctan(Ip_u)$, displayed in Figure 4.5. Here, $\bar{q}_a \in]0, \frac{2Q_a}{\pi}]$ and $I \in \mathbb{R}$ is a fixed control parameter.

This constraint does not perfectly recreate giant motion, during which the gymnast's legs are almost completely extended [45] – it instead pivots the legs partially during rotations. However, the behaviour looks similar enough that the constraint should provide a reasonable foundation for injecting energy into the acrobot. It is for this reason that we choose our acrobot's constraint to be

$$h(q,p) = q_a - \bar{q}_a \arctan(Ip_u). \tag{4.11}$$

Let us now compute the constrained dynamics under (4.11). Note that $dh_q = \begin{bmatrix} 0 & 1 \end{bmatrix}$, while

$$dh_{p_u} = \frac{-\bar{q}_a I}{1 + I^2 p_u^2}.$$

Inserting these into (2.16), we get the solution for p_a on the constraint manifold:

$$p_a(q_u, p_u) = \frac{(1 + c_a)(1 + I^2 p_u^2)p_u - m^2 g l^3 \bar{q}_a I (2 - c_a^2)(2s_u + s_{ua})}{ml^2(3 + 2c_a)(1 + I^2 p_u^2)}.$$

The dynamics for p_u do not contain p_a, so they remain unchanged. The constrained

dynamics for q_u are given by

$$\dot{q}_u = e_1^\mathsf{T} M^{-1}(q) \begin{bmatrix} p_u \\ p_a(q_u, p_u) \end{bmatrix},$$

which can be simplified into

$$\dot{q_u} = \frac{(1 + I^2 p_u^2) p_u + m^2 g l^3 \bar{q}_a I (2 s_u + s_{ua})(1 + c_a)}{m l^2 (1 + I^2 p_u^2)(3 + 2 c_a)}.$$

Hence, the constrained dynamics for the acrobot under (4.11) are

$$\begin{cases} \dot{q}_u &= \frac{(1+I^2 p_u^2) p_u + m^2 g l^3 \bar{q}_a I (2 s_u + s_{ua})(1+c_a)}{m l^2 (1+I^2 p_u^2)(3+2c_a)} \\ \dot{p}_u &= -mgl(2 s_u + s_{ua}) \end{cases} \Bigg|_{q_a = \bar{q}_a \arctan(I p_u)}. \tag{4.12}$$

These dynamics do not always gain energy; rather, energy gain is only guaranteed under certain conditions on the size of I. First, let

$$E(q_u, p_u) := \frac{p_u^2}{10 m l^2} + 3 m g l (1 - \cos(q_u)),$$

be the energy function obtained by setting $I = 0$. As we will see later, this is the mechanical energy of a simple pendulum with two masses. Next, define the set

$$\mathcal{O}_1 := \left\{ (q_u, p_u) \in \mathbb{S}^1 \times \mathbb{R} \mid E(q_u, p_u) < E(\pi, 0) \right\}, \tag{4.13}$$

as in Figure 4.6a. Finally, let $\bar{\rho} > \sqrt{60 m^2 g l^3}$ and define the set

$$\mathcal{O}_2(\bar{\rho}) := \left\{ (q_u, p_u) \in \mathbb{S}^1 \times \mathbb{R} \mid E(q_u, p_u) < E(0, \bar{\rho}) \right\}, \tag{4.14}$$

as in Figure 4.6b

For small enough I, our VNHC will inject energy on the open set $\mathcal{O}_1$ and (provided a suitable condition is met) on the open set $\mathcal{O}_2(\bar{\rho})$.

Theorem 4.2. *Consider the simple acrobot* (4.6) *constrained by the VNHC* (4.11)*, whose constraint manifold is* $\Gamma \simeq \mathbb{S}^1 \times \mathbb{R}$*.*

1. *There exists* $I^\star > 0$ *such that, for all* $I \in]0, I^\star]$*,* (4.11) *injects energy into the acrobot on* $\mathcal{O}_1$*. Moreover, almost every orbit will escape the closure of* $\mathcal{O}_1$ *in finite time. If instead* $I \in [-I^\star, 0[$*, the VNHC dissipates energy.*

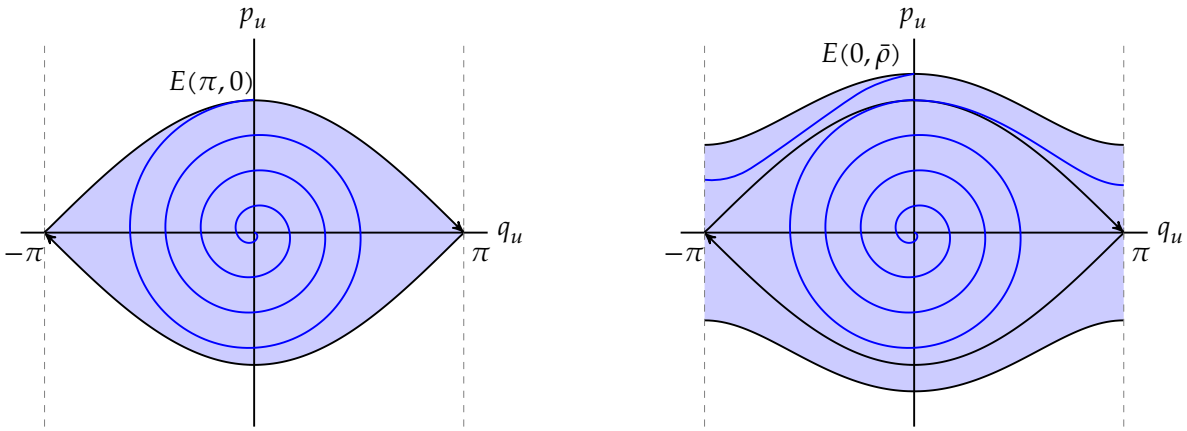

(A) The set $\mathcal{O}_1$. An orbit starting in this set (blue) will pass through the level set $E(\pi, 0)$ of the nominal pendulum.

(B) The set $\mathcal{O}_2(\bar{\rho})$. Orbits starting in this set are guaranteed to reach the level set $E(0, \bar{\rho})$ of the nominal pendulum.

Figure 4.6: The sets on which the acrobot gains energy, according to Theorem 4.2.

2. *Define* $b : \mathbb{S}^1 \times \mathbb{R}_{>0} \to \mathbb{R}$ *by*

$$b(\beta, \rho_0) := \frac{5m^2gl^3\bar{q}_a\left(m^2gl^3\left(18s_\beta^2 + 30c_\beta(1 - c_\beta)\right) - c_\beta\rho_0^2\right)}{|\rho_0|\sqrt{\rho_0^2 - 30m^2gl^3(1 - c_\beta)}},$$

and define $S(\rho_0) := \int_0^{2\pi} b(\sigma, \rho_0)d\sigma$. *Fix* $\bar{\rho} > \sqrt{60m^2gl^3}$. *Suppose there exists* $\epsilon > 0$ *so that* $S(\rho_0) \geq \epsilon$ *for all* $\rho_0 \in \left]\sqrt{60m^2gl^3}, \bar{\rho}\right]$. *Then there exists* $I^\star > 0$ *such that, for all* $I \in]0, I^\star]$ (4.11) *injects energy into the acrobot on* $\mathcal{O}_2(\bar{\rho})$. *If instead* $I \in [-I^\star, 0[$, *the VNHC dissipates energy.*

Notice that $\mathcal{O}_1 \subset \mathcal{O}_2(\bar{\rho})$, yet Theorem 4.2 considers these sets separately. This separation is advantageous because the first result holds for any m, g, l, and $\bar{q}_a$. That is, regardless of one's choice of acrobot, a small enough fixed value $I > 0$ will enable the acrobot to escape any compact subset of $\mathcal{O}_1$ in finite time. Therefore, the acrobot will display an oscillatory behaviour whereby the amplitude of oscillation increases with time. In so doing, the acrobot's orbit will exit in finite time the closure of $\mathcal{O}_1$ as in Figure 4.6a.

In other words, the first result of Theorem 4.2 states that all acrobots constrained by (4.11) will gain enough energy to begin rotating around the bar. In the worst case, the acrobot will at least perform a swing-up routine to reach the unstable equilibrium at $(q_u, p_u) = (\pi, 0)$.

The second result of Theorem 4.2 pertains to energy injection once the acrobot has

started rotating. For the acrobot to achieve giants with energy $E(0, \bar{\rho})$, it must satisfy the assumption on the integral of $b(\beta, \rho_0)$. The value of this integral depends on the acrobot's physical parameters. If the assumption holds, orbits will escape compact subsets of $\mathcal{O}_2(\bar{\rho})$ in finite time until the acrobot eventually reaches a momentum of at least $\bar{\rho}$. One example of this behaviour is displayed in Figure 4.6b. Note that the size of I will depend on $\bar{\rho}$.

The proof used in Chapter 3 does not readily transfer to the acrobot. Proving Theorem 4.2 requires an intelligent change of coordinates and the use perturbation theory [49]. We provide the full proof of this theorem in Chapter 4.5.

4.5 Proof of Theorem 4.2

To make the proof of Theorem 4.2 as clear as possible, we break it down into the following segments:

1. Background on perturbation theory.
2. Perturbation analysis for oscillations.
3. Perturbation analysis for rotations.

When $I = 0$, the constrained acrobot behaves like a single pendulum with masses at a distance l and $2l$ from the pivot (Figure 4.7a) whose energy

$$E(q_u, p_u) = \frac{p_u^2}{10ml^2} + 3mgl(1 - \cos(q_u)), \tag{4.15}$$

is conserved. Level sets of E are ellipses on the (q_u, p_u)-plane when $E(q_u, p_u) < E(\pi, 0)$, which we call "oscillations"; and they are open curves when $E(q_u, p_u) > E(\pi, 0)$, which we call "rotations". Examples of these can be seen in Figure 4.7b.

Using a method developed by Mohammadi et al. [20], we can find a change of coordinates $(q_u, p_u) \to (\alpha, \mu)$ with the following properties:

- The energy of oscillation in (α, μ) coordinates is uniquely defined by μ, which remains constant along oscillations of the simple pendulum.
- α is a pseudo-angle living in $\mathbb{S}^1$ which is always increasing along oscillations.

The coordinates (α, μ) can be thought of as deformed polar coordinates adapted to level sets of E below the value $E(\pi, 0)$, where μ specifies the level set and α identifies a point

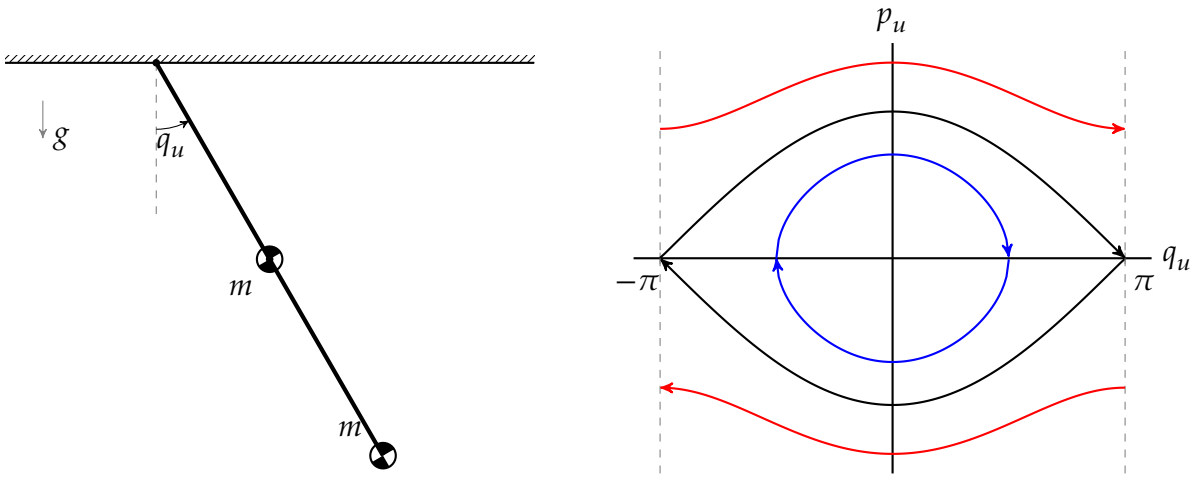

(A) A simple pendulum with two masses.

(B) Level sets of E. The blue ellipse is an oscillation; the red curves are rotations; and the black ellipse is the homoclinic orbit with energy $E(\pi, 0)$.

Figure 4.7: Our constrained acrobot is a simple pendulum when $I = 0$.

on that level set. Once we have these coordinates in hand, we can use perturbation theory to prove that μ increases on $\mathcal{O}_1$ when $I > 0$ is small enough.

Likewise, we will find a second set of coordinates (β, ρ) for rotations, where $\beta \in \mathbb{S}^1$ is always increasing along solutions, ρ is constant along rotations of the simple pendulum, and ρ increases for the acrobot when $I > 0$ is small enough. Using both (α, μ) and (β, ρ), we will show the acrobot is gaining energy on $\mathcal{O}_2(\bar{\rho})$.

4.5.1 Background on Perturbation Theory

Nonlinear systems like the acrobot are difficult (or even impossible) to solve analytically. Perturbation theory allows one to understand the behaviour of nonlinear systems by studying a simpler nominal system. Solutions of the nonlinear system can often be approximated by taking a Taylor expansion around a solution of the nominal system.

Khalil [49] considers a system of the form

$$\begin{cases} \dot{x} = f(t, x, I), \\ x(t_0) = \eta(I), \end{cases} \tag{4.16}$$

where $f : [t_0, t_1] \times D \times [-I_0, I_0] \to \mathbb{R}^n$ is smooth[1] on a domain $D \subset \mathbb{R}^n$. In the context of the acrobot, x is any pair of coordinates which make our analysis convenient; I is the control parameter of the system; the function f is the constrained dynamics in x-coordinates; and $\eta(I) \equiv \eta_0$ is a constant initial condition.

Setting $I = 0$ we get the nominal system

$$\begin{cases} \dot{x}_0 = f(t, x, 0), \\ x_0(t_0) = \eta_0, \end{cases} \tag{4.17}$$

which we need to solve for the explicit solution $x_0(t, \eta_0)$ on $[t_0, t_1]$. We assume this solution is contained in D.

Now consider the solution $x(t, \eta_0, I)$ to (4.16). Performing a first-order Taylor series expansion at $I = 0$, we get $x(t, \eta_0, I) = x_0(t, \eta_0) + Ix_1(t, \eta_0) + R(t, \eta_0, I)$, where the remainder term $R(t, \eta_0, I)$ is smooth and $O(I^2)$, *i.e.*,,

$$\lim_{I \to 0} \frac{R(t, \eta_0, I)}{I} = 0.$$

One can recover $x_1(t, \eta_0)$ as the solution to the scalar time-varying ODE

$$\begin{cases} \dot{x}_1 = \frac{\partial f}{\partial x}(t, x_0(t, \eta_0), 0)x_1 + \frac{\partial f}{\partial I}(t, x_0(t, \eta_0), 0), \\ x_1(t_0, \eta_0) = 0. \end{cases} \tag{4.18}$$

We now paraphrase Khalil's Theorem 10.1 [49] on the accuracy of perturbation analysis.

Theorem 4.3. *Fix $t_0, t_1 \in \mathbb{R}$ with $t_0 < t_1$. Suppose $f : [t_0, t_1] \times D \times [-I_0, I_0] \to \mathbb{R}^2$ is C^1, and that the nominal system (4.17) has a unique solution $x_0(t, \eta_0) \in D$ on $[t_0, t_1]$. Then there exists $I^\star > 0$ such that, for all I with $|I| < I^\star$, the solution $x(t, \eta_0, I)$ to (4.16) satisfies*

$$\|x(t, \eta_0, I) - \big(x_0(t, \eta_0) + Ix_1(t, \eta_0)\big)\| \leq k|I^2|$$

for some $k > 0$.

Theorem 4.3 tells us that we can approximate the solution of the nonlinear system by the Taylor approximation $x(t, \eta_0, I) \approx x_0(t, \eta_0) + Ix_1(t, \eta_0)$. When I is small enough, solutions of the nonlinear system and the Taylor approximation are the same up to

[1] Khalil actually considers $f(t, x, \epsilon)$ which is "sufficiently smooth". To more easily connect his theory to the acrobot constraint, we assume smoothness of f and replace ϵ with I.

order I^2 along compact time intervals. This is equivalent to saying that the remainder term $R(t, \eta_0, I)$ is bounded, because

$$\|x(t, \eta_0, I) - \big(x_0(t, \eta_0) + Ix_1(t, \eta_0)\big)\| = \|R(t, \eta_0, I)\| \leq k|I^2|.$$

Since we know that the acrobot behaves like a pendulum at $I = 0$, we can use this theory to prove energy injection properties on the acrobot by studying the simple pendulum.

4.5.2 Perturbation Analysis for Oscillations

As we have seen, setting $I = 0$ turns the acrobot into a nominal pendulum. This pendulum oscillates whenever the nominal energy (4.15) is less than $E(\pi, 0)$. Hence, the domain of oscillations for the nominal pendulum is given by

$$\mathcal{O}_1 := \left\{(q_u, p_u) \in \mathbb{S}^1 \times \mathbb{R} \mid E(q_u, p_u) < E(\pi, 0)\right\}.$$

Recall that orbits of a pendulum are level sets of E. From Figure 4.7b, we know that oscillation level sets look like ellipses contained in $\mathcal{O}_1$. Since perturbation theory requires us to analyze the nominal pendulum, we will make our analysis convenient by changing coordinates into a pseudo-radius $\mu > 0$ which remains constant on level sets of E, along with a pseudo-angle $\alpha \in \mathbb{S}^1$ satisfying $\dot{\alpha} > 0$ on $\mathcal{O}_1$.

Pseudo-Polar Coordinates

Once again, to define pseudo-polar coordinates, we consider the dynamics of the pendulum obtained by setting $I = 0$ in (4.12), resulting in

$$\begin{cases} \dot{q}_u = \frac{p_u}{5ml^2}, \\ \dot{p}_u = -3mgl \sin(q_u). \end{cases} \tag{4.19}$$

The above is a simple mechanical system whose total energy is precisely the function $E(q_u, p_u)$ defined in (4.15). The energy of oscillation can be determined by the intersection μ of an orbit of (4.19) with the q_u-axis (as in Figure 4.8). Since $q_u \in]-\pi, \pi[$ on $\mathcal{O}_1$, we set $\mu \in]0, \pi[$. The transformation we want is therefore a diffeomorphism of the form

$$\begin{aligned} T : \mathcal{O}_1 \backslash \{(0,0)\} &\to \mathbb{S}^1 \times]0, \pi[, \\ (q_u, p_u) &\mapsto (\alpha, \mu). \end{aligned}$$

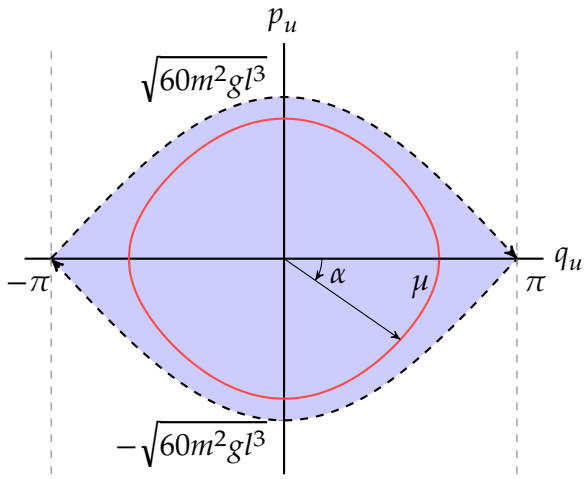

Figure 4.8: The domain $\mathcal{O}_1$ (blue) where a pendulum oscillates. The pseudo-radius μ corresponds to the intersection of an oscillation (red) with the q_u-axis. The psuedo-angle α is taken to be clockwise positive because oscillations of a pendulum move clockwise on $\mathcal{O}_1$.

The energy level set corresponding to the intersection $(q_u, p_u) = (\mu, 0)$ is

$$\left\{(q_u, p_u) \in \mathbb{S}^1 \times \mathbb{R} \mid E(q_u, p_u) = 3mgl(1 - \cos(\mu))\right\},$$

which gives the relationship

$$p_u^2 = 30m^2gl^3\left(\cos(q_u) - \cos(\mu)\right). \tag{4.20}$$

On this level set, q_u ranges between $[-\mu, \mu]$ and can be uniquely parameterized by $q_u = \mu\cos(\alpha)$, where α is our desired pseudo-angle. Substituting this into (4.20), we get

$$p_u^2 = 30m^2gl^3\left(\cos(\mu\cos(\alpha)) - \cos(\mu)\right).$$

We want to find p_u as a function of (α, μ); noting that we can determine the sign of p_u from the sign of $\sin(\alpha)$, we get the (clockwise) parameterization

$$p_u = -\operatorname{sgn}(\sin(\alpha))\sqrt{30m^2gl^3\left(\cos(\mu c_\alpha) - c_\mu\right)}, \tag{4.21}$$

which is smooth for all $\mu \in]0, \pi[$.

We have thus found a transformation $T^{-1}(\alpha, \mu) = (q_u, p_u)$. We need the inverse of this map to get our diffeomorphism $T(q_u, p_u)$. Notice from (4.20) that

$$\cos(\mu) = -\frac{p_u^2}{30m^2gl^3} + \cos(q_u) =: C_\mu(q_u, p_u).$$

Since $\mu \in]0, \pi[$, we can uniquely express μ by

$$\mu = \arccos\left(C_\mu(q_u, p_u)\right).$$

Next we need to find α. Recall that

$$\cos(\alpha) = \frac{q_u}{\mu}, \tag{4.22}$$

which means

$$\sin(\alpha) = \pm\sqrt{1 - \frac{q_u^2}{\mu^2}}. \tag{4.23}$$

Using (4.21), we determine that $\operatorname{sgn}(\sin(\alpha)) = -\operatorname{sgn}(p_u)$. Putting together (4.22) and (4.23), we deduce that

$$\alpha = \operatorname{arctan}_2\left(-\operatorname{sgn}(p_u)\sqrt{1 - \frac{q_u^2}{\mu^2}}, \frac{q_u}{\mu}\right)\Bigg|_{\mu=\arccos(C_\mu(q_u,p_u))}.$$

Thus, our transformation into (α, μ)-coordinates is

$$\alpha = \operatorname{arctan}_2\left(-\operatorname{sgn}(p_u)\sqrt{1 - \frac{q_u^2}{\mu^2}}, \frac{q_u}{\mu}\right)\Bigg|_{\mu=\arccos(C_\mu(q_u,p_u))}, \tag{4.24}$$

$$\mu = \arccos\left(C_\mu(q_u, p_u)\right). \tag{4.25}$$

The acrobot's constrained dynamics in (α, μ)-coordinates can be computed by evaluating

$$\begin{cases} \dot{\alpha} &= \frac{\partial\alpha(q_u,p_u)}{\partial q_u}\dot{q}_u + \frac{\partial\alpha(q_u,p_u)}{\partial p_u}\dot{p}_u \\ \dot{\mu} &= \frac{\partial\mu(q_u,p_u)}{\partial q_u}\dot{q}_u + \frac{\partial\mu(q_u,p_u)}{\partial p_u}\dot{p}_u \end{cases}\Bigg|_{(q_u,p_u)=T^{-1}(\alpha,\mu)}.$$

with $(\dot{q}_u, \dot{p}_u)$ given by (4.12).

These dynamics are much too large to write out, so we simply denote them by

$$\dot{\alpha} = f_\alpha(\alpha, \mu, I), \tag{4.26}$$

$$\dot{\mu} = f_\mu(\alpha, \mu, I). \tag{4.27}$$

MATLAB's symbolic toolbox evaluates the nominal dynamics (when $I = 0$) as

$$\dot{\alpha} = \sqrt{\frac{6g}{5l}}\sqrt{\frac{\cos(\mu\cos(\alpha)) - \cos(\mu)}{\mu^2\sin(\alpha)^2}}, \tag{4.28}$$

$$\dot{\mu} = 0. \tag{4.29}$$

Note that (4.28) has removable singularities at $\alpha \in \{0, \pi\}$. Taking the limit as α approaches these points yields

$$\lim_{\alpha\to 0}\dot{\alpha} = \lim_{\alpha\to\pi}\dot{\alpha} = \sqrt{\frac{6g\sin(\mu)}{10l\mu}},$$

which is smooth and well-defined for all $\mu \in]0, \pi[$. Taking these removable singularities into account, one can verify that $\dot{\alpha} > 0$ for every $\mu \in]0, \pi[$. By continuity of (4.26), there exists $I_1 > 0$ small enough that $\dot{\alpha}$ remains positive on $\mathcal{O}_1$ for $I \in [-I_1, I_1]$.

These pseudo-polar coordinates can be extended smoothly to the boundary of $\mathcal{O}_1$. Notice that, for each $\alpha \in \mathbb{S}^1$,

$$\lim_{\mu\to\pi}\dot{\alpha} = \sqrt{\frac{6g}{5l}}\sqrt{\frac{\cos(\pi\cos(\alpha)) + 1}{\pi^2\sin(\alpha)^2}} \geq 0, \tag{4.30}$$

with equality if and only if $\alpha \in \{0, \pi\}$. In other words, setting $\mu = \pi$ dictates the behaviour of the nominal pendulum on the homoclinic orbit with energy $E(\pi, 0)$. Hence, for small enough I we have $\dot{\alpha} \geq 0$ everywhere on the closure of $\mathcal{O}_1$, with equality only at the upright equilibrium $(q_u, p_u) = (\pi, 0)$. We will use this later to prove that all orbits starting in $\mathcal{O}_1$ will eventually begin rotating.

Time Scaling

We have observed in (4.27)-(4.26) that $\dot{\alpha} > 0$ on $\mathcal{O}_1$ for small enough I. Hence, we can use α as our time variable by reparameterizing t as a function $t(\alpha)$. This allows us to study the evolution of μ as a function of α rather than a function of time. Setting $\hat{\mu}(\alpha) := \mu(t(\alpha))$ yields the dynamics

$$\frac{d\hat{\mu}}{d\alpha} = \frac{d\mu}{dt}\frac{dt}{d\alpha}.$$

This reduces the system $(\dot{\alpha}, \dot{\mu})$ into the scalar time-varying ODE

$$\begin{cases} \frac{d\hat{\mu}}{d\alpha} = \frac{f_\mu(\tau(\alpha),\mu,I)}{f_\alpha(\tau(\alpha),\mu,I)} =: g(\alpha,\mu,I), \\ \hat{\mu}(0) = \mu_0. \end{cases} \tag{4.31}$$

Perturbation Analysis of the Time Scaled System

In the spirit of perturbation analysis, we will expand our time-scaled system $\hat{\mu}(\alpha, \mu_0, I)$. We begin by setting $I = 0$ to find the nominal system

$$\begin{cases} \frac{\partial \hat{\mu}_0}{\partial \alpha} = g(\alpha, \hat{\mu}_0, 0), \\ \hat{\mu}_0(0) = \mu_0. \end{cases}$$

Equations (4.28)-(4.29) reveal that $g(\alpha, \mu, 0) = 0$, so the solution to this nominal system is $\hat{\mu}_0(\alpha, \mu_0) \equiv \mu_0$ for all α.

We now take a first-order Taylor approximation of $\hat{\mu}(\alpha, \mu_0, I)$ around the nominal $\hat{\mu}_0(\alpha, \mu_0)$,

$$\hat{\mu}(\alpha, \mu_0, I) = \hat{\mu}_0(\alpha, \mu_0) + I\hat{\mu}_1(\alpha, \mu_0) + R(\alpha, \mu_0, I). \tag{4.32}$$

By (4.18), we know the function $\hat{\mu}_1(\alpha, \mu_0)$ is the solution to the linear time-varying scalar system

$$\begin{cases} \frac{\partial \hat{\mu}_1}{\partial \alpha} = \frac{\partial g}{\partial \hat{\mu}}(\alpha, \mu_0, 0)\hat{\mu}_1 + \frac{\partial g}{\partial I}(\alpha, \mu_0, 0), \\ \hat{\mu}_1(0) = 0. \end{cases} \tag{4.33}$$

These dynamics are difficult to compute by hand, so we resort to MATLAB symbolic computation to reveal that

$$\begin{aligned} \frac{\partial g}{\partial \hat{\mu}}(\alpha, \mu_0, 0) &= 0, \\ \frac{\partial g}{\partial I}(\alpha, \mu_0, 0) &= Ka(\alpha, \mu_0), \end{aligned}$$

where

$$\begin{aligned} K &:= \frac{\bar{q}_a\sqrt{30m^2gl^3}}{15}, \\ a(\alpha, \mu_0) &:= \frac{\mu_0|\sin(\alpha)|\left(5c_{\mu_0}\cos(\mu_0 c_\alpha) - 8\cos(\mu_0 c_\alpha)^2 + 3\right)}{\sin(\mu_0)\sqrt{\cos(\mu_0 c_\alpha) - c_{\mu_0}}}. \end{aligned}$$

Equation (4.33) can be solved by quadrature, giving

$$\hat{\mu}_1(\alpha, \mu_0) = K \int_0^{\alpha} a(\sigma, \mu_0) d\sigma.$$

Therefore, the first-order Taylor approximation of $\hat{\mu}(\alpha, \mu_0, I)$ is

$$\hat{\mu}(\alpha, \mu_0, I) = \mu_0 + IK \int_0^{\alpha} a(\sigma, \mu_0) d\sigma + R(\alpha, \mu_0, I). \tag{4.34}$$

Poincaré Analysis

Since $\dot{\alpha} > 0$, there is a well-defined Poincaré map describing how the pseudo-radius μ changes each time the orbit of $(q_u(t), p_u(t))$ intersects the q_u-axis, *i.e.*,, when $\alpha = 0$ or $\alpha = \pi$. Using our time-scaled system (4.31), we can define this Poincaré map as the change in $\hat{\mu}$ when α increases by π:

$$\begin{aligned} P_{\mathcal{O}} :]0, \pi[&\to \mathbb{R}_+, \\ \mu_0 &\mapsto \hat{\mu}(\pi, \mu_0, I). \end{aligned}$$

The Poincaré map expands into

$$P_{\mathcal{O}}(\mu_0) = \mu_0 + IK \int_0^{\pi} a(\sigma, \mu_0) d\sigma + R(\pi, \mu_0, I).$$

Let us define

$$Q(\mu_0) := \int_0^{\pi} a(\sigma, \mu_0) d\sigma. \tag{4.35}$$

Note that K is a positive constant which contains the acrobot's physical parameters m, g, l, and $\bar{q}_a$, while $a(\alpha, \mu)$ is adimensional. This means $Q(\mu_0)$ is identical for every acrobot. If $Q(\mu_0)$ is strictly positive, then $\hat{\mu}_1(\pi, \mu_0)$ will be positive for any acrobot.

We numerically compute $Q(\mu_0)$ for $\mu_0 \in [10^{-10}, \pi - 10^{-3}]$ in Figure 4.9. We see that it is strictly positive and monotonically increasing, with an asymptote at $\mu_0 = \pi$. Simulations with smaller μ_0 result in an infinite integral error due to a division by zero, so we believe that $Q(\mu_0)$ is in fact positive for all μ_0.

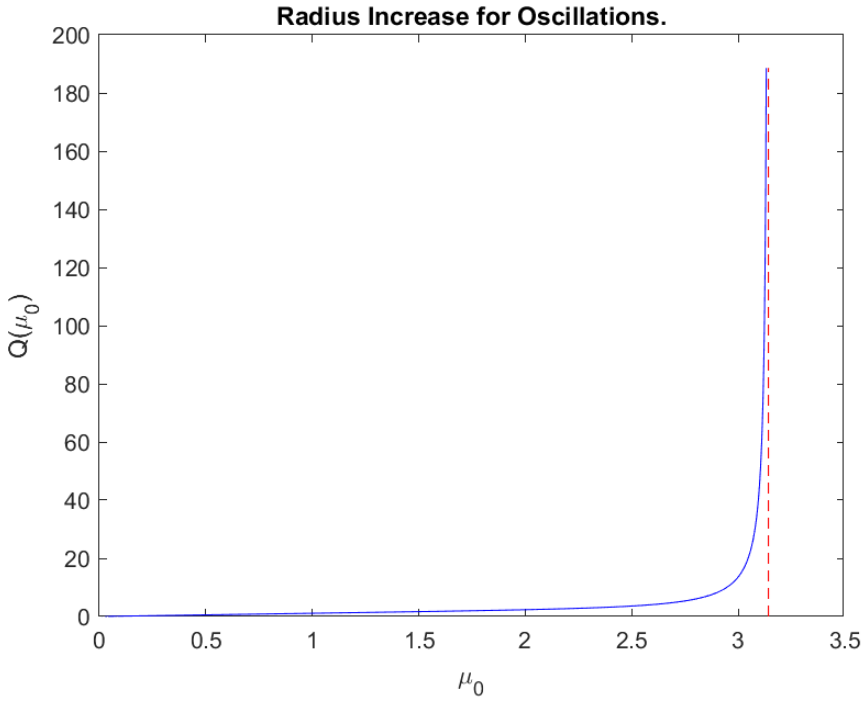

Figure 4.9: The plot of $Q(\mu_0)$.

Energy Gain on $\mathcal{O}_1$

The Poincaré map $P_{\mathcal{O}}$ allows us understand the evolution of $\hat{\mu}(\alpha, \mu_0, I)$ by studying the evolution of the discrete time system

$$\mu_{n+1} := P_{\mathcal{O}}(\mu_n) = \mu_n + IKQ(\mu_n) + R(\pi, \mu_n, I), \tag{4.36}$$

with initial condition μ_0. Here, μ_n represents the distance along the q_u-axis when an orbit of the constrained dynamics intersects the q_u-axis for the nth time, assuming the orbit was initialized at $(q_u, p_u) = (\mu_0, 0)$.

Proving the constrained dynamics gain energy on $\mathcal{O}_1$ is equivalent to showing μ_n eventually reaches π. That is, we want to find $I^\star \in]0, I_1]$ where, for all $\delta > 0$ and $\mu_0 \in]0, \pi - \delta]$, there exists $N > 0$ so that for all $n \geq N$, $\mu_n \notin [0, \pi - \delta]$.

A sufficient conditions for this characterization is to prove that $P_{\mathcal{O}}(\mu_0) \geq \mu_0 + \gamma$ for some $\gamma > 0$. We will perform our analysis in two sections. First, we will show the origin is a repeller of (4.36). This implies that orbits near the origin flow away from it. Then, we will use the sufficient condition above to guarantee all orbits reach $\mu = \pi$.

Linearizing (4.36) at $\mu_0 = 0$ yields

$$P'_{\mathcal{O}}(0) = 1 + IKQ'(0) + R'(\pi, 0, I),$$

where prime denotes differentiation with respect to μ. If there is some value of $I \in]0, I_1]$ for which this term is greater than 1, then 0 is a repeller of the discrete time system. To show such a value of I exists, we first compute

$$Q'(0) = \int_0^\pi \frac{\partial a}{\partial \mu}(\sigma, 0) d\sigma.$$

Numerical computations reveal that

$$\lim_{\mu_0 \to 0^+} \frac{\partial a}{\partial \mu}(\alpha, \mu_0) = -\frac{\sqrt{2}}{2}\left(11\sin(\alpha)^2 - 6\right),$$

which means

$$Q'(0) = \frac{\pi}{2\sqrt{2}} > 0.$$

Since the remainder term $R(\pi, 0, I)$ is $O(I^2)$, its partial derivative $R'(\pi, 0, I)$ is also $O(I^2)$. Hence, it can be written in the form $I^2\tilde{R}(I)$ where $\tilde{R}(I)$ is smooth and zero at $I = 0$. Thus, there exists $I_2 \in]0, I_1]$ such that

$$I_2 K Q'(0) + (I_2)^2 \tilde{R}(I) > 0.$$

Hence,

$$P'_{\mathcal{O}}(0) \geq 1 + IKQ'(0) + I^2\tilde{R}(I) > 1,$$

for all $I \in]0, I_2]$.

We have shown 0 is a repeller of the discrete time system, which means there exists some (unknown) $\epsilon > 0$ where the interval $]0, \epsilon[$ is negatively invariant for (4.36). What's more, all solutions starting in this interval will flow towards the value $\mu = \epsilon$.

To complete the proof, recall that $R(\pi, \mu_0, I)$ is smooth in all its parameters as well as being $O(I^2)$. It is therefore bounded below on the compact set $\mu_0 \in [\epsilon, \pi]$ by some value $\underline{R}(I)$. Theorem 4.3 asserts that there exists some $I_3 > 0$ and $r > 0$ so that, for all $I \in [-I_3, I_3]$,

$$R(\pi, \mu_0, I) \geq \underline{R}(I) > -I^2 r.$$

Note that we can assume $I_3 \leq I_2$ without loss of generality. Furthermore, $Q(\mu_0)$ is a strictly increasing function, so for $\mu_0 \in [\epsilon, \pi[$,

$$P_{\mathcal{O}}(\mu_0) > \mu_0 + IKQ(\epsilon) - I^2 r.$$

Picking a small $\gamma > 0$ and choosing $I^\star \in]0, I_3]$ so that

$$I^\star KQ(\epsilon) - (I^\star)^2 r \geq \gamma > 0,$$

means that $P_{\mathscr{O}}(\mu_0) \geq \mu_0 + \gamma$ for all $\mu_0 \in [\epsilon, \pi[$.

Looking at (4.36) we find that $\mu_{n+1} \geq \mu_n + \gamma$. This implies that all solutions of the discrete time system will flow towards $\mu = \pi$.

We conclude that, for all $m, g, l, \bar{q}_a$, there exists $I > 0$ small enough that the constraint (4.11) is injecting energy on $\mathscr{O}_1$.

By the same arguments presented in this section, the Poincaré section satisfies $P_{\mathscr{O}}(\mu_0) \leq \mu_0 - \gamma$ when $I < 0$. In this case, the constraint dissipates energy on $\mathscr{O}_1$.

Energy Gain on $\bar{\mathscr{O}}_1$

Before moving on to the rotation analysis, we must first confirm that any acrobot constrained by (4.11) will eventually start rotating. The definition of energy gain states that all orbits initialized in $\mathscr{O}_1$ will escape compact subsets of $\mathscr{O}_1$ in finite time. This is not enough to prove that all orbits will escape the boundary of $\mathscr{O}_1$.

Indeed, let E_π be the level set with energy $E(\pi, 0)$, which forms the boundary of $\mathscr{O}_1$. Define $\bar{\mathscr{O}}_1 = \mathscr{O}_1 \cup E_\pi$ to be the closure of $\mathscr{O}_1$. An orbit of the acrobot will only begin rotating if it escapes $\bar{\mathscr{O}}_1$ by crossing through E_π, and eventually remains outside this set. It is possible for orbits starting in $\mathscr{O}_1$ to always approach E_π without ever crossing into the rotation zone. We will prove this does not happen in general.

To begin, let us analyze the upright equilibrium. Taking the Jacobian of the constrained dynamics (4.12) at $(q_u, p_u) = (\pi, 0)$ yields

$$J = \begin{bmatrix} -\frac{6mgl\bar{q}_a I}{5} & \frac{1-2m^2gl^3\bar{q}_a^2 I^2}{5ml^2} \\ 3mgl & mgl\bar{q}_a I \end{bmatrix},$$

which has characteristic polynomial

$$\det(\lambda I_2 - J) = \lambda^2 + \frac{mgl\bar{q}_a I}{5}\lambda - 3g.$$

By Descartes' rule of signs, this polynomial has one root with positive real part. The equilibrium $(\pi, 0)$ is therefore unstable, so the stable manifold Π^+ of initial conditions converging to $(\pi, 0)$ is one-dimensional, and hence is of measure zero in $\mathbb{S}^1 \times \mathbb{R}$.

Using $x(t) := (q_u(t), p_u(t))$ as shorthand, let $x(0) \in \mathscr{O}_1$ be a nonzero initial condition

of the acrobot. Suppose by way of contradiction that the orbit $x(\mathbb{R})$ is confined within $\bar{\mathcal{O}}_1$, and does not exit through E_π into the rotation zone. Since $\bar{\mathcal{O}}_1$ is compact, the Birkhoff Theorem [50] implies:

- The positive limit set L_+ of $x(t)$ is non-empty, compact, and invariant.
- The solution $x(t)$ asymptotically tends to L_+.

Since the acrobot gains energy on $\mathcal{O}_1$, the positive limit set of $x(t)$ must be the largest invariant subset of E_π. From our discussion on pseudo-polar coordinates (in particular the extension (4.30) of $\dot{\alpha}$ to $\bar{\mathcal{O}}_1$), we know that $\dot{\alpha} \geq 0$ on E_π, with equality if and only if $\alpha \in \{0, \pi\}$. There are two possibilities: either E_π itself is invariant, or the largest invariant subset of E_π is $\{(\pi, 0)\}$. To rule out the first possibility, take the derivative of $E(q_u, p_u)$ at the p_u-axis to get

$$\dot{E}(0, p_u) = -\frac{g}{5l} \sin(q_a) p_u.$$

This is non-zero everywhere except at the origin, which means it is non-zero on E_π. This means E_π is not invariant, so the positive limit set of $x(t)$ must be the set $\{(\pi, 0)\}$. Hence, $x(t)$ converges to $(\pi, 0)$, which means $x(0) \in \Pi^+$. Since we know that Π^+ is a set of measure zero in $\mathbb{S}^1 \times \mathbb{R}$, almost every orbit initialized in $\mathcal{O}_1$ must escape through the boundary E_π into the rotation domain.

Escaping once into the rotation domain does not guarantee the acrobot orbit will never return to $\mathcal{O}_1$. Indeed, the orbit could escape through E_π and return to $\mathcal{O}_1$ several times. However, almost every orbit must eventually remain outside the closure of $\mathcal{O}_1$. If not, the positive limit set would once again be E_π; by the same argument as above, that orbit would be in Π^+.

We conclude that all orbits beginning in $\mathcal{O}_1$ will, in finite time, escape the closure of $\mathcal{O}_1$ and remain in the rotation domain forever after.

Summary

We have proven the first part of Theorem 4.2, which claims there exists a control value $I^\star > 0$ such that, for $I \in]0, I^\star]$, (4.11) injects energy into the acrobot on $\mathcal{O}_1$. Enough energy is injected that orbits will exit the closure of $\mathcal{O}_1$ and enter the rotation domain.

Here is a summary of the proof:

1. We found pseudo-polar coordinates (α, μ) adapted to level sets of the nominal pendulum's mechanical energy on $\mathcal{O}_1$, where $\alpha \in \mathbb{S}^1$ is a pseudo-angle and $\mu \in]0, \pi[$ is a pseudo-radius.

2. We showed there exists a value I_1 small enough where $\dot{\alpha} > 0$ everywhere on $\mathcal{O}_1$.

3. Using α as a time variable, we found the time-scaled pseudo-radius $\hat{\mu}$ and expanded it into (4.32) using perturbation theory.

4. Taking this expanded solution, we defined and expanded the Poincaré map $P_{\mathcal{O}}$ to analyze the discrete-time system (4.36).

5. We found a value $I_2 \leq I_1$ making the origin a repeller of (4.36), and a value $I_3 \leq I_2$ which drives μ_n towards $\mu = \pi$.

6. We showed that the upright equilibrium $(\pi, 0)$ is unstable, and used this fact to prove that almost every orbit crosses through E_π, thereby exiting the closure of $\mathcal{O}_1$ in finite time.

Choosing $I \in]0, I_3]$ guarantees energy injection on $\mathcal{O}_1$ because all orbits approach the pseudo-radius $\mu = \pi$. In fact, almost all orbits escape $\bar{\mathcal{O}}_1$. Likewise, choosing $I \in [-I_3, 0[$ guarantees energy dissipation on $\mathcal{O}_1$.

□

4.5.3 Perturbation Analysis for Rotations

Figure 4.7b reminds us that rotations of the nominal pendulum obtained by setting $I = 0$ look like open curves on some rotation domain $\mathscr{R} \subset \mathbb{S}^1 \times \mathbb{R}$, where

$$\mathscr{R} := \left\{ (q_u, p_u) \in \mathbb{S}^1 \times \mathbb{R} \mid E(q_u, p_u) > E(\pi, 0) \right\}.$$

Performing a similar process to what we did for oscillations, we wish to find a new set of coordinates (β, ρ) where the pseudo-radius $\rho \in \mathbb{R}$ remains constant on level sets of E and the pseudo-angle $\beta \in \mathbb{S}^1$ is always increasing on $\mathscr{R}$.

Pseudo-Polar Coordinates

In the oscillation region $\mathcal{O}_1$ we showed that the energy of the nominal pendulum (4.19) is uniquely determined by an orbit's intersection point μ with the q_u-axis. Likewise, on $\mathscr{R}$ the energy is determined by the orbit's intersection point ρ with the p_u-axis, as in Figure 4.10.

Note that the boundary of $\mathscr{R}$ intersects the p_u axis when $p_u^2 = 60m^2gl^3$. This boundary is the homoclinic orbit for the upright equilibrium of the pendulum, which is the level

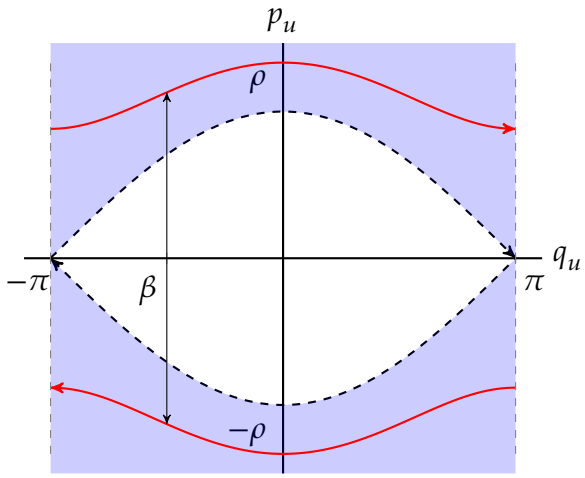

Figure 4.10: The domain $\mathscr{R}$ (blue) where a pendulum rotates. The pseudo-radius ρ corresponds to the intersection of an orbit of rotation with the p_u-axis. The pseudo-angle β selects a point on the rotation.

set with energy $E(\pi, 0)$. Hence, we must have $\rho > \sqrt{60m^2gl^3}$, if a rotation has momentum $p_u > 0$, and $\rho < -\sqrt{60m^2gl^3}$ if it has momentum $p_u < 0$. The energy level set associated with ρ is

$$\left\{(q_u, p_u) \in \mathbb{S}^1 \times \mathbb{R} \mid E(q_u, p_u) = \frac{\rho^2}{10ml^2}\right\},$$

which gives the relationship

$$\frac{p_u^2}{10ml^2} + 3mgl(1 - c_u) = \frac{\rho^2}{10ml^2}. \tag{4.37}$$

On this level set, q_u takes all values on $\mathbb{S}^1$, so our angle of rotation is uniquely parameterized by $\beta = q_u$. Since ρ does not change sign along the rotation, we have the smooth relationship

$$q_u = \beta, \tag{4.38}$$

$$p_u = \operatorname{sgn}(\rho)\sqrt{\rho^2 - 30m^2gl^3\left(1 - c_\beta\right)}. \tag{4.39}$$

Inverting this relationship gives our pseudo-polar coordinates

$$\beta = q_u, \tag{4.40}$$

$$\rho = \operatorname{sgn}(p_u)\sqrt{p_u^2 + 30m^2gl^3\left(1 - c_u\right)}. \tag{4.41}$$

Computing the acrobot's constrained dynamics in (β, ρ)-coordinates and setting

$I = 0$ yields the dynamics of the nominal pendulum. MATLAB evaluates those dynamics as

$$\dot{\beta} = \operatorname{sgn}(\rho)\, \frac{\sqrt{\rho^2 - 30m^2gl^3(1 - c_\beta)}}{5ml^2}, \tag{4.42}$$

$$\dot{\rho} = 0. \tag{4.43}$$

As expected, $\dot{\beta}$ does not change sign on $\mathscr{R}$ because the orbits always flow clockwise. If $\rho > 0$, the rotation curve goes from $\beta = -\pi$ to $\beta = \pi$; if $\rho < 0$, it goes from $\beta = \pi$ to $\beta = -\pi$. By continuity of (4.40), there exists $I_1 > 0$ small enough that $\dot{\beta}$ is non-zero and does not change sign on $\mathscr{R}$ for all $I \in [-I_1, I_1]$.

Time Scaling

Using β as our new time variable (via a time reparameterization $t = t(\beta)$) produces the time-scaled pseudo-radius $\hat{\rho}(\beta) := \rho(t(\beta))$. This reduces the system $(\dot{\beta}, \dot{\rho})$ into the scalar time-varying ODE

$$\begin{cases} \frac{d\hat{\rho}}{d\beta} = \frac{\dot{\rho}}{\dot{\beta}}, \\ \hat{\rho}(0) = \rho_0. \end{cases} \tag{4.44}$$

Perturbation Analysis of the Time Scaled System

In the spirit of perturbation analysis, we expand the time-scaled system $\hat{\rho}(\beta, \rho_0, I)$. From (4.17) we know the nominal system at $I = 0$ is

$$\begin{cases} \frac{d\hat{\rho}_0}{d\beta} = 0, \\ \hat{\rho}_0(0) = \rho_0, \end{cases}$$

which has solution $\hat{\rho}_0(\beta, \rho_0) \equiv \rho_0$.

We take a first-order Taylor approximation of $\hat{\rho}(\beta, \rho_0, I)$ around $\hat{\rho}_0(\beta, \rho_0)$ to get

$$\hat{\rho}(\beta, \rho_0, I) = \hat{\rho}_0(\beta, \rho_0) + I\hat{\rho}_1(\beta, \rho_0) + R(\beta, \rho_0, I), \tag{4.45}$$

where $R(\beta, \rho_0, I)$ is smooth and $O(I^2)$.

Using MATLAB's symbolic toolbox and (4.18), we discover that $\hat{\rho}_1(\beta, \rho_0)$ is the

solution to the linear time-varying scalar ODE

$$\begin{cases} \frac{d\hat{\rho}_1}{d\beta} = \frac{5m^2gl^3\bar{q}_a\left(m^2gl^3\left(18s_\beta^2+30c_\beta(1-c_\beta)\right)-c_\beta\rho_0^2\right)}{|\rho_0|\sqrt{\rho_0^2-30m^2gl^3(1-c_\beta)}} =: b(\beta,\rho_0), \\ \hat{\rho}_1(0) = 0, \end{cases} \tag{4.46}$$

whose solution is

$$\hat{\rho}_1(\beta,\rho_0) = \int_0^\beta b(\sigma,\rho_0)d\sigma.$$

Poincaré Analysis

Suppose we initialize the acrobot at $(\beta,\rho) = (0,\rho_0)$. One full rotation amounts to β traversing 2π rad in a clockwise direction; that is, when β goes from 0 to $\text{sgn}\left(\rho_0\right)2\pi$. Since $\dot{\beta}$ does not change sign on $\mathscr{R}$, there is a well-defined Poincaré map describing how the pseudo-radius ρ changes each time the orbit $(q(t),p(t))$ hits the p_u axis, *i.e.*,, every time β changes by 2π. We define this Poincaré map as

$$P_{\mathscr{R}}(\rho_0) := \hat{\rho}\left(\text{sgn}\left(\rho_0\right)2\pi,\rho_0,I\right),$$

which expands into

$$P_{\mathscr{R}}(\rho_0) = \rho_0 + I\hat{\rho}_1(\text{sgn}\left(\rho_0\right)2\pi,\rho_0) + R(\text{sgn}\left(\rho_0\right)2\pi,\rho_0,I).$$

Let us pause here for a moment to remember what we are trying to accomplish. The second part of Theorem 4.2 states that, under suitable conditions on the integral of $b(\beta,\rho_0)$, the acrobot will gain energy on

$$\mathscr{O}_2(\bar{\rho}) := \left\{(q_u,p_u) \in \mathbb{S}^1\times\mathbb{R} \mid E(q_u,p_u) < E(0,\bar{\rho})\right\},$$

for some $\bar{\rho} > \sqrt{60m^2gl^3}$. Recall from Section 4.5.2 that any acrobot initialized in $\mathscr{O}_1$ will eventually remain in the rotation region $\mathscr{R}$. What remains, then, is to prove that the acrobot's orbits will also gain energy on

$$\mathscr{R}_{\bar{\rho}} := \mathscr{R} \cap \mathscr{O}_2(\bar{\rho}).$$

This can be proven by analyzing the Poincaré map $P_{\mathscr{R}}(\rho_0)$. Looking at Figure 4.11, it is

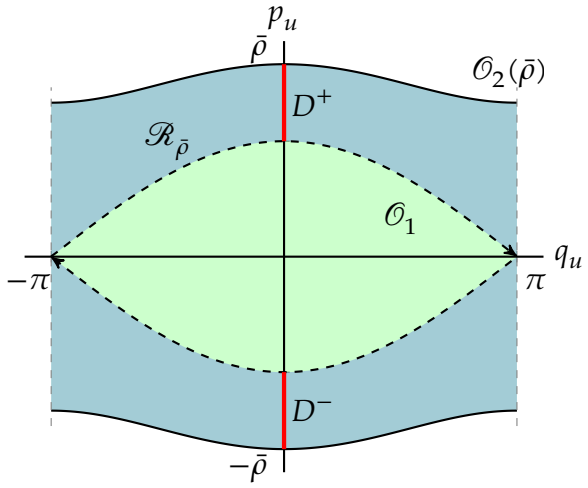

Figure 4.11: The region $\mathscr{R}_{\bar{\rho}}$ of rotations in $\mathscr{O}_2(\bar{\rho})$ is coloured in blue, while the domain $D = D^- \cup D^+$ of the Poincaré map is coloured in red.

clear that $P_{\mathscr{R}}$ has the domain

$$D := \left[-\bar{\rho}, -\sqrt{60m^2gl^3}\right[\ \cup \ \left]\sqrt{60m^2gl^3}, \bar{\rho}\right],$$

which is the intersection of $\mathscr{R}_{\bar{\rho}}$ with the p_u-axis. We label the part of D contained in the negative p_u-axis as

$$D^- := \left[-\bar{\rho}, -\sqrt{60m^2gl^3}\right[,$$

and the part contained in the positive p_u-axis as

$$D^+ := \left]\sqrt{60m^2gl^3}, \bar{\rho}\right],$$

so that $D = D^- \cup D^+$. If $P_{\mathscr{R}}(\rho_0)$ is always further from the origin than ρ_0 (*i.e.*, it is "expanding" on D), the acrobot will be gaining energy on $\mathscr{O}_2(\bar{\rho})$.

Mirroring the Poincaré analysis for oscillations, let us find a function $S(\rho_0)$ which is positive on D. This will be the rotational analogue to $Q(\mu_0)$ from (4.35).

Notice that the function $b(\beta, \rho_0)$ is even and 2π-periodic in β, which implies that

$$\begin{aligned}
\hat{\rho}_1(\operatorname{sgn}(\rho_0)\, 2\pi, \rho_0) &= \int_0^{\operatorname{sgn}(\rho_0)2\pi} b(\sigma, \rho_0) d\sigma, \\
&= \operatorname{sgn}(\rho_0) \int_0^{2\pi} b(\sigma, \rho_0) d\sigma, \\
&= \operatorname{sgn}(\rho_0)\, \hat{\rho}_1(2\pi, \rho_0).
\end{aligned}$$

Defining $S(\rho_0) := \hat{\rho}_1(2\pi, \rho_0)$, the Poincaré map becomes

$$P_{\mathscr{R}}(\rho_0) = \rho_0 + I \operatorname{sgn}(\rho_0) S(\rho_0) + R(\operatorname{sgn}(\rho_0) 2\pi, \rho_0, I). \tag{4.47}$$

Proving expansion of $P_{\mathscr{R}}(\rho_0)$ becomes easier if $S(\rho_0)$ is positive on D. Recall the assumption that there exists $\epsilon > 0$ where $S(\rho_0) \geq \epsilon$ for all $\rho_0 \in D^+$. Since $b(\beta, \rho_0)$ is even in ρ_0, its integral $S(\rho_0)$ is also even in ρ_0, which means $S(\rho_0) \geq \epsilon$ for every $\rho_0 \in D$.

Energy Gain on $\mathscr{O}_2(\bar{\rho})$

The Poincaré section $P_{\mathscr{R}}$ allows us understand the evolution of $\hat{\rho}(\beta, \rho_0, I)$ by studying the evolution of the discrete time ODE

$$\rho_{n+1} := P_{\mathscr{R}}(\rho_n) = \rho_n + I \operatorname{sgn}(\rho_n) S(\rho_n) + R(\operatorname{sgn}(\rho_n) 2\pi, \rho_n, I). \tag{4.48}$$

Here, ρ_n represents the distance along the p_u-axis when an orbit of the constrained dynamics intersects the p_u-axis for the n^{th} time, assuming the orbit was initialized at $(q_u, p_u) = (0, \rho_0)$.

To prove energy gain on $\mathscr{R}_{\bar{\rho}}$, it is enough to prove that $|\rho_n|$ eventually reaches $\bar{\rho}$. This is true if there exists some $\gamma > 0$ whereby $|P_{\mathscr{R}}(\rho_0)| \geq |\rho_0| + \gamma$ for all $\rho_0 \in D$

We begin with $\rho_0 \in D^+$. Recall that $R(\beta, \rho_0, I)$ is $O(I^2)$ and smooth in all its parameters. Therefore, it is bounded below on the compact set $\rho_0 \in \left[\sqrt{60m^2gl^3}, \bar{\rho}\right]$ by some value $\underline{R}(I)$. Theorem 4.3 asserts that there exists some $I_2 > 0$ and $r > 0$ so that, for all $I \in [-I_2, I_2]$,

$$R(2\pi, \rho_0, I) \geq \underline{R}(I) > -I^2 r.$$

Since $S(\rho_0) \geq \epsilon$, we find that

$$P_{\mathscr{R}}(\rho_0) > \rho_0 + I\epsilon - I^2 r,$$

for all $\rho_0 \in D^+$. Choosing $I_3 \in]0, I_2]$ so that

$$I_3\epsilon - (I_3)^2 r \geq \gamma,$$

makes $P_{\mathscr{R}}(\rho_0) \geq \rho_0 + \gamma$ for all $\rho_0 \in D^+$.

Now take $\rho_0 \in D^-$, where we wish to show that $P_{\mathscr{R}}(\rho_0) \leq \rho_0 - \gamma$. The remainder $R(\beta, \rho_0, I)$ is bounded above on the compact set $\rho_0 \in \left[-\bar{\rho}, -\sqrt{60m^2gl^3}\right]$, and Theorem

4.3 asserts that there exists some $I_4 > 0$ and $r' > 0$ so that, for all $I \in [-I_4, I_4]$,

$$R(-2\pi, \rho_0, I) < I^2 r'.$$

Hence,

$$P_{\mathscr{R}}(\rho_0) < \rho_0 - I\epsilon + I^2 r'.$$

Choosing $I_5 \in]0, I_4]$ so that

$$I_5\epsilon - (I_5)^2 r' \geq \gamma,$$

makes $P_{\mathscr{R}}(\rho_0) \leq \rho_0 - \gamma$ for all $\rho_0 \in D^-$.

To connect the two subregions of D together, choose $I^\star \in]0, \min\{I_3, I_5\}]$. Then $|P_{\mathscr{R}}(\rho_0)| \geq |\rho_0| + \gamma$ for all $\rho_0 \in D$, so the constrained dynamics are gaining energy on $\mathscr{R}_{\bar{\rho}}$.

By the same arguments presented in this section, the Poincaré section satisfies $|P_{\mathscr{R}}(\rho_0)| \leq |\rho_0| - \gamma$ when $I < 0$.

Conclusion

We have proven the second part of Theorem 4.2: if the acrobot satisfies the assumptions on $S(\rho_0)$, there exists $I > 0$ small enough that the constraint (4.11) injects energy into the acrobot on $\mathscr{O}_2(\bar{\rho})$.

Here is a summary of the proof:

1. We found pseudo-polar coordinates (β, ρ) adapted to level sets of the nominal pendulum's mechanical energy on $\mathscr{R}$, where $\beta \in \mathbb{S}^1$ is a pseudo-angle and $\rho \in D$ is a pseudo-radius.

2. We showed there exists a value I_1 small enough where $\dot{\beta} > 0$ everywhere on $\mathscr{R}$.

3. Using β as a time variable, we found the evolution of the time-scaled pseudo-radius $\hat{\rho}$ and expanded it into (4.45) using perturbation theory.

4. Taking this expanded solution, we defined and expanded the Poincaré map $P_{\mathscr{R}}$ on the domain $D = D^- \cup D^+$ which shows how the acrobot's orbits behave on $\mathscr{R}_{\bar{\rho}}$.

5. Using the Poincaré map to analyze the discrete-time system (4.48), we found values I_2, I_4 bounding the remainder term $R(\beta, \rho_0, I)$ on D^+ and D^- (respectively), then found values I_3, I_5 which drive all orbits of (4.48) towards $|\rho| = \bar{\rho}$.

Table 4.1: Physical parameters for the real acrobot, as measured by Wang [1].

m_u	m_a	l_u	l_a	l_{c_u}	l_{c_a}	J_u	J_a	g
0.2112	0.1979	0.148	0.145	0.073	0.083	0.00129	0.00075	9.81

Recall from Section 4.5.2 that there exists $I^\star > 0$ making orbits escape $\bar{\mathcal{O}}_1$ into $\mathscr{R}$. Choosing $I \in]0, \min\{I_3, I_5, I^\star\}]$ guarantees energy injection on $\mathcal{O}_2(\bar{\rho})$. Likewise, choosing $I \in [-\min\{I_3, I_5, I^\star\}, 0[$ guarantees energy dissipation on $\mathcal{O}_2(\bar{\rho})$.

This analysis, together with that of section 4.5.2, completes the proof of Theorem 4.2.

□

4.6 Experimental Results

In this section, we test our VNHC on the physical acrobot built by Xingbo Wang [1] (Figure 4.12). This acrobot is not simple, that is, the torso and leg rods have unequal mass and differ in length. Furthermore, the centers of mass are not located at the tip of each rod. These experiments will therefore test whether VNHCs are robust to model mismatch, since our VNHC is only proven to inject energy on simple acrobots. As we will see, our VNHC does inject energy on the general acrobot model.

Wang's acrobot has inertia matrix as in (4.1) and potential function as in (4.2). The physical parameters are written explicitly in Table 4.1.

This acrobot's actuator is a servo motor with a built-in PID controller, so we can set $q_a = \arctan(Ip_u)$ directly without needing to solve for the VNHC's torque input τ. The control parameter I needs to be small, but it also needs to be large enough to overcome friction in the servo motor. Since the acrobot's mass and length values are small, its momentum is also small. Through various experiments, we determined that $I = 10$ is sufficient to ensure the actuator can fully rotate in its allowable range $q_a \in \left[-\frac{\pi}{2}, \frac{\pi}{2}\right]$.

4.6.1 Simulations

To compute the energy of the nominal pendulum, we evaluate the system at the VNHC $q_a = 0$, which yields

$$E(q_u, p_u) \approx 396.5501 p_u^2 + 0.5997(1 - \cos(q_u)).$$

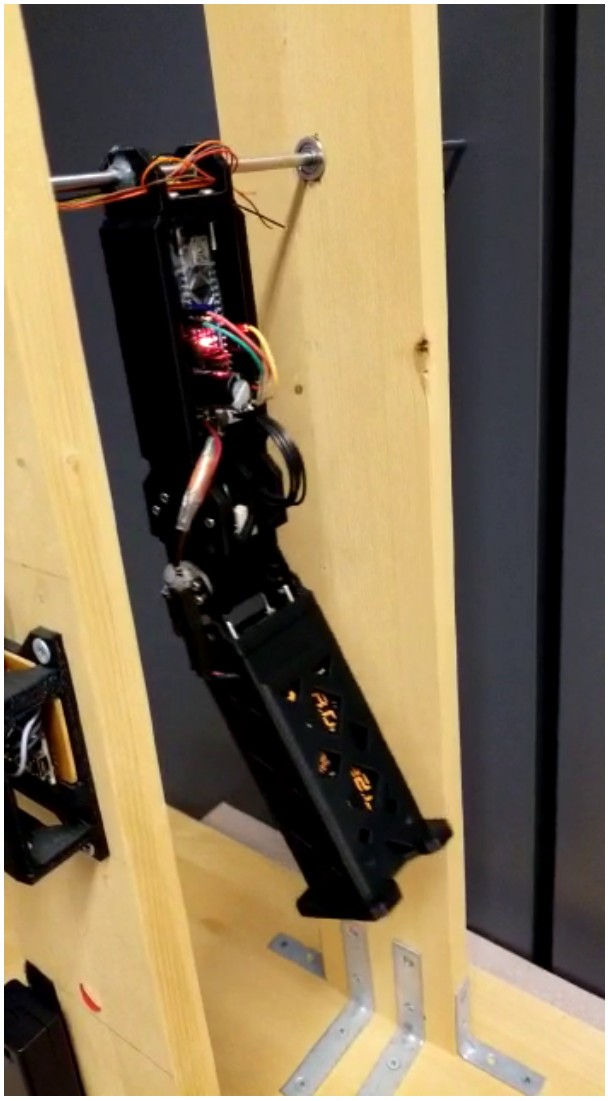

Figure 4.12: The acrobot built by Wang [1].

Hence, the level set of E_π of the energy $E(\pi, 0)$ is parameterized by

$$p_u \approx \pm\sqrt{\frac{1.1994}{793.1001}(1 + \cos(q_u))},$$

for each $q_u \in]-\pi, \pi]$.

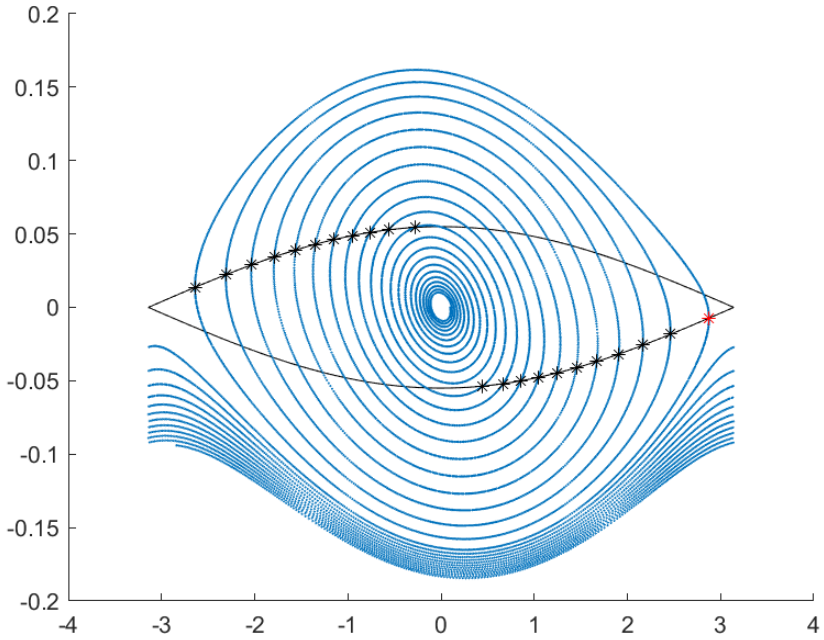

Figure 4.13: A simulation of the acrobot from [1].

We initialize the simulation for this acrobot at $(q_u, p_u) = \left(\frac{\pi}{32}, 0\right)$ and plot the resulting orbit in Figure 4.13. The nominal energy level set E_π is outlined in black. Because this acrobot is not simple, E_π is not the boundary between rotations and oscillations. The oscillation domain is actually much larger: orbits rotate once they hit the p_u-axis at $|p_u| \approx 0.15$, while E_π intersects the p_u-axis at $|p_u| \approx 0.055$. Despite this, we see that eventually the acrobot remains outside E_π. The points where the orbit exits E_π are highlighted with black stars, with the final departure highlighted in red. At this final departure, the acrobot begins rotating and continues to gain energy over time.

To verify that the acrobot will consistently begin rotating, we use a Monte Carlo method [51] to simulate this acrobot 1000 times. At each iteration, we initialize the acrobot randomly inside the sublevel set

$$\left\{(q_u, p_u) \in \mathbb{S}^1 \times \mathbb{R} \mid E(q_u, p_u) \leq E\left(\frac{\pi}{32}, 0\right)\right\},$$

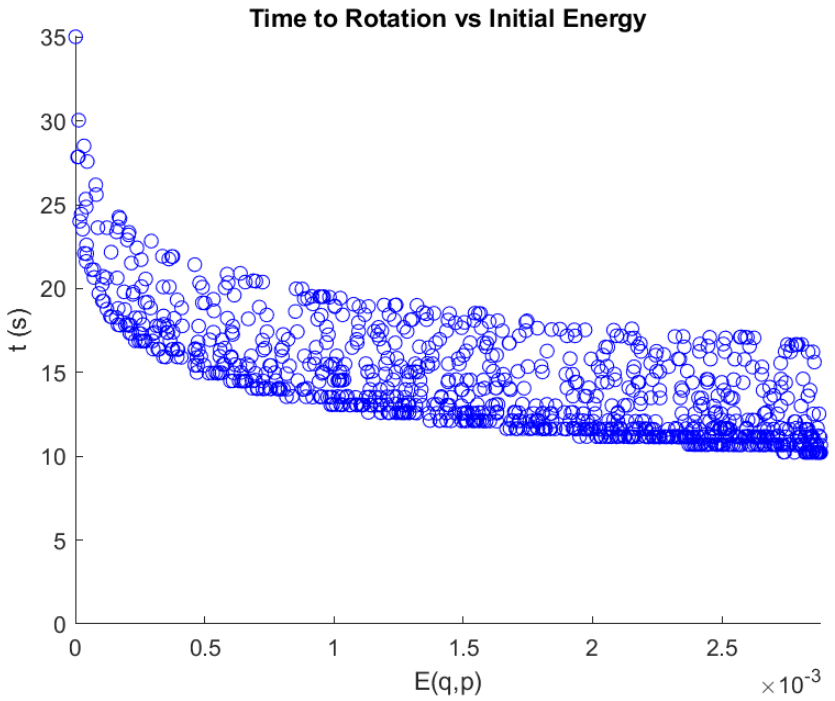

Figure 4.14: Monte Carlo simulation results for the acrobot from [1].

and measure how long it takes the acrobot to begin rotating. The results are plotted in Figure 4.14. The acrobot always rotates within 10–35 seconds.

4.6.2 Physical Experiments

To complete this chapter, we perform four experiments with the physical acrobot:

1. An undisturbed test to validate that the acrobot reaches rotations.
2. A test where we stop the acrobot once it has started rotating.
3. A test where we push the acrobot in its direction of motion after it has started rotating.
4. A test where we push the acrobot against its direction of motion.

The acrobot has an encoder at the pivot which measures q_u and $\dot{q}_u$, and the servo provides a measurement of q_a. We estimate $\dot{q}_a$ through sequential values of q_a and compute p_u through $p_u = e_1^T M(q)\dot{q}$. The actuator value at iteration $k \in \mathbb{Z}_{>0}$ is assigned through the equation

$$q_a^k = \arctan(Ip_u^{k-1}).$$

Test 1: No Disturbances

For this test we initialize the acrobot at $(q_u, p_u) \approx \left(\frac{\pi}{8}, 0\right)$. The resulting orbit is shown in Figure 4.15, which is clearly gaining energy over time.

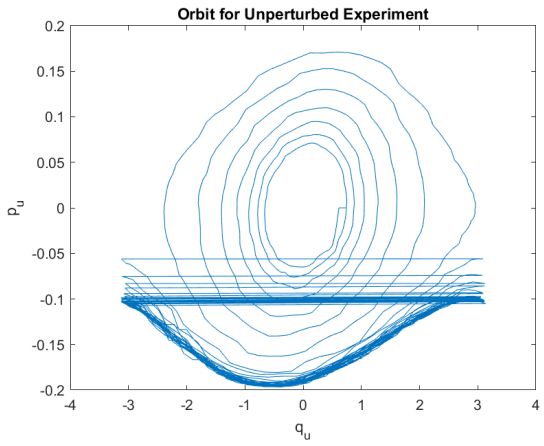

Figure 4.15: The orbit of the physical acrobot during an unperturbed test.

Test 2: Stopping the Acrobot

For this test we initialize the acrobot at $(q_u, p_u) \approx (\pi, 0)$ and let it run for 15 seconds, then stop the acrobot as it reaches the bottom of its arc. The resulting orbit is shown in Figure 4.16. The blue curves correspond to the orbit before the disturbance, while the red spiral shows that the acrobot begins oscillating after it is stopped. Despite the disturbance, it gains energy and eventually starts rotating again.

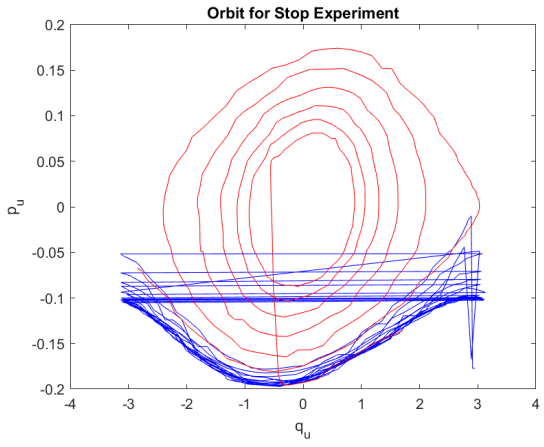

Figure 4.16: The orbit of the physical acrobot before (blue) and after (red) it is stopped.

Test 3: Pushing the Acrobot Forwards

To see how the acrobot responds when pushed in its direction of motion, we allow the acrobot to rotate undisturbed for 15 seconds and then give it a push in its direction of motion. The orbit in Figure 4.17 shows that the acrobot speeds up to rotate with energy $E(0, 0.22)$, but then slows down until it reaches a stable rotation with energy $E(0, -0.195)$.

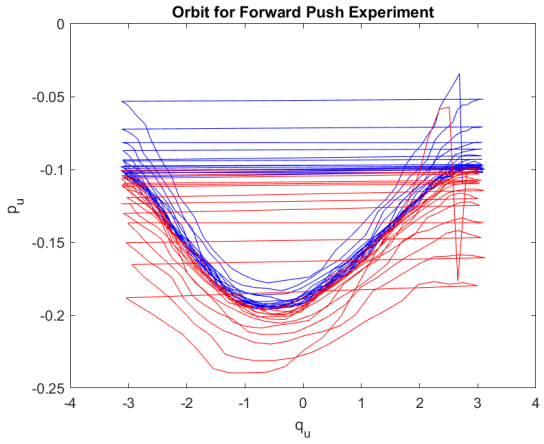

Figure 4.17: The orbit of the physical acrobot before (blue) and after (red) it is pushed in its current direction of motion.

Test 4: Pushing the Acrobot Backwards

In this final experiment, we test whether the acrobot can easily change directions when pushed against its current direction of motion. We again allow the acrobot to rotate undisturbed for 15 seconds, then push it the opposite way. The orbit in Figure 4.18 demonstrates that the acrobot responds by readily changing direction, and quickly achieves its maximum speed with energy $E(0, 0.195)$.

4.6.3 Summary of Experimental Results

The simulations and experiments in this section show that VNHCs are excellent tools for injecting energy even in non-simple acrobots. Furthermore, the experimental results show that the energy gain is robust against a variety of disturbances. Finally, the two push tests suggest that Wang's acrobot constrained by our VNHC will gain energy on $\mathcal{O}_2(0.195)$.

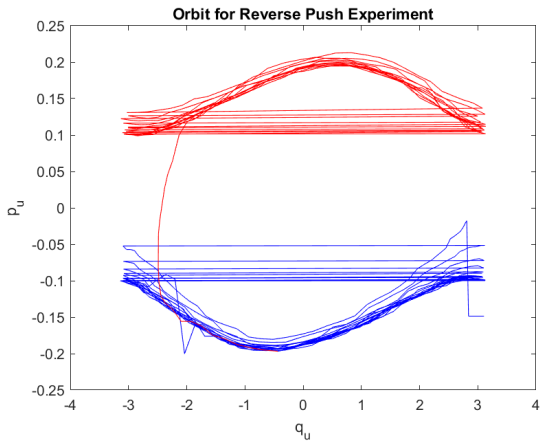

Figure 4.18: The orbit of the physical acrobot before (blue) and after (red) it is pushed against its current direction of motion.

Chapter 5

Conclusion

This thesis has shown the utility of VNHCs as a means of injecting energy into mechanical systems. In Chapter 2 we developed the framework of VNHCs for underactuated mechanical systems, with a focus on VNHCs for simply actuated Hamiltonian systems. We then applied this framework to two benchmark systems: the variable-length pendulum and the acrobot. In Chapter 3 we proved that a certain class of VNHCs will always inject energy into the VLP, while in Chapter 4 we designed a constraint inspired by gymnastics and proved it injects energy into the acrobot. At the end of each chapter we performed simulations and experiments which validated the theory, and which showed the efficacy and robustness of VNHC-driven motion. In the end, we demonstrated that virtual nonholonomic constraints are capable of injecting and dissipating energy in a robust manner, all while producing realistic biological motion.

5.1 Limitations and Future Research

Our VNHC framework relies on the following assumptions:

1. The Hamiltonian of the system is of the form
$$H(q,p) = \frac{1}{2}p^{\mathsf{T}}M^{-1}(q)p + V(q).$$
2. The input matrix $B(q) \equiv B \in \mathbb{R}^{n\times k}$ is constant and full rank.
3. The input matrix has a left-annihilator $B^{\perp} \in \mathbb{R}^{(n-k)\times n}$.
4. The annihilator matrix $B^{\perp}$ is right semi-orthogonal.
5. The inertia matrix of the system satisfies $\nabla_{q_u} M(q) = \mathbf{0}_{n(n-k)\times n}$.

6. On the constraint manifold Γ, one can solve for q_a as a function of (q_u, p_u).

If any of these assumptions are not satisfied, one may not be able to find the constrained dynamics in simply actuated coordinates, and the results of this thesis may not hold. In particular, the theoretical guarantees of this thesis do not apply to systems with physical nonholonomic constraints (*e.g.*,friction), nor do they apply to vehicles with wheels.

These limitations guide us to the following research directions. First, one might relax the assumptions on the input and inertia matrices, thereby widening the class of systems to which VNHCs can be applied. Second, one might forgo the assumption that q_a is solvable on the constraint manifold; instead, one could borrow from the VHC literature and parameterize the constraint manifold with a different set of coordinates than (q_u, p_u). This might result in the same dynamics as Horn et al. [18], albeit in Hamiltonian rather than Lagrangian mechanics. Third, one might consider more general mechanical systems with dynamics given by

$$\begin{cases} \dot{q} = M^{-1}(q)p, \\ \dot{p} = -(I_n \otimes p^\mathsf{T})\nabla_q M^{-1}(q)p - \nabla_q V(q) + Q_{nh}(q,p) + B(q)\tau, \end{cases}$$

where $Q_{nh}(q,p) \in \mathbb{R}^n$ are terms corresponding to physical nonholonomic constraints like friction. Fourth, one can investigate a smoother method for energy stabilization, where a VNHC is explicitly designed to inject energy below some energy level, and dissipate energy above it. For example, one might devise a mechanism for smoothly transferring between VNHCs while maintaining certain safety requirements.

Finally, the proof of Theorem 4.2 in Chapter 4.5 opens a door to the possibility of VNHC generation. One might search for suitable conditions on VNHCs where the Poincaré sections for oscillations and rotations are increasing. Then, one can extend Otsason's "virtual constraint generator" [52] to generate regular VNHCs which satisfy these energy injection/dissipation conditions. In this way, one could automatically generate regular VNHCs which stabilize a desired energy level.

Bibliography

[1] X. Wang, "Motion control of a gymnastics robot using virtual holonomic constraints," Master's thesis, University of Toronto, 2016.

[2] G. K. A. e.V., "Jonas e. auf der kiik," online; accessed on 19 December 2020. [Online]. Available: https://kiikinggermany.de/media/pictures/post/2/das-ist-kiiking.jpg

[3] B. Piccoli and J. Kulkarni, "Pumping a swing by standing and squatting: Do children pump time-optimally?" *IEEE Control Systems Magazine*, vol. 25, no. 4, pp. 48 – 56, August 2005.

[4] M. Maggiore and L. Consolini, "Virtual holonomic constraints for euler-lagrange systems," *IEEE Transactions on Automatic Control*, vol. 58, no. 4, pp. 1001 – 1008, April 2013.

[5] J. A. Acosta, R. Ortega, A. Astolfi, and A. Mahindrakar, "Interconnection and damping assignment passivity-based control of mechanical systems with underactuation degree one," *IEEE Transactions on Automatic Control*, vol. 50, no. 12, pp. 1936 – 1955, December 2005.

[6] A. Mahindrakar, A. Astolfi, R. Ortega, and G. Viola, "Further constructive results on interconnection and damping assignment control of mechanical systems: The acrobot example," in *Proceedings of the 2006 American Control Conference*. Minneapolis, Minnesota, USA: American Control Conference, June 2006.

[7] R. Ortega, A. J. van der Schaft, I. Mareels, and B. Maschke, "Energy shaping control revisited," in *Advances in the control of nonlinear systems*, A. Baños, F. Lamnabhi-Lagarrigue, and F. J. Montoya, Eds. Springer, 2001, pp. 227–307.

[8] X. Xin and Y. Liu, "Trajectory tracking control of variable length pendulum by partial energy shaping," *Communications in Nonlinear Science and Numerical Simulations*, vol. 19, no. 5, pp. 1544 – 1556, May 2014.

[9] X. Xin and M. Kaneda, "The swing up control for the acrobot based on energy control approach," in *Proceedings of the 41st IEEE Conference on Decision and Control*. Las Vegas, USA: IEEE, March 2003.

[10] T. Henmi, M. Chujo, Y. Ohta, and M. Deng, "Reproduction of swing-up and giant swing motion of acrobot based on a technique of the horizontal bar gymnast," in *Proceedings of the 11th World Congress on Intelligent Control and Automation*. Shenyang, China: IEEE, June 2014.

[11] B. Griffin and J. Grizzle, "Nonholonomic virtual constraints for dynamic walking," in *2015 54th IEEE Conference on Decision and Control*. Osaka, Japan: IEEE, December 2015.

[12] T. Takubo, H. Arai, and K. Tanie, "Virtual nonholonomic constraint for human-robot cooperation in 3-d space," in *2000 IEEE/RSJ International Conference on Intelligent Robots and Systems*. Takamatsu, Japan: IEEE, October 2000.

[13] B. Griffin and J. Grizzle, "Nonholonomic virtual constraints and gait optimization for robust walking control," *The International Journal of Robotics Research*, vol. 36, pp. 895–922, May 2017.

[14] W. K. Chan, Y. Gu, and B. Yao, "Optimization of output functions with nonholonomic virtual constraints in underactauted bipedal walking control," in *2018 Annual American Control Conference*. Milwaukee, USA: IEEE, June 2018.

[15] S. Vozar, Z. Chen, P. Kazanzides, and L. L. Whitcomb, "Preliminary study of virtual nonholonomic constraints for time-delayed teleoperation," in *2015 IEEE/RSJ International Conference on Intelligent Robots and Systems*. Hamburg, Germany: IEEE, October 2015.

[16] S. Shibata and T. Murakami, "Psd based virtual nonholonomic constraint for human interaction of redundant manipulator," in *Proceedings of the 2004 IEEE International Conference on Control Applications*. Taipei,Taiwan: IEEE, September 2004.

[17] J. D. Castro-Díaz, P. Sánchez-Sánchez, A. Gutiérrez-Giles, M. Arteaga-Pérez, and J. Pliego-Jiménez, "Experimental results for haptic interaction with virtual holonomic and nonholonomic constraints," *IEEE Access*, vol. 8, pp. 120 959 – 120 973, July 2020.

[18] J. Horn, A. Mohammadi, K. Hamed, and R. Gregg, "Hybrid zero dynamics of bipedal robots under nonholonomic virtual constraints," *IEEE Control Systems Letters*, vol. 3, no. 2, pp. 386 – 391, April 2019.

[19] J. C. Horn, A. Mohammadi, K. A. Hamed, and R. D. Gregg, "Nonholonomic virtual constraint design for variable-incline bipedal robotic walking," *IEEE Robotics and Automation Letters*, vol. 5, pp. 3691 – 3698, February 2020.

[20] A. Mohammadi, M. Maggiore, and L. Consolini, "Dynamic virtual holonomic constraints for stabilization of closed orbits in underactuated mechanical systems," *Automatica*, vol. 94, pp. 112 – 124, August 2018.

[21] ——, "On the lagrangian structure of reduced dynamics under virtual holonomic constraints," *ESAIM: Control, Optimization and Calculus of Variations*, vol. 23, no. 3, pp. 913 – 935, June 2017.

[22] D. T. Greenwood, *Principles of Dynamics*, 2nd ed. Englewood Cliffs, NJ: Prentice Hall, 1987.

[23] L. D. Landau and E. M. Lifschitz, *Mechanics*, 3rd ed. Butterworth-Heinemann, January 1982.

[24] R. D. Schafer, *An Introduction to Non-Associative Algebras*. New York: Dover Publications, 1996.

[25] G. Golub and W. Kahan, "Calculating the singular values and pseudo-inverse of a matrix," *Journal of the Society for Industrial and Applied Mathematics: Series B, Numerical Analysis*, vol. 2, no. 2, pp. 204–224, 1965.

[26] J. Grizzle, C. Chevallereau, R. Sinnet, and A. Ames, "Models, feedback control, and open problems of 3d bipedal robotic walking," *Automatica*, vol. 50, no. 8, pp. 1955 – 1988, August 2014.

[27] F. Plestan, J. Grizzle, E. R. Westervelt, and G. Abba, "Stable walking of a 7-dof biped robot," *IEEE Transactions on Robotics and Automation*, vol. 19, no. 4, pp. 653–668, August 2003.

[28] L. Consolini and M. Maggiore, "Control of a bicycle using virtual holonomic constraints," *Automatica*, vol. 49, no. 9, pp. 2831–2839, September 2013.

[29] S. Westerberg, U. Mettin, A. S. Shiriaev, L. B. Freidovich, and Y. Orlov, "Motion planning and control of a simplified helicopter model based on virtual holonomic constraints," in *2009 International Conference on Advanced Robotics*. Munich, Germany: IEEE, June 2009, pp. 1–6.

[30] A. Mohammadi, E. Rezapour, M. Maggiore, and K. Y. Pettersen, "Maneuvering control of planar snake robots using virtual holonomic constraints," *IEEE Transactions on Control Systems Technology*, vol. 24, no. 3, pp. 884 – 899, May 2015.

[31] S. Wirkus, R. Rand, and A. Ruina, "How to pump a swing," *The College Mathematics Journal*, vol. 29, no. 4, pp. 266 – 275, 1998.

[32] V. Sevrez, E. Berton, G. Rao, and R. J. Bootsma, "Regulation of pendulum length as a control mechanism in performing the backward giant circle in gymnastics," *Human Movement Science*, vol. 28, no. 2, pp. 250 – 262, March 2009.

[33] L. Wang, W. Shi, and Y. Zhou, "Study on self-adjustable variable pendulum tuned mass damper," *The structural design of tall and special buildings*, vol. 28, January 2019.

[34] A. O. Belyakov, A. P. Seyranian, and A. Luongo, "Dynamics of the pendulum with periodically varying length," *Physica D*, vol. 238, pp. 1589 – 1597, August 2009.

[35] E. A. Barbashin and N. N. Krasovskii, "On the stability of motion as a whole (in russian)," *Doklady Akademii Nauk SSSR*, vol. 86, pp. 453–456, 1952.

[36] L. Perko, *Differential equations and dynamical systems*, 3rd ed. New York, USA: Springer, 2013, vol. 7.

[37] I. Bendixson, "Sur les courbes définies par les équations différentielles," *Acta Math*, vol. 24, pp. 1–88, 1901.

[38] H. Kaarma, G. Veldre, L. Saluste, M. Lintsi, J. Kasmel, E.-M. Tiit, R. Stamm, M. Toomsalu, and A. Arend, "On systematisation of estonians' body build data," *Papers on Anthropology*, vol. 26, no. 1, pp. 9–27, 2017.

[39] kiiking.com, "Kiiking.com sale," online; accessed on 20 December 2020. [Online]. Available: https://kiiking.com/index.php/en/sale

[40] J. Hauser and R. Murray, "Nonlinear controllers for non-integrable systems: the acrobot example," in *1990 American Control Conference*. San Diego, USA: IEEE, May 1990.

[41] E. Westervelt, "Toward a coherent framework for the control of planar biped locomotion," Ph.D. dissertation, University of Michigan, Michigan, USA, 2003.

[42] M. W. Spong, "The swing up control problem for the acrobot," *IEEE Control Systems Magazine*, vol. 15, pp. 49–55, February 1995.

[43] A. D. Mahindrakar and R. N. Banavar, "A swing-up of the acrobot based on a simple pendulum strategy," *International Journal of Control*, vol. 78, no. 6, pp. 424 – 429, 2005.

[44] T. Henmi, M. Akiyama, and T. Yamamoto, "Motion control of underactuated linkage robot based on gymnastic skill," *Electrical Engineering in Japan*, vol. 206, pp. 42–50, January 2009.

[45] P. E. Pidcoe, "The biomechanics principles behind training giant swings," Online, Virginia Commonwealth University, Richmond, VA, USA, August 2005, accessed 11 September 2020. https://usagym.org/pages/home/publications/technique/2005/8/giant.pdf.

[46] E. Papadopoulos and G. Papadopoulos, "A novel energy pumping strategy for robotic swinging," in *2009 17th Mediterranean Conference on Control and Automation*. Thessaloniki, Greece: IEEE, June 2009.

[47] X. Zhang, H. Cheng, Y. Zhao, and B. Gao, "The dynamical servo control problem for the acrobot based on virtual constraints approach," in *The 2009 IEEE/RSJ International Conference on Intelligent Robots and Systems*. St. Louis, USA: IEEE, October 2009.

[48] K. Ono, K. Yamamoto, and A. Imadu, "Control of giant swing motion of a two-link horizontal bar gymnastic robot," *Advanced Robotics*, vol. 15, no. 4, pp. 449 – 465, 2001.

[49] H. K. Khalil, *Nonlinear Systems*, 3rd ed. Upper Saddle River, NJ 07485: Prentice Hall, 2002.

[50] G. D. Birkhoff, *Dynamical Systems*. Colloquium Publications, 1927, vol. 9.

[51] N. Metropolis, "The beginning of the monte carlo method," *Los Alamos Science*, pp. 125–130, 1987, 1987 special issue dedicated to Stanislaw Ulam.

[52] R. D. Otsason, "Virtual constraint generation," Master's thesis, University of Toronto, 2020.